



# **Modelling of Magnetizing Inductance Saturation in a Three-phase Self- excited Induction Generator**

Abdlrhman Mohammed N Alfrhan

School of Electrical and Electronic Engineering

Newcastle University

A thesis submitted for the degree of

Doctor of Philosophy

Dec, 2016







# Abstract

---

Self-excited induction generators are used in small-scale generation systems such as small wind turbines and micro-hydro schemes where a grid connection is not available. In such applications, there is a strong need to model the generator as accurately as possible in order to obtain a realistic estimation of machine behaviour and dynamics. This study presents a generalized dynamic analytical model of a three-phase self-excited induction generator (SEIG) in the natural three-phase ABC/abc reference frame. The developed model accounts for the significant effects of magnetic saturation by expressing the magnetizing inductance as an exponential function of the magnetizing current, considering both variation in magnetizing inductance and its rate of change with magnetizing current ( $dL_m/di_m$ ). This more accurately predicts the dynamic behaviour. The proposed model has the capability to include the effects of mutual saturation between the stator windings as well as that between the rotor windings. Additionally, the proposed model is extended to cover leakage saturation, such that, the effect of the derivative of leakage inductance with respect to magnetizing current is taken into account. The proposed dynamic saturated model is used to successfully predict the performance of the SEIG at steady state, load perturbation, faults, and balanced and unbalanced conditions. The results are verified experimentally using a 7.5kW induction generator test rig. A high level of agreement has been obtained between experimental waveforms and those from the proposed model.

# Acknowledgements

---

First and foremost, I would like to express my gratitude to Dr. Shady Gadoue, my main supervisor, for his valuable guidance, endless support and knowledgeable comments throughout my PhD project. I would also like to show my appreciation for my second supervisor, Dr. Mohammed Elgendy, for this help throughout my time at Newcastle University, particularly for his reading and valuable comments on this thesis. Additionally I would like to express my gratitude to my previous supervisor, Dr. Bashar Zahawi, for his support and help in the initial stages of this work, and for his subsequent direction.

I would like to thank the following people for their invaluable help:

The technical support staff in the Power Electronic Machines and Drives Laboratory and Mechanical workshop at the School for their help in constructing my rig, and providing the testing equipment. Special thanks go to Stephen Robson, Stephen Mitchell, Gordon Marshall, Darren Mackie, and James Richardson.

The administrative staff in the Electrical Engineering school for their help. Special thanks to Gillian Webber for her help during the project period.

Yasser Alamoudi and Mohammed Shalby, for helping to solve any problems and for our discussions.

And finally, I would like to thank my family for supporting me throughout the work of my PhD, and for their great influence on the work and its completion. Thanks, to my wife, my daughters Sarah, Rahaf, Reema, Ghala and my son Meshari.

Special thanks go to my brother Saud for his full support and enthusiasm and inspiration at all times throughout my study.

*To the memory of my Mother*  
*who departed at the end of my studies*

# Table of Contents

---

Abstract	i
Acknowledgements	ii
Table of Contents	iii
List of Figures	vi
List of Tables	ix
Acronyms and symbol	x
<b>Chapter 1. Introduction</b>	<b>1</b>
1.1 Background	1
1.2 Objectives and scope of the research	4
1.3 Novelty and contributions	5
1.4 Published Material	6
1.5 Structure of the thesis	6
<b>Chapter 2. Review, analysis and modelling of the SEIG</b>	<b>9</b>
2.1 Introduction	9
2.2 The self-excitation phenomenon	9
2.3 Steady-state operation of SEIGs	14
2.4 Voltage regulation of SEIGs	16
2.5 Transient analysis of SEIGs	17
2.6 The main saturation effects of SEIGs	19

2.7	The leakage saturation effect of SEIGs	22
2.8	Conclusion	23
<b>Chapter 3. Mathematical model of the saturation of the SEIG</b>		<b>25</b>
3.1	Introduction	25
3.2	Conventional dynamic model of induction machine	26
3.3	Proposed dynamic model of the SEIG	35
3.4	Flux linkage model of SEIGs	46
3.5	Electromagnetic torque equation of SEIGs	46
3.6	Mechanical torque equation of SEIGs	49
3.7	Mathematical model of the load and excitation capacitors	50
3.7.1	Resistive load	50
3.7.2	Inductive and resistive load	52
3.8	Modelling the residual flux of SEIGs	54
3.9	Magnetizing current equation for SEIGs	54
3.10	Conclusion	56
<b>Chapter 4. Representation of variation in magnetizing inductance</b>		<b>58</b>
4.1	Introduction	58
4.2	Methods used to model magnetizing inductance	59
4.3	The exponential method to represent the magnetizing inductance	60
4.4	Conclusion	66

<b>Chapter 5. The experimental system</b>	<b>67</b>
5.1 Introduction	67
5.2 The experimental system under study	69
5.3 Determination of induction machine parameters	71
5.3.1 DC test	71
5.3.2 Locked rotor test	72
5.3.3 No load test	74
5.4 Magnetizing characteristics	76
5.5 Speed measurements	77
5.6 Conclusion	77
<b>Chapter 6. Simulation results and experimental validation</b>	<b>79</b>
6.1 Introduction	79
6.2 No-load results	80
6.3 Balanced load results	88
6.4 Unbalanced-load results	92
6.5 Load perturbation results	96
6.6 Fault response results	109
6.7 Sudden change in speed results	113
6.8 Conclusion	117
<b>Chapter 7. The effects of dynamic inductance</b>	<b>119</b>

7.1	Introduction	119
7.2	Results and discussion	120
7.3	Conclusion	127
<b>Chapter 8. The effects of leakage saturation</b>		<b>128</b>
8.1	Introduction	128
8.2	Leakage inductance characteristic	129
8.3	Modelling leakage saturation	129
8.4	Model results and experimental validation	131
8.5	Conclusion	137
<b>Chapter 9. Conclusion and future work</b>		<b>138</b>
9.1	Conclusion	138
9.2	Future work	142
<b>Appendix A. Derivation of the exponential function</b>		<b>143</b>
<b>Appendix B. The determination of the minimum capacitor value</b>		<b>147</b>
<b>Appendix C. Laboratory tools</b>		<b>148</b>
<b>Appendix D. Lagrange polynomial</b>		<b>151</b>
<b>References</b>		<b>153</b>

# List of Figures

---

<i>Figure 1.1 Renewable energy share in 2020: (target 2020: 20%)[10].....</i>	<i>2</i>
<i>Figure 2.1 Per-phase equivalent circuit of the induction machine referred to the stator. ....</i>	<i>10</i>
<i>Figure 2.2 The self-excitation phenomena. ....</i>	<i>11</i>
<i>Figure 2.3 The direction of flux, current and volt of self-excitation phenomena [66].....</i>	<i>12</i>
<i>Figure 2.4 Determination of stable operation of self-excited induction generator.....</i>	<i>13</i>
<i>Figure 3.1 Schematic diagram of self-excited induction generator driven by a wind .....</i>	<i>26</i>
<i>Figure 3.2 Machine diagram in natural reference frame[53]. ....</i>	<i>27</i>
<i>Figure 3.3 Configuration of the system when a resistive load is connected. ....</i>	<i>51</i>
<i>Figure 3.4 Single-phase diagram of the system under study.....</i>	<i>52</i>
<i>Figure 3.5 Configuration of the system under study when R-L load is connected. ....</i>	<i>53</i>
<i>Figure 4.1 Determination of stable operation of self-excited induction generator.....</i>	<i>59</i>
<i>Figure 4.2 Calculated induction machine magnetization curve.....</i>	<i>62</i>
<i>Figure 4.3 Induction machine magnetization curve. ....</i>	<i>63</i>
<i>Figure 4.4 Magnetizing characteristics of the induction machine under study. ....</i>	<i>64</i>
<i>Figure 4.5 Flow chart describing the performance evaluation.....</i>	<i>65</i>
<i>Figure 5.1 Circuit diagram of the experimental setup. ....</i>	<i>67</i>
<i>Figure 5.2 Mechanical coupling between the SEIG and a DC motor for the system .....</i>	<i>68</i>

<b>Figure 5.3</b> Experimental bench for the system.....	70
<b>Figure 5.4</b> Approximate equivalent circuit for the locked rotor test. ....	72
<b>Figure 5.5</b> Approximate equivalent circuit for no load test.....	74
<b>Figure 5.6</b> Magnetization characteristics for the 7.5 kW induction machine.....	77
<b>Figure 6.1</b> Measured phase voltage (a); calculated phase voltage (b), during the build-up process of the SEIG at $C= 30 \mu\text{F}$ per phase and 1450 rpm. ....	81
<b>Figure 6.2</b> Measured phase voltage (a) and calculated phase current (b), during the build-up process of the SEIG at $C= 30 \mu\text{F}$ per phase and 1450 rpm.....	82
<b>Figure 6.3</b> The variation of the flux in the stator windings during the build-up process of the SEIG at $C= 30 \mu\text{F}$ per phase and 1450 rpm: (a) phase a (b) in a three-dimension (abc frame). ....	83
<b>Figure 6.4</b> Variation in: (a) magnetizing current; (b) magnetizing inductance; (c) dynamic inductance in stator phase a; (d) dynamic inductance in the rotor phase a, during the build-up process of the SEIG at $C= 30 \mu\text{F}$ per phase and 1450 rpm. ....	85
<b>Figure 6.5</b> Variation in: (a) mechanical torque and (b) electromagnetic torque during the build-up process of the phase of the voltage of the SEIG at $C= 30 \mu\text{F}$ per phase and 1450 rpm.....	86
<b>Figure 6.6</b> No-load generated voltage and current waveforms at 1450 rpm; $C=30\mu\text{F}$ per phase. ....	87
<b>Figure 6.7</b> Steady-state generated voltage (a) and current (b) waveforms with a balanced resistive load of $500 \Omega$ per phase, $C = 30\mu\text{F}$ per phase.....	88
<b>Figure 6.8</b> Waveforms of phase voltage (oscilloscope screenshot) (a); phase voltage (rms) (b); phase current (oscilloscope screenshot) (c) and phase current (rms) (d) during switching on a balanced load at 8.1 seconds; $R=500\Omega$ per	

<i>phase.</i> .....	90
<b>Figure 6.9</b> <i>Steady-state generated voltage (a) and current (b) waveforms with a balanced R-L load, <math>R=365\Omega</math> per phase, <math>L=1H</math> per phase, <math>C = 37\mu F</math> per phase.</i> .....	91
<b>Figure 6.10</b> <i>Configuration of the system under study when R-L load is connected.</i> .....	92
<b>Figure 6.11</b> <i>Steady-state generated voltage and current waveforms; unbalanced resistive load (<math>R_{1a} = R_{1b} = 620\Omega</math> and <math>R_{1c} = 500\Omega</math>), <math>C = 30\mu F</math> per phase.</i> .....	93
<b>Figure 6.12</b> <i>Generated voltage and current waveforms; <math>500\Omega</math> resistive load connected to phases b and c while phase a is open circuited; <math>C = 30\mu F</math> per phase.</i> .....	94
<b>Figure 6.13</b> <i>Steady-state of voltage (a) and current(b) waveforms; unbalance R-L load, <math>C = 37\mu F</math> per phase, 1400 rpm.</i> .....	95
<b>Figure 6.14</b> <i>Waveforms of phase voltage (a), phase current (b), during switching of a balanced load at 10.3 seconds; <math>R=500\Omega</math> per phase.</i> .....	97
<b>Figure 6.15</b> <i>Waveforms of: (a) phase voltage; (b) phase current, during the removal of a balanced load; <math>R=365\Omega</math> per phase, <math>L=1H</math> per phase, <math>C=37\mu F</math> per phase.</i> .....	99
<b>Figure 6.16</b> <i>Behaviour of phase voltage: (a) phase a; (b) phase b; (c) phase c, during load perturbation at unbalanced conditions with two phase load rejection, <math>C = 30\mu F</math> per phase, 1450 rpm.</i> .....	100
<b>Figure 6.17</b> <i>Behaviour of the generated current (r.m.s): (a) phase a; (b) phase b; (c) phase c, during load perturbation at unbalanced conditions with two phase load rejection, <math>C = 30\mu F</math> per phase, 1450 rpm.</i> .....	102
<b>Figure 6.18</b> <i>Behaviour of the stator current: (a) phase a; (b) phase b; (c) phase c; of SEIG after removing one phase (phase a) of the load.</i> .....	104
<b>Figure 6.19</b> <i>The Behaviour of output voltage: (a) phase a; (b) phase b; (c) phase c, of SEIG after removing phase a of the load.</i> .....	106
<b>Figure 6.20</b> <i>SEIG performance after adding an excessive three-phase load when running</i>	

at 1330rpm at no-load: (a) phase current (oscilloscope screenshot);(b)phase current (rms) (c) phase voltage (oscilloscope screenshot) (d) phase voltage (rms).....	108
<b>Figure 6.21</b> SEIG performance after adding an excessive three-phase load when running at 1330rpm at no-load: (a) flux, (b) dynamic inductance. ....	109
<b>Figure 6.22</b> Fault behavior of the SEIG with a three-phase fault at the generator terminals. ....	111
<b>Figure 6.23</b> Fault behaviour of the SEIG with a line-to-line fault at the generator terminals. ....	113
<b>Figure 6.24</b> Shaft speed of self-excited induction generator during a DL fault. ....	113
<b>Figure 6.25</b> Variation in shaft speed of the prime mover of the SEIG.....	114
<b>Figure 6.26</b> Performance of the SEIG during a sudden change in rotor speed: (a) phase stator current; (b) screen shot of the oscilloscope of the phase current, with a balanced R-L load.....	115
<b>Figure 6.27</b> Performance of the SEIG during a sudden change in rotor speed:(a) phase stator voltage; (b) screen shot of the oscilloscope of the phase voltage when a balanced R-L load was connected. ....	116
<b>Figure 6.28</b> Change in the dynamic inductance of phase-a in: (a) the stator; (b) the rotor, due to sudden change in speed. ....	117
<b>Figure 7.1</b> Comparison of the performance of the proposed and conventional models following sudden disconnection of balanced three-phase R-L load, $R=365\Omega$ per phase, $L=1H$ per phase, $C = 37\mu F$ per phase, 1400 rpm. ....	121
<b>Figure 7.2</b> Behaviour of the dynamic effects in the stator phase-a (a), and the rotor phase-a (b) for same case as figure 7.1. ....	122
<b>Figure 7.3</b> Comparison of the behaviour of (a) the flux of stator windings in phase-a and	

(b) electromagnetic torque obtained by the proposed and conventional models during sudden removal of balanced three phase R-L load,  $R=365\Omega$  per phase,  $L=1H$  per phase,  $C = 37\mu F$  per phase, speed =1400 rpm.....123

**Figure 7.4** Comparison of the proposed and conventional models during three-phase fault when parallel R-L load is connected,  $R=365\Omega$  per phase,  $L=1H$  per phase,  $C = 37\mu F$  per phase, 1400 rpm. ....125

**Figure 7.5** Comparison of the stator current phase-a (a) and phase-b (b) produced by proposed and conventional models during line-to-line fault when parallel R-L load is connected,  $R=365\Omega$  per phase,  $L=1H$  per phase,  $C = 37\mu F$  per phase, 1400 rpm. ....126

**Figure 8.1** Effect of leakage inductance saturation. ....129

**Figure 8.2** Behaviour of stator current (a) and output voltage (b) of SEIG during a three-phase fault with and without including leakage saturation. ....132

**Figure 8.3** Behaviour of dynamic inductance of stator (as defined in the equation 3.45) (a) and rotor (b) in phase a during a three-phase fault when leakage saturation is included. ....133

**Figure 8.4** Behaviour of dynamic matrix of stator (as defined in the equation 3.45) (a) and rotor (b) in phase a during a three-phase fault when leakage saturation is not included. ....134

**Figure 8.5** Prediction of the behaviour of current (a) and voltage (b) of the SEIG with and without including leakage saturation after removing a three phase R-L load.....135

**Figure 8.6** Behaviour of dynamic matrix of stator phase-a (a) and rotor phase-a (b) during the removal of three-phase load with and without including leakage saturation. ....136

# List of Tables

---

<i>Table 5.1 Results of the DC test.</i> .....	71
<i>Table 5.2: Results of the locked rotor test.</i> .....	73
<i>Table 5.3: Results of the no load test.</i> .....	75
<i>Table 5.4: Induction machine parameters.</i> .....	76

# Acronyms and symbols

---

SEIG	Self-excited induction generator
MATLAB	Matrix laboratory
EMTP	Electro-magnetic transient program
rpm	Revolutions per minute
MMF	Magnet motive force
DLG	Double line to ground fault
Kw	Kilowatts
DC	Direct current
AC	Alternating current
d-q	Direct-quadrature
EMF	Electro motive force
IM	Induction machine
IG	Induction generator
STATCOM	Static synchronous compensator

ELC	Electronic load controller
$\rho$	Air density in $\text{kg/m}^3$
$T_e$	Electromagnetic torque
$T_L$	Mechanical torque in N.m
J	The inertia of the rotor in $\text{Kg.m}^2$
$B_m$	Damping coefficient associated with the rotational system of the machine in N.m.s/rad
B	Flux density
$v_s, v_r$	Stator and rotor phase voltages respectively
P	Pole pair number
N	Number of turns
I	RMS current
$I_m$	Magnetization current
$\mu_0$	Permeability of free space
s	Slip
$\mu_m$	Permeability of magnet

$i_{sa}, i_{sb}, i_{sc}$	Stator abc phase currents
$i_{ra}, i_{rb}, i_{rc}$	Rotor abc phase currents
$R_s$	Stator winding resistance
$R_r$	Rotor winding resistance
$R_c$	Core resistance
$V_g$	No-load air gap voltage across the magnetizing reactance
$i_m$	Magnetizing current
$X_m$	Magnetizing reactance
$X_{ls}$	Stator leakage reactance
$X_{lr}$	Rotor leakage reactance
$L_m$	Magnetizing inductance
$L_{ls}$	Leakage stator inductance
$L_{lr}$	Leakage rotor inductance
$L_{sr}$	Stator-rotor mutual inductance
$M_s$	Mutual inductance between stator windings

$M_r$	Mutual inductance between rotor windings
$C_a, C_b, C_c$	Excitation capacitors of phases a, b and c respectively
$X_{ca}, X_{cb}, X_{cc}$	Excitation capacitors reactance of phase a, b and c respectively
$\lambda$	Linkage flux in Webers
$F$	Per unit frequency
$f_{base}$	Reference frequency used in the test to obtain the excitation curve
$\omega$	Angular frequency in rads per second
$\theta$	Rotor electrical displacement in rads
$\theta_r$	Rotor position in rads
$p$	Differentiation operator ( $d/dt$ )
$RMS_e$	Root mean squared error

### **Subscripts**

s	Stator
r	Rotor
a, b, c	Stator and rotor phases



---

# Chapter 1. Introduction

---

## 1.1 Background

In recent years, research efforts have been focused on renewable energy because of serious environmental and geopolitical concerns related to the use of fossil fuels [1-3]. Wind, biomass and small-scale hydro (micro-hydro) systems are good alternative clean energy sources, particularly in rural areas where the power grid is not available. In such remote areas, the self-excited induction generator (SEIG) is an attractive and viable option for power generation [4-9].

Environmental degradation, the increase in the fossil fuel prices particularly during the 1970s and the increasing rate of depletion of oil resources within the next 50 years support the crucial role to be played by renewable energy in the future [5]. As a result, research efforts have been focused on renewable energy such as wind, photovoltaic, and hydro power plants. The European Commission (EC) plan to achieve a target of 20% of the European Union's (EU) energy consumption to be derived from renewable resources by 2020. Renewable energy share in 2020 is shown in Figure 1.1. By 2030, it is expected the target of at least 27 % of renewable energy should be achieved [10].

Induction generators are widely used in renewable energy sources such as wind and small hydroelectric (micro-hydro) energy conversion [11-15]. Micro-hydro units up to a few hundred kilowatts which can operate on an off-grid basis are preferred as they do not cause problems such as deforestation, environmental degradation, or the displacement of populations [5]. This make them suitable to be used in rural areas, in particular where there is no access to the grid.

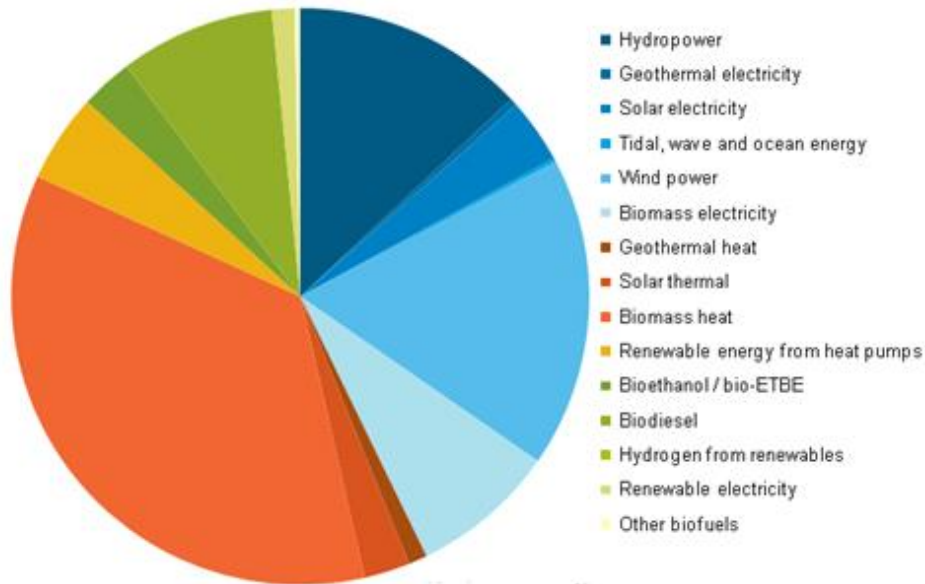


**Figure 1.1** Renewable energy share in 2020: (target 2020: 20%)[10]

What has helped the SEIG to gain this momentum are its inherent advantages, including the absence of a DC power supply for excitation, brushless construction with the squirrel-cage rotor, low maintenance costs, reduced size, simple construction and better transient performance and stability [8, 13, 14, 16-29]. Induction generators are used as highly reliable generators for critical areas such as fire-fighting equipment [30] and as reliable and accurate applications for instance, auxiliary braking for heavy vehicles [31, 32]. However, there are certain drawbacks associated with the use of this type of generator, such as its reactive-power consumption, and poor voltage and frequency regulation [8, 16].

The SEIG is a cage induction machine that does not rely on the grid to obtain its reactive power requirement. Instead, the reactive power requirement of the SEIG is provided by excitation capacitors connected to its stator terminals. The self-excitation process of the SEIG can take place if there is sufficient residual magnetic flux in the rotor [11] or if an initial voltage is imposed across the terminals of the excitation capacitors. The value of the excitation capacitance must be sufficient to provide all the reactive power requirement of the isolated system. Many publications have considered the calculation of the minimum capacitance value

required for self-excitation and, for a particular capacitance value, the corresponding minimum prime-mover speed for building up the generator voltage [33-35]. The development of robust control systems for overcoming the poor voltage and frequency regulation of the SEIG has also been the subject of many investigations [5, 7, 36-38].

The performance of the SEIG has been analysed and investigated, although some authors have neglected the effect of saturation, [39-43]. In these literatures, a simple machine model is employed considering the machine parameters with constant values. However, such a model is suitable to study the performance of the induction machine model only at a specific operating point. Hence, at a variable operating point this approach would not be accurate, as there will be variations in the parameters since flux magnitude and frequency vary.

Other papers [44-48] have accounted for the saturation effect in the induction machine by using the conventional equivalent circuit (EC) of an induction machine such that it is applicable in steady state conditions but cannot be employed to predict transient performance.

Several authors [9, 16, 49] have taken into consideration the non-linearity in the induction machine in the steady state and dynamic response by representing the variation in the relationship between inductance and magnetizing current. However, these conventional machine saturation models have ignored the effects of the derivative of magnetizing inductance with respect to magnetizing current (i.e., dynamic inductance) ( $dL_m/di_m$ ), which may lead to a noticeable error in the dynamic state. This will be shown and highlighted in this study.

A few studies [50, 51] have included the saturation effect by both representing the variation in the relationship between magnetizing inductance and magnetizing current, and taking into account the effect of the change in magnetic inductance with current compromising model accuracy. Furthermore, the proposed models in these papers were developed in the d-q synchronous reference frame and therefore would not be appropriate for unbalanced conditions [49, 52-54]. Additionally, these models include neither the mutual saturation between stator windings, nor that between rotor windings; moreover, the leakage path saturation is not included in these models. In addition, the models that include dynamic inductance have been tested only at constant speed, and none of them were tested under variable speed.

Although the main aim in some papers [16, 49, 55] is to predict the dynamic performance of the SEIG, the effects of dynamic inductance are neglected, which may lead to insufficient accuracy in the results. For this reason, one of the aims of this study is to highlight and include the derivative of magnetizing inductance with respect to magnetizing current. This will be implemented by comparing both a model that includes dynamic inductance with one that neglects this effect.

For a more accurate representation of the variation in magnetizing inductance with current, a polynomial function is conventionally used to model the nonlinearity caused by magnetic saturation [50, 56]. The nonlinear relationship between the air-gap voltage ( $V_g$ ) and the magnetizing current ( $I_m$ ) has also been represented by piecewise linear and exponential functions [1].

## 1.2 Objectives and scope of the research

The steady-state performance characteristics of the SEIG circuit have been extensively studied and reported in literature [23, 38, 39, 57, 58]. For a certain speed and excitation capacitance, the steady-state machine equivalent circuit is solved for the generated frequency and the magnetizing reactance. The magnetizing reactance is then substituted in the magnetization characteristic to obtain the air-gap induced voltage in the stator which is used to calculate other quantities of interest, such as terminal voltage, load current and power [57-59]. However, a noticeable disparity is observed when comparing the results obtained from these models with actual experimental results. This can be attributed to the absence of an accurate representation of magnetic saturation effects in the machine [50, 54], which plays a crucial role in the process of voltage build up and the stable operation of the SEIG [50, 56]. Accounting for the main flux saturation is important in any analysis of the self-excitation, because the induction machine relies on the intersection between capacitor voltage line and the magnetizing curve to determine the steady state operation point [60].

This thesis aims to develop a new general dynamic mathematical model of a three-phase self-excited induction generator (SEIG) by including the non-linearity of the induction machine such that the model can represent the main path saturation, mutual saturation between stator

winding, mutual saturation between rotor windings and leakage path saturation. This developed model should be able to predict the performance of the induction machine precisely at different conditions not only in terms of magnitude but also as phase. These conditions can be steady state, balanced and unbalanced conditions or even at more stressful conditions such as transient conditions. In addition, this study aims to represent the variation in the relationship between the magnetizing inductance and magnetizing current using an accurate and simple methodology.

### 1.3 Novelty and contributions

A new general dynamic mathematical model in the natural three-phase  $ABC/abc$  reference frame has been developed which has the capability to represent the nonlinearity of a self-excited induction generator accurately under different conditions. This model has the ability to represent the main path saturation, leakage path saturation, and the mutual saturation between the stator windings as well as that between the rotor windings. For a more accurate prediction of the performance of the SEIG during the dynamic state, the rate of change of magnetizing inductance with magnetizing current ( $dL_m/di_m$ ) is included in this model.

An improved model of SEIG saturation is developed in which the magnetizing inductance is modelled as an exponential function of the magnetizing current, taking the variation of  $L_m$  with respect to the magnetizing current fully into account. The model is developed in the natural  $ABC/abc$  frame of reference so as to be universal and applicable under various unbalanced operating conditions and to allow the tracking of the natural phase currents directly at any time during a transient [52]. The determination of the magnetizing inductance function requires only three measurement points of the open-circuit magnetizing curve of the generator, avoiding the need to take measurements at high current values.

The model is implemented in Matlab/Simulink environment and used to investigate the generator's operating characteristics at different operating conditions, including voltage build-up, steady-state and transient operation when operating under balanced and unbalanced conditions. The results are validated experimentally using a 7.5kW SEIG test rig. The experimental investigation demonstrates a high level of agreement between the measured waveforms and those obtained from the proposed model.

The interest of the magnetizing inductance derivative with respect to the magnetizing current

has been demonstrated clearly in this study. The results obtained by the proposed model which includes the magnetizing inductance derivative with respect to the magnetizing current are compared with those yields from a conventional model.

The following section gives an outline of each chapter of this thesis.

#### 1.4 Published Material

A. Alfarhan, S. M. Gadoue, B. Zahawi, M. Shalaby, and M. A. Elgendy, "Modelling of magnetizing inductance saturation in self-excited induction generators," in *2016 IEEE 16th International Conference on Environment and Electrical Engineering (EEEIC)*, Florence, 2016, pp.

#### 1.5 Structure of the thesis

The work carried out in this thesis is organised in nine main chapters. An outline of each chapter is given as follows:

- **Chapter 1:** This chapter gives an introduction to the thesis. It provides the background to the self-excited induction generator, describes some of the more important points in the research field of the three-phase self-excited induction generator (SEIG), and emphasises the importance of this research. The chapter presents and highlights the objectives of the study and gives an overview of the thesis.
- **Chapter 2:** The phenomena of self-excitation has been described intensively. This chapter provides a review of the literature relevant to the self-excited induction generator, describing the background and development of this type of generator. In addition, the applications of this generator are highlighted, including its advantages and drawbacks and how to overcome the drawbacks. Reference is also made to different approaches to the inclusion of nonlinearity in this type of generator.

- **Chapter 3:** This chapter presents the background of the conventional dynamic model of the three-phase induction machine. Additionally, a step-by-step generalized dynamic model of a three-phase self-excited induction generator in the natural three-phase *abc* reference frame is derived and clearly explained. Furthermore, this chapter demonstrates how to simulate mathematically the resistive load, inductive load, electromagnetic torque, mechanical torque, residual flux and magnetizing current.
- **Chapter 4:** This chapter focuses on how to represent the variation in the magnetizing inductance as a function in magnetizing current by using an exponential function. Different methods for mathematically representing the variation in the magnetizing inductance with respect to magnetizing current are also discussed.
- **Chapter 5:** This chapter describes the experimental rig used and its components. The circuit diagram of the experiment set-up is shown. The identified parameters of the machine under study are analysed and the methods of determining these parameters are explained. The magnetizing characteristics test of the machine under study is presented and explained in this chapter. The experimental results of this test are compared with those obtained by the exponential method are also depicted in this chapter. The method used for measuring and controlling the speed of the shaft experimentally is highlighted and its positive effects are mentioned.
- **Chapter 6:** The aim of this chapter is to test the performance of the proposed mathematical model in different operational conditions. The developed model is implemented in the Matlab/Simulink environment to solve its differential equations. This numerical technic is used to investigate the generator's operating characteristics at different operating conditions including voltage build-up, steady-state and transient operation, and under balanced, unbalanced, load perturbation and fault conditions. The results obtained by the developed model are validated against those obtained in the laboratory.
- **Chapter 7:** The importance of including the derivative of magnetizing inductance with respect to magnetizing current during the dynamic response is demonstrated and explained clearly in this chapter. To appreciate this effect, the proposed model will be

compared with a model which ignores this derivative effect together with experimental results in order to validate the results.

- **Chapter 8:** The effect of leakage saturation is investigated in this chapter. The leakage saturation path has been included in the developed mathematical model. The results obtained by a model which includes both the main path saturation and leakage path saturation along with experimental results are compared with those produced by a model which includes only the main path saturation. Both models are verified against experimental results.
- **Chapter 9:** This chapter presents the conclusions of the research together with a summary. Suggestions for future research are discussed.

# Chapter 2. Review, analysis and modelling of the SEIG

---

## 2.1 Introduction

In the last three decades, there has been immense interest in the various issues related to the use of the SEIG as a potential alternative to the synchronous generator to feed power to remote areas where there is no access to the grid. This chapter, therefore, reviews developments in self-excited induction generator research and development since its first invention. In particular, studies of the dynamic modelling of induction machines that can adequately account for the non-linearity of the machine as a result of saturation effects are highlighted.

In this chapter, an overview of the self-excited induction generator is presented, and the self-excitation phenomenon, steady-state operation, voltage regulation, transient analysis, the main saturation effects, and leakage saturation effects in SEIGs are discussed.

## 2.2 The self-excitation phenomenon

The self-excitation phenomenon in induction machines is considered to be a complex physical phenomenon which has been well-known since the 1930s and has been investigated extensively in the past [60] since being discovered by Basset and Potter [61]. This initial work was followed by further work by C.F Wagner, the purpose of which was to analyse the circumstances under which self-excitation becomes possible, based on the equivalent circuit shown in Figure 2.1. Wagner concluded that the voltage at which a machine can be excited at a specific frequency depends upon its no-load excitation characteristics at that frequency.

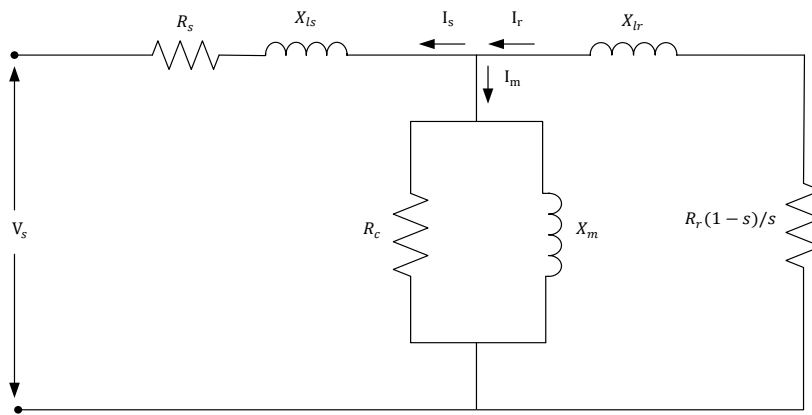


**Figure 2.1** Per-phase equivalent circuit of the induction machine referred to the stator.

Doxy [62] described the principle of the self-excitation phenomena of an induction generator as follows: “After starting, a residual magnetism must be present in the rotor. Hence, an emf will be induced in the stator winding at a frequency proportional to the rotor speed. A leading current flowing in the capacitor which is the same current passing through the stator windings, will produce an armature reaction flux assisting the originally existing one.” Although this phenomenon has been known for a long time, it is still a subject to close attention [11, 60].

The phenomenon of self-excitation can take place if the following conditions are satisfied:

- There is sufficient residual magnetic field in the rotor [11, 63] or if an initial voltage is imposed across the terminals of the excitation capacitors.
- The value of the bank of three shunt capacitors should be sufficient (with a minimum capacitance value) [11, 15, 64]

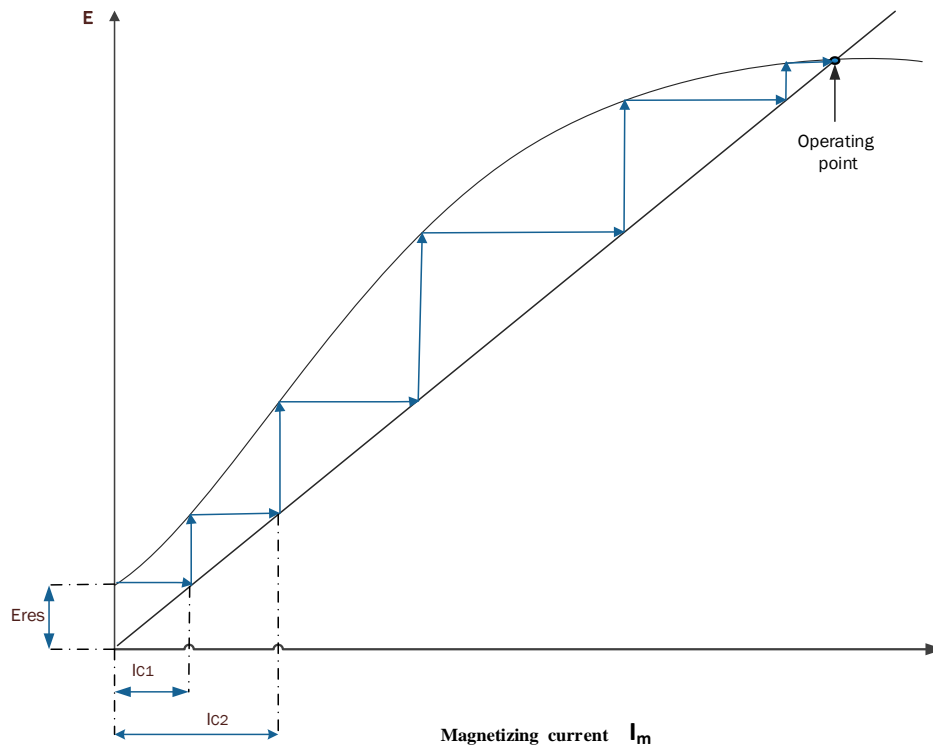


**Figure 2.2** The self-excitation phenomena.

When the induction generator is running at suitable speed while three excitation capacitors are connected to its terminals, and there is a sufficient residual magnetism, an electromotive force  $E_{res}$  will be induced in the winding. The induced stator voltage causes a capacitor current that generates a corresponding flux in the generator. This flux will aid the residual flux because it is in the same direction as shown in the phasor diagrams shown in Figure 2.3. Again because the total flux will now be higher than the residual flux, therefore a voltage  $E_{tot}$  will be generated across the stator terminals which is greater than  $E_{res}$ . Therefore the capacitor current  $I_C$  will follow in the circuit, and then flow through the stator windings and cause a corresponding magnetic field. This in turn causes a higher induced stator voltage leading to a successive increase in current and flux [65].

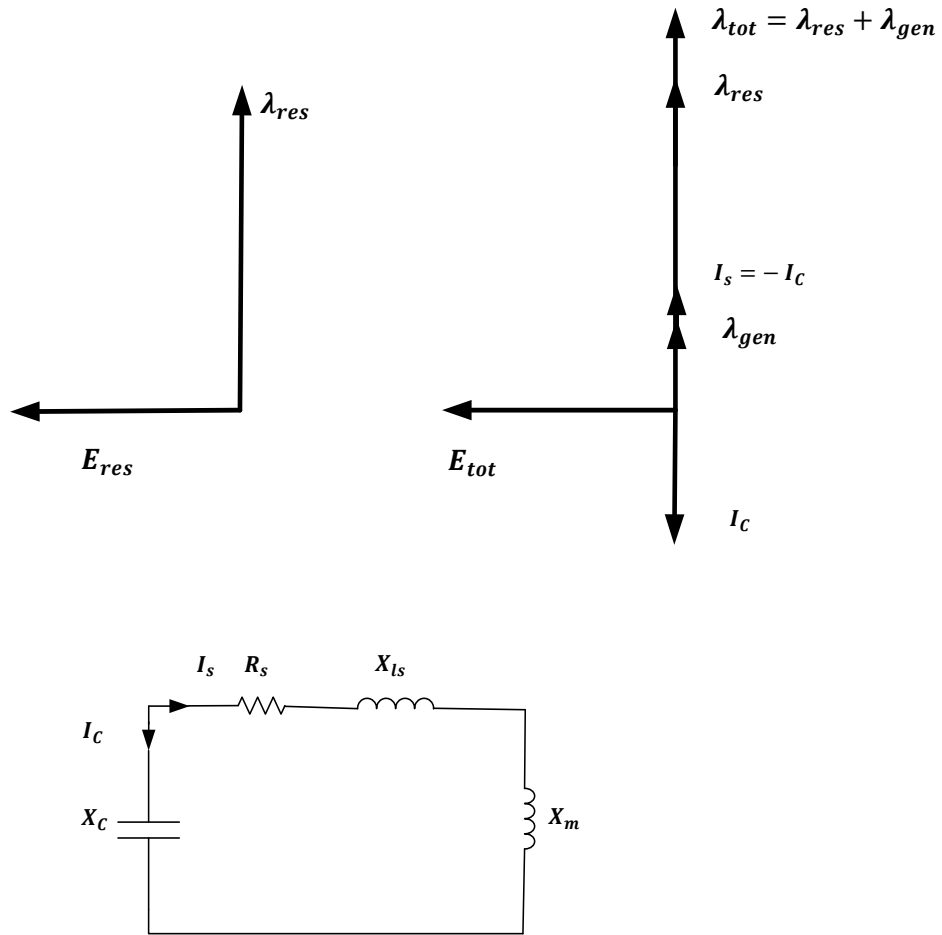


**Figure 2.3** The direction of flux, current and volt of self-excitation phenomena [66].

This process will continue until the capacitor voltage curve intersects the no-load curve of the induction generator. At this point, the generator will reach its steady- state operating point, the current passing through the shunt capacitor must be equal to the magnetizing current ( $I_c = I_m$ ) at no load. The slope of the load line is given by  $\tan^{-1} \left[ \frac{1}{\omega C} \right]$  [63] as illustrated in Figure 2.4.

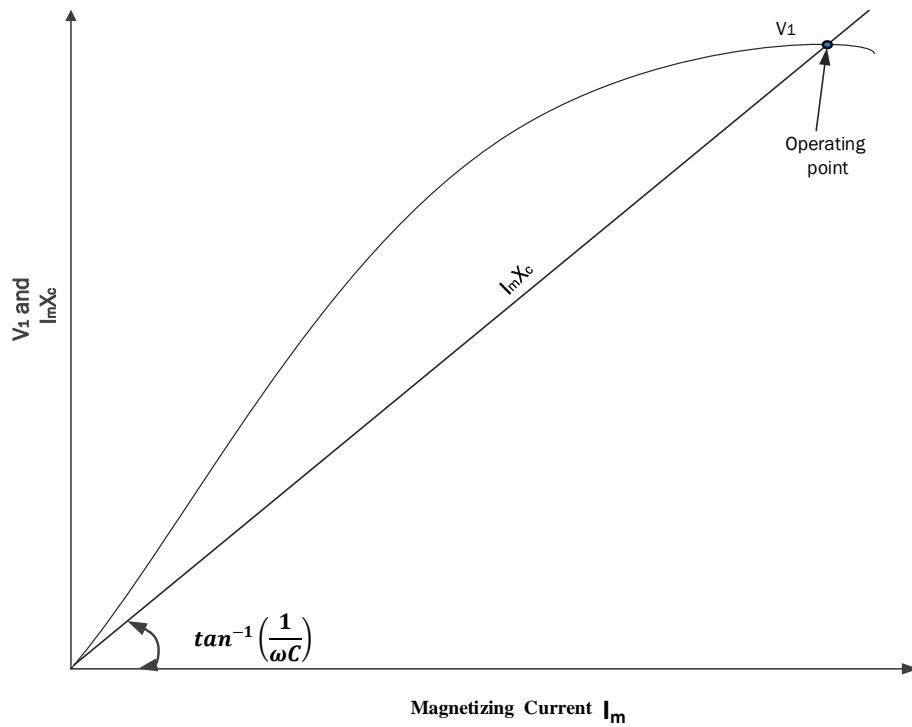


**Figure 2.4** Determination of stable operation of self-excited induction generator.

One of the major problems which may face the self-excited induction generator (SEIG) at starting is guaranteeing that there is a sufficient residual magnetism in the rotor [18]. A reduction in residual flux can occur when there is fault on the terminals of the induction generator or if the generator's speed is allowed to slow down while a small resistive load is connected to its terminals. An insufficiency of the residual magnetism in the induction generator results in failure to initiate self-excitation, and thus, failure to build up the voltage. Several methods can be employed to overcome this problem as follows [18]:

- 1) Applying a DC voltage source to the terminals of the machine before it is run up to speed.
- 2) Increasing the machine speed above the rated speed value of the machine.
- 3) Connecting sufficient terminal capacitance and then running the generator at a suitable speed.

According to the experimental work conducted in this study, the most practical and easiest method is the third method. A long time may be taken for the induction machine to gain

a sufficient residual magnetism if the second method is employed. Care should be taken in applying the second and third methods, and it is imperative to avoid a high voltage which may be generated suddenly when the machine becomes excited.

### 2.3 Steady-state operation of SEIGs

Previous studies focusing on the self-excitation process and the operation of the SEIG can be classified into two major groups. One deals with various aspects of steady-state operation whereas the other is concerned with dynamic models and the transient simulation of self-excited induction generators at different conditions under various no-load and loading conditions [60].

Many of the previous studies on the SEIG have analysed the steady-state conditions [5-8]. For a certain speed and excitation capacitance, the steady-state equivalent circuit is solved for the generated frequency and the magnetizing reactance. The magnetizing reactance is then substituted in the magnetization characteristics to obtain the air-gap induced voltage in the stator which is used to calculate other quantities of interest, such as terminal voltage, load current and power [44-46]. C.F Wagner [67] analysed the circumstances under which the SEIG becomes possible based on the equivalent circuit shown in Figure 2.1. Wagner concluded that the voltage at which the machine can be excited at a specific frequency depends upon its no-load excitation characteristics at that frequency.

Although the phenomena of self-excitation has been well known since the 1930s, the interaction between load, excitation capacitance, speed and various machine parameters remained unclear until the 1980s [23] when some papers were published such as [17] [71]. Murthy et al. [17] developed a very efficient analytical technique using the Newton-Raphson method to determine the steady state performance and to obtain the magnetising reactance and output frequency of a self-excited induction generator for a given capacitance, speed and load. Performance was computed using the steady-state equivalent circuit.

Based on the per-phase steady-state equivalent circuit of the induction machine, several researchers relied on concepts of loop impedance [35, 68] and nodal admittance [59, 69, 70] to analyse the steady-state performance of the induction generator. At given speed, capacitance and load conditions, the performance of the machine can be determined provided that its

parameters are known. In the loop impedance and nodal admittance the principle of the conservation of active and reactive powers was employed and to satisfy the conditions for self-excitation, the sum of the loop must be equal to zero, which implies that both the real and imaginary parts would separately also equal zero. These methods were used effectively to find the minimum value of the terminal capacitance which is sufficient for self-excitation. Another method used to predict the steady state performance of the SEIG is based on a generalized machine theory in which a numerical technic is used to solve the equation of the operational impedance matrix.

Several researchers have described different techniques to determine the suitable value of terminal capacitance of the SEIG [22, 34, 35, 68, 71]. A formula to calculate the minimum excitation capacitance value required to ensure that a SEIG can initiate its build-up process at no load conditions has been given as shown below [35]:

$$C_{min} = \frac{1}{\omega^2 v^2 (L_m + L_{ls})} \quad (2.1)$$

where is  $\omega$  the base angular frequency,  $v$  is the per unit speed and  $L_{ls}$ , and  $L_m$  are the stator leakage and magnetizing inductances respectively. It was found that the value of minimum excitation capacitor is inversely proportional to the unsaturated magnetizing inductance and inversely proportional to the square of per unit speed of the machine. In this study, it was concluded that the SEIG requires a higher capacitance value when it is loaded than when at no load conditions. Eltamaly [69] relied on nodal analysis instead of loop analysis to present a new formula to determine the minimum value of capacitance required for the SEIG. By using an eigenvalue based approach, the minimum and maximum values of capacitance required for the self-excitation of the induction generator was predicted by Wang et al. [72].

Generally, the induction machine must work at a speed above the synchronous speed (negative slip) to work as a generator, whereas to work as a motor the speed should be lower than the synchronous speed (positive slip). The output voltage and generated frequency in SEIG mode are affected by the speed, load, and capacitance value in Farads [73]. J. Bjornsted et al. [74] proposed a method to determine the steady state performance of a loaded SEIG by extending the method of determining the operating point of the steady state at no-load conditions which relies on the intersection between the generator no-load curve and the capacitor characteristics,

as illustrated in Figure 2.4. In addition, the effect of resistance on the remaining flux was experimentally investigated, and the flux was found to initially decrease with increasing applied resistance until the SEIG voltage generated due to the remaining flux was too low to be measured.

## 2.4 Voltage regulation of SEIGs

The main drawback of a SEIG is unsatisfactory voltage and frequency regulation at varying loads, which has been a major barrier to its application [22]. To overcome this problem, several papers have been published discussing different techniques to regulate voltage and frequency [5, 75, 76]. The poor voltage regulation of the SEIG occurs even at regulated speeds [22]. The proposed voltage regulating schemes use switched capacitors, variable inductors, and saturable core reactors, which are considered to be the three most popular schemes [23, 77, 78]. Of these the voltage regulating use of the switched capacitor is a simple and cheap scheme.

To avoid the high installation costs of using a speed governor, uncontrolled turbines are used in off-grid applications [5]. Therefore, to maintain constant generated power, electronic load controllers (ELCs) have been used by several authors [5, 7, 37, 38] to dissipate the excess power in dump resistors. Chilipe et al [37] proposed a new voltage and frequency controller (VFC) for standalone parallel operated self-excited induction generators driven by constant power micro hydro turbines. An electronic load controller (ELC) is used to balance the generated power such that the ELC does not dissipate the excess energy in a dump resistor as designed in previous papers, instead it uses the excess energy to feed useful load such as pump system. Additionally, a STATCOM in this VFC is used to regulate the voltage during load variation such that, it works as a reactive power compensator.

To overcome the problem of the temporary loss of synchronization due to the severe fluctuations created by the random load variation in the SEIG system, Chen et al. [79] developed a new advanced STATCOM which is almost totally immune to frequency fluctuations. In a paper by Chilipe et al [5], the performance of a self-excited induction generator with a voltage and frequency controller (VFC) in a standalone micro-hydro power generating system is presented.

## 2.5 Transient analysis of SEIGs

Although the self-excitation phenomena has positive effects, in some practical circumstances it can be undesirable due to a destructive voltage which can be generated during transient conditions which may cause damage to the machine insulation [80-82] or it may cause winding overheating [81, 83].

The literature indicates that the steady-state operation of the SEIGs has been covered by intensive experimental investigation. However, only a few papers have focused on transient analysis [60]. Most of this research focuses on the grid mode rather than the self-excited mode.

The failure of shunt capacitor banks at the terminals of an induction generator driven by a wind turbine was investigated by Le Tang et al. [84]. They concluded that this failure is likely to be due to the phenomena which happens when a windfarm is disconnected from the utility networks leading to a total loss of load which can result in a high magnitude of voltage.

M.A Ouhrouche et al. [21] studied the transient behaviour of an induction generator by using EMTP software package. It was noted that, when it is sufficiently compensated, the induction generator remains excited after it is disconnected from the power grid. Induction generators in this situation will either accelerate or slow down, depending on the value of the capacitive compensation level used. Theoretically, a new equilibrium point should be reached where the electromagnetic torque is equal to the mechanical torque applied by the prime mover. At this equilibrium state, high overvoltage is generated at the IG terminals.

Wang et al. [16] derived the dynamic equations of a SEIG with unbalanced excitation capacitors using an ABC/abc natural frame model for a three-phase induction machine. It was concluded that, when one of the three balanced excitation capacitors is suddenly switched off, the studied SEIG can maintain self-excitation and generates adequate voltage in the other two phases. In this case, if the neutral line is connected between the excitation capacitor bank and the SEIG, the transient recovery time to return to the steady state value can be effectively minimized. In addition, when two of the three balanced excitation capacitors are suddenly switched off from the machine, the generated voltage of the SEIG collapses and gradually declines to zero.

In order to analyse the transient behaviour of an SEIG, Kishore et al. [85] developed a general dynamic model for a three phase SEIG using d-q variables in a stationary reference frame. The effect of main and cross flux saturation was included to investigate the behaviour of the SEIG in various transient conditions. The consideration of main flux and cross-saturation gave good results. One of the main advantages of this approach is the separation of machine parameters from the self-excitation capacitors and the load parameters, and therefore, the transient analysis can be effectively conducted.

Wang et al. [86] studied the difference between the short-shunt and long-shunt connections of an isolated self-excited induction generator feeding an induction motor load. Their comparison of different shunt capacitor topologies showed that the short shunt connection provide better voltage regulation, whereas the long-shunt connection might cause unwanted oscillation.

The influence of different capacitor excitation configurations (shunt, short-shunt and long-shunt) on the steady state and dynamic performance of a single phase SEIG has been investigated by Ojo [87]. In this study, it was observed that, when the induction generator is overloaded, the voltage collapses while with neither a long shunt or short shunt connection, the generator is able to sustain the load at a lower operating voltage and larger load current.

S.K Jain et al. [88] presented the transient performance of a three-phase SEIG. They developed a generalised dynamic model of a SEIG in a stationary reference frame using d-q variables. The effect of main and cross-saturation was considered in the model. Although this study focuses on the dynamic response of the SEIG, the effects of the derivative of the magnetizing inductance with respect to the magnetizing current is neglected in this study, which may affect the accuracy of the results. The delta configuration was chosen because it does not have a zero-sequence component in the line current and phase voltage. It was observed that the faults result in voltage collapse and de-excitation. The authors recommended that, during shaft design, the excessive high torque during short-circuit and the sustained pulsating torque which results from imbalance disturbance may be taken into account.

Alsalloum et al. [9] derived a general model in direct phase (a-b-c reference) quantities in order to analyse the performance of the SEIG and its load and excitation capacitor under different balanced and unbalanced conditions. The effect of saturation was simulated by a corresponding

change in the value of  $L_m$ . Variations in magnetizing inductance were represented by a linear piecewise method in this study, and on the other hand the effects of the derivative of magnetizing inductance with respect to magnetizing current was neglected. Furthermore, the effects of leakage saturation were not taken into account.

## 2.6 The main saturation effects of SEIGs

In order to maximize torque production for a given machine frame, the induction machine is usually designed to be slightly saturated at the operating point [89]. It has been reported that it is unsatisfactory to assume that the circuit is linear in induction machine modelling and analysis in many transient conditions such as switching on and switching off the transients [12, 73, 90].

The value of voltage reached after the self-excitation process in an SEIG is initiated, due to the magnetic saturation, which balances the excitation capacitance and machine voltage [22].

The nonlinearity of the iron has to be taken into account in the model of an induction machine in order to enhance the accuracy of the simulation, because it is well known that the air gap in the induction machine is generally narrow [50, 51, 91, 92]. The disparity between simulated results achieved using the traditional model and experimental results can be attributed to the main saturation being neglected [93]. Basically, there are two main types of saturation effects that influence the performance of induction machines. The first is main flux saturation (i.e. magnetizing inductance saturation). The second type is leakage flux saturation. The saturation in the magnetic circuit of an induction generator plays a crucial role in the process of voltage build-up and stabilization of the operation at loaded and unloaded conditions [56, 94]. Not only that, but also the linear model is not capable of describing the behaviour of different conditions of the system such as studying the voltage build-up [92, 95]. Saturation considerably affects the stability and dynamic conditions of induction machines [50, 96]. Several methods have been used by researchers to represent the relationship between magnetizing inductance and magnetizing current. Generally, the two most popular methods used to represent the variation between magnetizing inductance and magnetizing current (or the air-gap voltage in some studies, which is the voltage across the magnetizing inductance), are linear piecewise and a polynomial function. A linear piecewise association within the range of the magnetizing current is used to approximate the variation in the magnetizing inductance. Several authors have applied

this method [9, 16, 86]. Wang et al. [16] approximated the nonlinear relationship between  $i_m$  and  $X_m$  using piecewise linear approximation. Four straight lines were used to represent saturated curve and one for an unsaturated curve. In this method, the magnetizing reactance versus air gap voltage (or exciting current) can be represented as a constant for unsaturated, low values of voltage, and this is decreased when it saturates [16, 86]. The magnetizing reactance  $X_m = \omega L_m$  can be expressed as follows:

$$X_m = \begin{cases} a_0 & \text{for } 0 \leq i_m < i_1 \\ \frac{a_1}{(i_m + b_1)} & \text{for } i_1 \leq i_m < i_2 \\ \frac{a_2}{(i_m + b_2)} & \text{for } i_2 \leq i_m < i_3 \\ \frac{a_3}{(i_m + b_3)} & \text{for } i_3 \leq i_m < i_4 \\ \frac{a_4}{(i_m + b_4)} & \text{for } i_4 \leq i_m \end{cases} \quad (2.2)$$

This means that the straight line  $a_0$  represents the unsaturated line. However, the approximation in this method does not reflect the actual variation in magnetizing inductance. Therefore, it does not predict the behaviour of actual phenomena during the initiation of self-excitation [56, 94] where all of the constants can be obtained experimentally. Another method used to represent the nonlinear relationship between air-gap voltage (Vg) and magnetizing current ( $i_m$ ) is a polynomial function to express the magnetising inductance with respect to magnetising current  $i_m$  as shown:

$$L_m = a_5 i_m^5 + a_4 i_m^4 + a_3 i_m^3 + a_2 i_m^2 + a_1 i_m + a_0 \quad (2.3)$$

This polynomial function is of degree 5, but a polynomial function of different degrees can be used. The degree of the polynomial obviously influences accuracy, such that a higher polynomial degree gives higher accuracy [50]. The coefficient in the equation above ( $a_0, a_1, a_2 \dots etc$ ) can be obtained experimentally. For better results in representing the variation in magnetizing inductance, a polynomial function is used by many authors [9, 44, 50,

56]. For example, in K. Idjdarene et al. [50] used a polynomial function of the 12th degree with respect to the magnetizing current in order to model the nonlinearity caused by the saturation effect. The effect of the variation in magnetizing inductance with voltage on self-excitation has also been presented by Seyoum et al. [56]. This effect is taken into account in order to predict accurately whether or not self-excitation will occur in the SEIG for various speed and capacitance values at both no load and loaded cases. It was concluded that the relationship between magnetizing inductance,  $L_m$ , and the induced stator voltage determines the regions of stable operation in addition to the minimum generated voltage without loss of self-excitation. In addition, it was concluded that the speed required to initiate self-excitation is always more than the speed at which self-excitation ceases. Additionally, Coussens et al [97] modelled nonlinearity in the magnetizing inductance by using the hyperbolic tangent function.

The no-load test is the traditional method for identifying the magnetizing inductance of induction machine; however, some alternative methods have been proposed to avoid the very lengthy measurements required in this test [94, 98, 99]. Luká's et. al. [94] proposed an alternative method which avoids complex and lengthy measurement to obtain the measured no-load curve. The results show a good correspondence between measurements and the new method; however, this model was not tested in practice. To overcome the complexity in the conventional method of determine magnetizing inductance, novel method was presented by A. Stnkovic et. al. [98] using a static DC excitation technique. The disadvantage of this method is that it can be employed only if the neutral of the induction machine is accessible. In addition, leakage inductance cannot be measured using this method.

However, most previous studies [16, 49, 56, 100] neglect the effects of the derivative of magnetizing inductance with respect to magnetizing current even if the main aim of these studies is to predict the dynamic performance of SEIG, which may lead to significant errors in predicting the behaviour of the SEIG during the dynamic state. There are only a few studies which consider the effects of saturation taking the derivative of magnetizing inductance with respect to magnetising current into account when the dynamic response of self-excited induction generator is investigated [50, 51, 101]. Furthermore, the proposed models in these papers were developed in the d-q reference frame and therefore would not be appropriate for unbalanced conditions [49, 52-54]. Additionally, these models include neither the mutual

saturation between stator windings nor mutual saturation between rotor windings; moreover, the leakage path saturation is not included.

A recent study which does include the dynamic inductance effects is by K. Idjdarene et al. [50]. In this study, a diphas model to allow main path saturation effects to be taken into account has been developed, while the leakage saturation is still neglected in the model. In order to approximate the nonlinearity caused by saturation effects, the authors used a polynomial function of the 12th degree, which is a function in the magnetizing current. The effects of the derivative of magnetizing inductance with respect to the magnetizing current is taken into account in this approach; however, the effects of mutual saturation between stator windings and that between rotor windings are neglected. Additionally, the effect of leakage saturation is neglected. The residual magnetism is represented in the simulation, which was implemented in a Matlab / Simulink environment, by a small voltage source and so the relationship between residual magnetism and rotor frequency is also neglected in this approach. In this study, it was observed that, within a specific load range, there is no significant change in the phase voltage magnitudes and frequencies, and therefore it can be concluded that it is possible to use the SEIG as an efficient and cheap system to feed an isolated load even if the load is unbalanced, irrespective of whether static converters are used.

Hallenius et al. [101] developed a d-q model to study the transient performance of induction machines which included the effects of main path saturation by utilizing the magnetizing inductance and its derivative with respect to magnetizing current. The computed results in this study give good agreement with experimental results. This study was followed by another by E. Levi [51] to investigate the effects of cross saturation on the accuracy of the orthogonal axis model of induction machines taking dynamic inductance into consideration. However, neither of these studies consider leakage saturation and mutual saturation and the models are not appropriate for the study of unbalanced conditions.

## 2.7 The leakage saturation effect of SEIGs

The assumption of considering the stator leakage and rotor leakage inductances to be constant values becomes inadequate if the stator phase current of the SEIG is high; hence, in order to obtain a realistic modelling for the SEIG, the leakage saturation should be considered [102]. If

a very high level of accuracy is required, where the stator current and rotor currents are expected to have very high values, taking leakage inductance saturation into account becomes imperative [49]. Lipo et al. [102] presented a method for modelling the stator and rotor leakage reactance saturation. In this approach, the total stator and rotor leakage inductances are separated into iron-dependent and air-dependent portions, such that the iron-portion is considered a saturable quantity (nonlinear inductance), whereas the air-dependent part is considered unsaturable (constant inductance). The representation of leakage inductance in this approach relies on the saturation factor.

A new approach to the analysis of induction machines in a d-q frame has been presented by Keyhani et al. [96] which assumes that the leakage inductances are nonlinear. The degree of saturated leakage inductance in this approach is represented by a nonlinear function. This approach was implemented and simulated with the help of IGSPICE. In this paper, the stator current and rotor speed of a machine during free acceleration, were measured experimentally and the results were then compared with those from their proposed method. Okoro [49] has studied the effects of leakage saturation, and the variation in leakage inductance in this study was represented using a polynomial function of degree third which is a function of magnetizing current. It was concluded that including the saturation improved the results and for the accurate prediction of induction machines in dynamic states, the effect of saturation must be taken into account. However, in these papers [49, 96, 102] the inclusion of the derivative leakage inductances with respect to magnetizing current was not taken into consideration.

## 2.8 Conclusion

An overview of studies of the SEIG has been presented in this chapter. Most of the previous literature has investigated the performance of SEIGs at steady state conditions focusing on improving voltage and frequency regulation. However, studies interested in representing the saturation effects in dynamic conditions are scarce. The simplicity and low cost of maintenance and operation mean that the self-excited induction generator could be preferable to the synchronous generator in remote isolated areas.

From this chapter, it can be concluded that a general model for the SEIG that accounts for saturation effects, has not yet been proposed, so that it can be applicable for different conditions

and in particular, for unbalanced conditions with the ability to include mutual and leakage saturation. Also, it should cope with changes in speed. In addition, the importance of the derivative of magnetizing inductance with respect to magnetizing current has not yet been highlighted and thus some recent studies still ignore the effects of this derivative even while trying to predict the dynamic response of the SEIG.

# Chapter 3. Mathematical model of the saturation of the SEIG

---

## 3.1 Introduction

Predicting the performance of the SEIG is important in order to investigate its behaviour in different conditions, such as transient states, since this type of generator is beginning to be used as a highly reliable generator in critical areas like fire-fighting [18] and electrical vehicles [32]. In such applications, accuracy is important for reliable and safe operation. It has been reported that an appropriate dynamic saturated machine model is required for the successful simulation of any of the transients associated with an SEIG's operation [60]. While d-q reference frames have a very wide area of application, they are not appropriate in studying the unbalanced operation of the motor [49, 52]. Hence, the aim of this chapter is to derive a generalized dynamic mathematical model of a three-phase self-excited induction generator in an ABC/abc natural frame taking into account the nonlinearity effect in the induction machine due to saturation phenomena. This model could then be suitable for steady state, dynamic response and balanced and unbalanced conditions. For more realistic representation, saturation effects in the mutual inductances between stator windings and between rotor windings are both taken into account in this proposed model, whereas the effects of leakage saturation is neglected. This dynamic model is derived based on the basic voltage equations for an induction machine in the natural three-phase ABC/abc reference frame. In order to accurately predict the performance of this type of generator, the model is implemented in the MATLAB/ SIMULINK.

In order to simulate the load and excitation capacitors in this numerical package, a mathematical model for a pure resistive load, resistive and inductive load, and magnetizing current, is derived in this chapter.

### 3.2 Conventional dynamic model of induction machine

A three-phase, star-connected cage induction generator is considered in this study. The output terminals of the generator are connected to a three-phase capacitor bank for excitation and a three phase load, as shown in Figure 3.1. According to Krause [53], the three phase stator voltage equations can be written in the following matrix form:

$$[v_s]_{abc} = [R][i_s]_{abc} + p[\lambda_s]_{abc} \quad (3.1)$$

Whereas, the three equations for the three phase rotor voltages can be expressed as follows:

$$[v_r]_{abc} = [R][i_r]_{abc} + p[\lambda_r]_{abc} \quad (3.2)$$

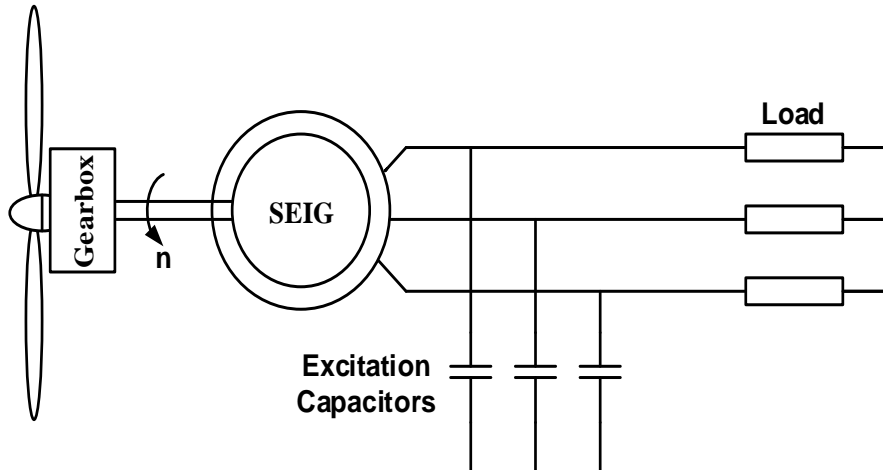


**Figure 3.1** Schematic diagram of self-excited induction generator driven by a wind turbine feeding a three-phase load

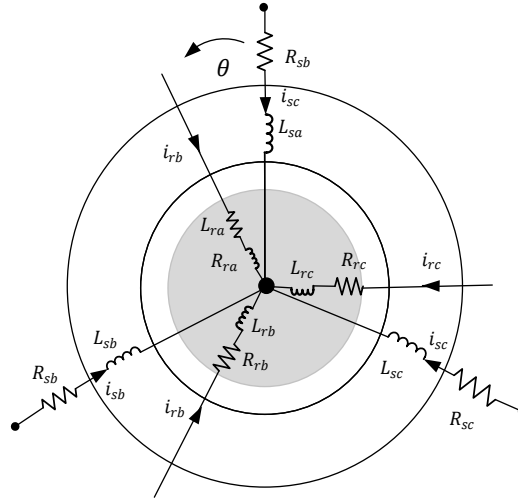


**Figure 3.2** Machine diagram in natural reference frame[53].

The three phase stator flux linkage equations can be written in the following matrix form:

$$[\lambda_s]_{abc} = [L_s][i_s]_{abc} + [L_{sr}][i_r]_{abc} \quad (3.3)$$

And the three phase rotor flux linkage equations can be written in the following matrix form:

$$[\lambda_r]_{abc} = [L_{sr}]^T [i_s]_{abc} + [L_r][i_r]_{abc} \quad (3.4)$$

Therefore, the derivative of the three phase stator and rotor flux linkage equations can be written in the following matrix form:

$$p[\lambda_s]_{abc} = p[L_s] \cdot [i_s]_{abc} + [L_s]p[i_s]_{abc} + p[L_{sr}] \cdot [i_r]_{abc} + [L_{sr}]p[i_r]_{abc} \quad (3.5)$$

$$p[\lambda_r]_{abc} = p[L_{sr}]^T [i_s]_{abc} + [L_{sr}]^T p[i_s]_{abc} + p[L_r][i_r]_{abc} + [L_r]p[i_r]_{abc} \quad (3.6)$$

For a magnetically linear system (where the saturation effect is neglected such that  $L_m$  is considered constant and therefore  $p[L_s]$  and  $p[L_r] = 0$ , whereas,  $L_{sr}$  considered as a function in the displacement) the flux linkages for the induction machine in equations 3.5 and 3.6 may be rewritten as follows:

$$p[\lambda_s]_{abc} = [L_s]p[i_s]_{abc} + [L_{sr}]p[i_r]_{abc} + \frac{\partial[L_{sr}]}{\partial\theta} \frac{\partial\theta}{\partial t} [i_s]_{abc} \quad (3.7)$$

$$p[\lambda_r]_{abc} = [L_{sr}]^T p[i_s]_{abc} + [L_r]p[i_r]_{abc} + \frac{\partial[L_{sr}]}{\partial\theta} \frac{\partial\theta}{\partial t} [i_r]_{abc} \quad (3.8)$$

where  $[R_s]$ ,  $[R_r]$ ,  $[L_s]$ ,  $[L_r]$ ,  $[L_{sr}]$  and  $[L_{sr}]^T$  are a matrix which can be expressed as follows:

$$[R_s] = \begin{bmatrix} r_{as} & 0 & 0 \\ 0 & r_{bs} & 0 \\ 0 & 0 & r_{cs} \end{bmatrix} \quad (3.9)$$

$$[R_r] = \begin{bmatrix} r_{ar} & 0 & 0 \\ 0 & r_{br} & 0 \\ 0 & 0 & r_{cr} \end{bmatrix} \quad (3.10)$$

$$[i_s] = \begin{bmatrix} i_{as} \\ i_{bs} \\ i_{cs} \end{bmatrix}, \quad [i_r] = \begin{bmatrix} i_{ar} \\ i_{br} \\ i_{cr} \end{bmatrix} \quad (3.11)$$

$$[L_{sr}] = L_{sr} \begin{bmatrix} a_1 & a_2 & a_3 \\ a_3 & a_1 & a_2 \\ a_2 & a_3 & a_1 \end{bmatrix} \quad (3.12)$$

$$[L_{sr}]^T = L_{sr} \begin{bmatrix} a_1 & a_3 & a_2 \\ a_2 & a_1 & a_3 \\ a_3 & a_2 & a_1 \end{bmatrix} \quad (3.13)$$

where,

$$a_1 = \cos(\theta)$$

$$a_2 = \cos\left(\theta + \frac{2\pi}{3}\right)$$

$$a_3 = \cos\left(\theta - \frac{2\pi}{3}\right)$$

$$b_1 = \sin(\theta)$$

$$b_2 = \sin\left(\theta + \frac{2\pi}{3}\right)$$

$$b_3 = \sin\left(\theta - \frac{2\pi}{3}\right)$$

$$\theta = \omega_r t$$

$$\frac{d\theta}{dt} = \omega_r$$

$$[L] = \begin{bmatrix} L_s & L_{sr} \\ L_{sr}^T & L_r \end{bmatrix}$$

and therefore:

$$[L_s] = \begin{bmatrix} L_s & -0.5L_m & -0.5L_m \\ -0.5L_m & L_s & -0.5L_m \\ -0.5L_m & -0.5L_m & L_s \end{bmatrix} \quad (3.14)$$

$$[L_r] = \begin{bmatrix} L_r & -0.5L_m & -0.5L_m \\ -0.5L_m & L_r & -0.5L_m \\ -0.5L_m & -0.5L_m & L_r \end{bmatrix} \quad (3.15)$$

By substituting equation 3.7 in equation 3.1 and equation 3.8 in equation 3.2, then equations 3.1 and 3.2 can be rewritten as follows:

$$[v_s]_{abc} = [R][i_s]_{abc} + [L_s]p[i_s]_{abc} + [L_{sr}]p[i_r]_{abc} + \frac{\partial[L_{sr}]}{\partial\theta} \frac{\partial\theta}{\partial t} [i_s]_{abc} \quad (3.16)$$

$$[v_r]_{abc} = [R][i_r]_{abc} + [L_{sr}]^T p[i_s]_{abc} + [L_r]p[i_r]_{abc} + \frac{\partial[L_{sr}]}{\partial\theta} \frac{\partial\theta}{\partial t} [i_r]_{abc} \quad (3.17)$$

Equations 3.16 and 3.17 can be combined and rewritten in a general form as follows:

$$[v] = [R][i] + [L] \frac{d[i]}{dt} + \frac{\partial[L]}{\partial\theta} \frac{\partial\theta}{\partial t} [i] \quad (3.18)$$

since

$$\frac{\partial\theta}{\partial t} = \omega_r$$

then,

$$[v] = [R][i] + [L] \frac{d[i]}{dt} + \omega_r \frac{\partial[L]}{\partial\theta} [i] \quad (3.19)$$

where

$$[R] = \begin{bmatrix} r_{as} & 0 & 0 & 0 & 0 & 0 \\ 0 & r_{bs} & 0 & 0 & 0 & 0 \\ 0 & 0 & r_{cs} & 0 & 0 & 0 \\ 0 & 0 & 0 & r_{ar} & 0 & 0 \\ 0 & 0 & 0 & 0 & r_{br} & 0 \\ 0 & 0 & 0 & 0 & 0 & r_{cr} \end{bmatrix} \quad (3.20)$$

$$[v] = [v_{as} \quad v_{bs} \quad v_{cs} \quad v_{ar} \quad v_{br} \quad v_{cr}]^T \quad (3.21)$$

$$[i] = [i_{as} \quad i_{bs} \quad i_{cs} \quad i_{ar} \quad i_{br} \quad i_{cr}]^T \quad (3.22)$$

$$[\lambda] = [\lambda_{as} \quad \lambda_{bs} \quad \lambda_{cs} \quad \lambda_{ar} \quad \lambda_{br} \quad \lambda_{cr}]^T \quad (3.23)$$

$$[L] = \begin{bmatrix} L_{As} & M_s & M_s & M_{sr} a_1 & M_{sr} a_2 & M_{sr} a_3 \\ M_s & L_{Bs} & M_s & M_{sr} a_3 & M_{sr} a_1 & M_{sr} a_2 \\ M_s & M_s & L_{Cs} & M_{sr} a_2 & M_{sr} a_3 & M_{sr} a_1 \\ M_{sr} a_1 & M_{sr} a_3 & M_{sr} a_2 & L_{ar} & M_r & M_r \\ M_{sr} a_2 & M_{sr} a_1 & M_{sr} a_3 & M_r & L_{br} & M_r \\ M_{sr} a_3 & M_{sr} a_2 & M_{sr} a_1 & M_r & M_r & L_{cr} \end{bmatrix} \quad (3.24)$$

Equation 3.19 can be rewritten in extended matrix form as shown below:

$$\begin{bmatrix} v_{as} \\ v_{bs} \\ v_{cs} \\ v_{ar} \\ v_{br} \\ v_{cr} \end{bmatrix} = \begin{bmatrix} r_{as} & 0 & 0 & 0 & 0 & 0 \\ 0 & r_{bs} & 0 & 0 & 0 & 0 \\ 0 & 0 & r_{cs} & 0 & 0 & 0 \\ 0 & 0 & 0 & r_{ar} & 0 & 0 \\ 0 & 0 & 0 & 0 & r_{br} & 0 \\ 0 & 0 & 0 & 0 & 0 & r_{cr} \end{bmatrix} \begin{bmatrix} i_{as} \\ i_{bs} \\ i_{cs} \\ i_{ar} \\ i_{br} \\ i_{cr} \end{bmatrix} +$$

$$\begin{bmatrix} L_{As} & M_s & M_s & M_{sr} a_1 & M_{sr} a_2 & M_{sr} a_3 \\ M_s & L_{Bs} & M_s & M_{sr} a_3 & M_{sr} a_1 & M_{sr} a_2 \\ M_s & M_s & L_{Cs} & M_{sr} a_2 & M_{sr} a_3 & M_{sr} a_1 \\ M_{sr} a_1 & M_{sr} a_3 & M_{sr} a_2 & L_{ar} & M_r & M_r \\ M_{sr} a_2 & M_{sr} a_1 & M_{sr} a_3 & M_r & L_{br} & M_r \\ M_{sr} a_3 & M_{sr} a_2 & M_{sr} a_1 & M_r & M_r & L_{cr} \end{bmatrix} \begin{bmatrix} \frac{di_{as}}{dt} \\ \frac{di_{bs}}{dt} \\ \frac{di_{cs}}{dt} \\ \frac{di_{ar}}{dt} \\ \frac{di_{br}}{dt} \\ \frac{di_{cr}}{dt} \end{bmatrix} +$$

$$\omega_r \begin{bmatrix} 0 & 0 & 0 & M_{sr} b_1 & M_{sr} b_2 & M_{sr} b_3 \\ 0 & 0 & 0 & M_{sr} b_3 & M_{sr} b_1 & M_{sr} b_2 \\ 0 & 0 & 0 & M_{sr} b_2 & M_{sr} b_3 & M_{sr} b_1 \\ M_{sr} b_1 & M_{sr} b_3 & M_{sr} b_2 & 0 & 0 & 0 \\ M_{sr} b_2 & M_{sr} b_1 & M_{sr} b_3 & 0 & 0 & 0 \\ M_{sr} b_3 & M_{sr} b_2 & M_{sr} b_1 & 0 & 0 & 0 \end{bmatrix} \begin{bmatrix} i_{as} \\ i_{bs} \\ i_{cs} \\ i_{ar} \\ i_{br} \\ i_{cr} \end{bmatrix}$$

(3.25)

In the above equations the variables and parameters associated with the stator circuit are denoted with the 's' subscript, whereas those associated with the rotor circuit are denoted with the 'r' subscript, and the 'sr' subscript denotes the mutual inductance between stator and rotor circuits. The subscripts a, b, c denote variables and parameters associated with phase a, phase b, and phase c respectively in the stator and rotor circuits,

where,

$v_s$  and  $v_r$  are the stator and rotor phase voltages,

$i_{sa}$ ,  $i_{sb}$ , and  $i_{sc}$  are the stator abc phase currents,

$i_{ra}$ ,  $i_{rb}$ , and  $i_{rc}$  are the rotor abc phase currents,

$R_s$ , and  $R_r$  are the stator and rotor winding resistances,

$L_m$  is the magnetizing inductance,

$L_{ls}$ , and  $L_{lr}$  are the stator and rotor leakage inductances,

$L_{sr}$  is the stator-rotor mutual inductance,

$\omega$  is the angular frequency in rad/sec,

$\theta$  is the rotor position in rad,

$p$  is the differentiation operator ( $d/dt$ ), and

$\lambda$  is the linkage flux in weber.

$$L_s = L_{ls} + L_{ms}$$

$$L_r = L_{lr} + L_{mr}$$

$$M = -0.5L_m$$

$$M_s = M_r = -0.5L_m$$

and  $M_{sr} = L_{sr} = L_m$

By substituting these values in the previous matrix, we can obtain the dynamic equations of the conventional induction machine; however, these equations do not take the nonlinearity into account and can be written as follows:

$$\begin{bmatrix} v_{as} \\ v_{bs} \\ v_{cs} \\ v_{ar} \\ v_{br} \\ v_{cr} \end{bmatrix} = \begin{bmatrix} r_{as} & 0 & 0 & 0 & 0 & 0 \\ 0 & r_{bs} & 0 & 0 & 0 & 0 \\ 0 & 0 & r_{cs} & 0 & 0 & 0 \\ 0 & 0 & 0 & r_{ar} & 0 & 0 \\ 0 & 0 & 0 & 0 & r_{br} & 0 \\ 0 & 0 & 0 & 0 & 0 & r_{cr} \end{bmatrix} \begin{bmatrix} i_{as} \\ i_{bs} \\ i_{cs} \\ i_{ar} \\ i_{br} \\ i_{cr} \end{bmatrix} +$$

$$\begin{bmatrix} L_s & -0.5L_m & -0.5L_m & L_{sr} a_1 & L_{sr} a_2 & L_{sr} a_3 \\ -0.5L_m & L_s & -0.5L_m & L_{sr} a_3 & L_{sr} a_1 & L_{sr} a_2 \\ -0.5L_m & -0.5L_m & L_s & L_{sr} a_2 & L_{sr} a_3 & L_{sr} a_1 \\ L_{sr} a_1 & L_{sr} a_3 & L_{sr} a_2 & L_r & -0.5L_m & -0.5L_m \\ L_{sr} a_2 & L_{sr} a_1 & L_{sr} a_3 & -0.5L_m & L_r & -0.5L_m \\ L_{sr} a_3 & L_{sr} a_2 & L_{sr} a_1 & -0.5L_m & -0.5L_m & L_r \end{bmatrix} \begin{bmatrix} \frac{di_{as}}{dt} \\ \frac{di_{bs}}{dt} \\ \frac{di_{cs}}{dt} \\ \frac{di_{ar}}{dt} \\ \frac{di_{br}}{dt} \\ \frac{di_{cr}}{dt} \end{bmatrix} +$$

$$\omega_r \begin{bmatrix} 0 & 0 & 0 & L_{sr} b_1 & L_{sr} b_2 & L_{sr} b_3 \\ 0 & 0 & 0 & L_{sr} b_3 & L_{sr} b_1 & L_{sr} b_2 \\ 0 & 0 & 0 & L_{sr} b_2 & L_{sr} b_3 & L_{sr} b_1 \\ L_{sr} b_1 & L_{sr} b_3 & L_{sr} b_2 & 0 & 0 & 0 \\ L_{sr} b_2 & L_{sr} b_1 & L_{sr} b_3 & 0 & 0 & 0 \\ L_{sr} b_3 & L_{sr} b_2 & L_{sr} b_1 & 0 & 0 & 0 \end{bmatrix} \begin{bmatrix} i_{as} \\ i_{bs} \\ i_{cs} \\ i_{ar} \\ i_{br} \\ i_{cr} \end{bmatrix} \quad (3.26)$$

### 3.3 Proposed dynamic model of the SEIG

In the previous section, the inductance matrix is considered as a function of rotor position ( $\theta$ ) only in the case of  $L_{sr}$ , whereas  $L_s$  and  $L_r$  are considered as constants. The aim of this section

is to derive a novel general model in the natural  $ABC/abc$  frame taking into account the saturation effect by assuming that the magnetizing inductance is variable, and including dynamic inductance effects. This approach has the benefits of keeping the original arrangement with no need to transform the stator and rotor voltage and current quantities, in addition to the possibility of modelling unbalanced conditions and nonlinearities which may arise from the use of electronic switches even under complex unbalanced conditions [52]. The voltage equation can therefore be re-written as follows:

$$[v] = [R][i] + [L] \frac{d[i]}{dt} + [i] \frac{\partial[L]}{\partial t} \quad (3.27)$$

and since  $L$  is a function in  $(\theta, i_m)$ , then:

$$\frac{\partial[L]}{\partial t} = \frac{\partial[L]}{\partial \theta} \frac{\partial \theta}{\partial t} + \frac{\partial[L]}{\partial i_m} \frac{\partial i_m}{\partial t} = \omega_r \frac{\partial[L]}{\partial \theta} + \frac{\partial[L]}{\partial i_m} \frac{\partial i_m}{\partial t} \quad (3.28)$$

$$[v] = [R][i] + [\omega_r \frac{\partial[L]}{\partial \theta}] [i] + [\frac{\partial[L]}{\partial i_m} \frac{\partial i_m}{\partial t}] [i] + [L] \frac{d[i]}{dt} \quad (3.29)$$

Based on equation 3.27 the voltage equation for stator phase-a can be derived again taking into consideration  $L$  as a function in  $(\theta, i_m)$ . Hence, the voltage for phase a in the stator circuit can be derived as follows:

$$\begin{aligned} v_{as} = & r_{as} i_{as} + p(L_s i_{as}) + p(M_s i_{bs}) + p(M_s i_{cs}) + p(M_{sr} a_1 i_{ar}) \\ & + p(M_{sr} a_2 i_{br}) + p(M_{sr} a_3 i_{cr}) \end{aligned} \quad (3.30)$$

$$\begin{aligned}
v_{as} = & r_{as} i_{as} + L_s p i_{as} + i_{as} p L_s + M_s p i_{bs} + i_{bs} p M_s + M_s p i_{cs} \\
& + i_{cs} p M_s + M_{sr} a_1 p i_{ar} + i_{ar} p M_{sr} a_1 + i_{ar} M_{sr} p a_1 + \\
& M_{sr} a_2 p i_{br} + i_{br} p M_{sr} a_2 + i_{br} M_{sr} p a_2 + M_{sr} a_3 p i_{cr} + \\
& i_{cr} p M_{sr} a_3 + i_{cr} M_{sr} p a_3
\end{aligned} \tag{3.31}$$

$$\begin{aligned}
v_{as} = & r_{as} i_{as} + L_s \frac{d}{dt} i_{as} + i_{as} \frac{d}{dt} L_s + M_s \frac{d}{dt} i_{bs} + i_{bs} \frac{d}{dt} M_s + M_s \frac{d}{dt} i_{cs} \\
& + i_{cs} \frac{d}{dt} M_s + M_{sr} a_1 \frac{d}{dt} i_{ar} + i_{ar} \frac{d}{dt} M_{sr} a_1 + i_{ar} M_{sr} \frac{d}{dt} a_1 \\
& + M_{sr} a_2 \frac{d}{dt} i_{br} + i_{br} \frac{d}{dt} M_{sr} a_2 + i_{br} M_{sr} \frac{d}{dt} a_2 + M_{sr} a_3 \frac{d}{dt} i_{cr} \\
& + i_{cr} \frac{d}{dt} M_{sr} a_3 + i_{cr} M_{sr} \frac{d}{dt} a_3
\end{aligned} \tag{3.32}$$

Substituting the values of  $a_1$ ,  $a_2$  and  $a_3$  and taking into account that  $\frac{d}{dt} L_s$ ,  $\frac{d}{dt} M_s$ , and  $\frac{d}{dt} M_{sr}$  are not equal to zero yields:

$$\begin{aligned}
v_{as} = & r_{as} i_{as} + L_s \frac{d}{dt} i_{as} + i_{as} \frac{d}{dt} L_s + M_s \frac{d}{dt} i_{bs} + i_{bs} \frac{d}{dt} M_s + M_s \frac{d}{dt} i_{cs} + i_{cs} \frac{d}{dt} M_s + \\
& M_{sr} \cos(\theta) \frac{d}{dt} i_{ar} + i_{ar} \frac{d}{dt} M_{sr} \cos(\theta) + i_{ar} M_{sr} \frac{d}{dt} \cos(\theta) + M_{sr} \cos\left(\theta + \frac{2\pi}{3}\right) \frac{d}{dt} i_{br} \\
& + i_{br} \frac{d}{dt} M_{sr} \cos\left(\theta + \frac{2\pi}{3}\right) + i_{br} M_{sr} \frac{d}{dt} \cos\left(\theta + \frac{2\pi}{3}\right) + M_{sr} \cos\left(\theta - \frac{2\pi}{3}\right) \frac{d}{dt} i_{cr} \\
& + i_{cr} \frac{d}{dt} M_{sr} \cos\left(\theta - \frac{2\pi}{3}\right) + i_{cr} M_{sr} \frac{d}{dt} \cos\left(\theta - \frac{2\pi}{3}\right) \quad (3.33)
\end{aligned}$$

or

$$\begin{aligned}
v_{as} = & r_{as} i_{as} + L_s \frac{d}{dt} i_{as} + i_{as} \frac{d}{dt} L_s + M_s \frac{d}{dt} i_{bs} + i_{bs} \frac{d}{dt} M_s + M_s \frac{d}{dt} i_{cs} + i_{cs} \frac{d}{dt} M_s + \\
& M_{sr} \cos(\theta) \frac{d}{dt} i_{ar} + i_{ar} \frac{d}{dt} M_{sr} \cos(\theta) - i_{ar} M_{sr} \sin(\theta) \omega_r + M_{sr} \cos\left(\theta + \frac{2\pi}{3}\right) \frac{d}{dt} i_{br} \\
& + i_{br} \frac{d}{dt} M_{sr} \cos\left(\theta + \frac{2\pi}{3}\right) - i_{br} M_{sr} \sin\left(\theta + \frac{2\pi}{3}\right) \omega_r + M_{sr} \cos\left(\theta - \frac{2\pi}{3}\right) \frac{d}{dt} i_{cr} + \\
& i_{cr} \frac{d}{dt} M_{sr} \cos\left(\theta - \frac{2\pi}{3}\right) - i_{cr} M_{sr} \sin\left(\theta - \frac{2\pi}{3}\right) \omega_r \quad (3.34)
\end{aligned}$$

Since we know that

$$\frac{dL_m}{dt} = \frac{dL_m}{di_m} \frac{di_m}{dt} \quad (3.35)$$

or

$$\frac{dL_m}{dt} = L'_m \frac{di_m}{dt} \quad (3.36)$$

then:

$$\begin{aligned} v_{as} = & r_{as}i_{as} + L_s \frac{d}{dt} i_{as} + i_{as} L'_{as} \frac{di_m}{dt} - 0.5L_{mb} \frac{d}{dt} i_{bs} - i_{bs} 0.5L'_m \frac{di_m}{dt} - 0.5L_{mb} \frac{d}{dt} i_{cs} \\ & - i_{cs} 0.5L'_m \frac{di_m}{dt} + L_{sr} \cos(\theta) \frac{d}{dt} i_{ar} + i_{ar} L'_{sr} \frac{di_m}{dt} \cos(\theta) - i_{ar} L_{sr} \sin(\theta) \omega_r \\ & + L_{sr} \cos\left(\theta + \frac{2\pi}{3}\right) \frac{d}{dt} i_{br} + i_{br} L'_{sr} \frac{di_m}{dt} \cos\left(\theta + \frac{2\pi}{3}\right) - i_{br} L_{sr} \sin\left(\theta + \frac{2\pi}{3}\right) \omega_r \\ & + L_{sr} \cos\left(\theta - \frac{2\pi}{3}\right) \frac{d}{dt} i_{cr} + i_{cr} L'_{sr} \frac{di_m}{dt} \cos\left(\theta - \frac{2\pi}{3}\right) - i_{cr} L_{sr} \sin\left(\theta - \frac{2\pi}{3}\right) \omega_r \end{aligned} \quad (3.37)$$

By using the same method for voltage in phase b in the stator circuit, the following equation can be obtained:

$$\begin{aligned}
v_{bs} = & r_{bs}i_{bs} + L_{sb}\frac{d}{dt}i_{bs} - \frac{1}{2}L_{ma}\frac{d}{dt}i_{as} - i_{as}\frac{1}{2}L'_m\frac{di_m}{dt} - i_{bs}L'_{bs}\frac{di_m}{dt} - \frac{1}{2}L_{mc}\frac{d}{dt}i_{cs} - \\
& i_{cs}\frac{1}{2}L'_{mc}\frac{di_m}{dt} + L_{sr}\cos\left(\theta - \frac{2\pi}{3}\right)\frac{d}{dt}i_{ar} + i_{ar}L'_{sr}\frac{di_m}{dt}\cos\left(\theta - \frac{2\pi}{3}\right) - i_{ar} \\
& L_{sr}\sin\left(\theta - \frac{2\pi}{3}\right)\omega_r + L_{sr}\cos(\theta)\frac{d}{dt}i_{br} + i_{br}L'_{sr}\frac{di_m}{dt}\cos(\theta) - i_{br}L_{sr}\sin(\theta)\omega_r + \\
& L_{sr}\cos\left(\theta + \frac{2\pi}{3}\right)\frac{d}{dt}i_{cr} + i_{cr}L'_{sr}\frac{di_m}{dt}\cos\left(\theta + \frac{2\pi}{3}\right) - i_{cr}L_{sr}\sin\left(\theta + \frac{2\pi}{3}\right)\omega_r]
\end{aligned} \tag{3.38}$$

In addition, for voltage in phase c in the stator circuit, the equation below can be obtained:

$$\begin{aligned}
v_{cs} = & r_{cs}i_{cs} + L_{sc}\frac{d}{dt}i_{cs} - \frac{1}{2}L_{ma}\frac{d}{dt}i_{as} - i_{as}\frac{1}{2}L'_m\frac{di_m}{dt} - i_{cs}L'_{cs}\frac{di_m}{dt} - \frac{1}{2}L_{mb}\frac{d}{dt}i_{bs} - \\
& i_{bs}\frac{1}{2}L'_{mb}\frac{di_m}{dt} + L_{sr}\cos\left(\theta + \frac{2\pi}{3}\right)\frac{d}{dt}i_{ar} + i_{ar}L'_{sr}\frac{di_m}{dt}\cos\left(\theta + \frac{2\pi}{3}\right) - i_{ar}L_{sr}\sin \\
& \left(\theta + \frac{2\pi}{3}\right)\omega_r + L_{sr}\cos\left(\theta - \frac{2\pi}{3}\right)\frac{d}{dt}i_{br} + i_{br}L'_{sr}\frac{di_m}{dt}\cos\left(\theta - \frac{2\pi}{3}\right) - i_{br}L_{sr}\sin \\
& \left(\theta - \frac{2\pi}{3}\right)\omega_r + L_{sr}\cos(\theta)\frac{d}{dt}i_{cr} + i_{cr}L'_{sr}\frac{di_m}{dt}\cos(\theta) - i_{cr}L_{sr}\sin(\theta)\omega_r]
\end{aligned}$$

(3.39)

By using the same method for voltage in phase a in the rotor circuit, this equation can be obtained:

$$\begin{aligned}
v_{ar} = & r_{ar}i_{ar} + L_{ra}\frac{d}{dt}i_{ar} - \frac{1}{2}L_{mb}\frac{d}{dt}i_{br} + i_{ar}L'_{ar}\frac{di_m}{dt} - i_{br}\frac{1}{2}L'_m\frac{di_m}{dt} - \frac{1}{2}L_{mc} \\
& \frac{d}{dt}i_{cr} - i_{cr}\frac{1}{2}L'_{mb}\frac{di_m}{dt} + L_{sr}\cos(\theta)\frac{d}{dt}i_{as} + i_{as}L'_{sr}\frac{di_m}{dt}\cos(\theta) - i_{as}L_{sr} \\
& \sin(\theta)\omega_r + L_{sr}\cos\left(\theta - \frac{2\pi}{3}\right)\frac{d}{dt}i_{bs} + i_{bs}L'_{sr}\frac{di_m}{dt}\cos\left(\theta - \frac{2\pi}{3}\right) - i_{bs}L_{sr} \\
& \sin\left(\theta - \frac{2\pi}{3}\right)\omega_r + L_{sr}\cos\left(\theta + \frac{2\pi}{3}\right)\frac{d}{dt}i_{cs} + i_{cs}L'_{sr}\frac{di_m}{dt}\cos\left(\theta + \frac{2\pi}{3}\right) - \\
& i_{cs}L_{sr}\sin\left(\theta + \frac{2\pi}{3}\right)\omega_r] \tag{3.40}
\end{aligned}$$

Similarly, for voltage in phase b in the rotor circuit, the following equation can be obtained:

$$\begin{aligned}
v_{br} = & r_{br}i_{br} + L_{rb}\frac{d}{dt}i_{br} - \frac{1}{2}L_{ma}\frac{d}{dt}i_{ar} + i_{ar}L'_{ar}\frac{di_m}{dt} - i_{br}\frac{1}{2}L'_m\frac{di_m}{dt} - \frac{1}{2}L_{mc}\frac{d}{dt}i_{cr} - \\
& i_{cr}\frac{1}{2}L'_{mb}\frac{di_m}{dt} + L_{sr}\cos\left(\theta + \frac{2\pi}{3}\right)\frac{d}{dt}i_{as} + i_{as}L'_{sr}\frac{di_m}{dt}\cos\left(\theta + \frac{2\pi}{3}\right) -
\end{aligned}$$

$$\begin{aligned}
& i_{as} L_{sr} \sin\left(\theta + \frac{2\pi}{3}\right) \omega_r + L_{sr} \cos(\theta) \frac{d}{dt} i_{bs} + i_{bs} L'_{sr} \frac{di_m}{dt} \cos(\theta) - \\
& i_{bs} L_{sr} \sin(\theta) \omega_r + L_{sr} \cos\left(\theta - \frac{2\pi}{3}\right) \frac{d}{dt} i_{cs} + i_{cs} L'_{sr} \frac{di_m}{dt} \cos\left(\theta - \frac{2\pi}{3}\right) - \\
& i_{cs} L_{sr} \sin\left(\theta - \frac{2\pi}{3}\right) \omega_r] \tag{3.41}
\end{aligned}$$

In the same manner, for voltage in phase c in the rotor circuit, the next equation can be obtained:

$$\begin{aligned}
v_{cr} = & r_{cr} i_{cr} + L_{rc} \frac{d}{dt} i_{cr} - \frac{1}{2} L_{ma} \frac{d}{dt} i_{ar} + i_{cr} L'_{cr} \frac{di_m}{dt} - i_{ar} \frac{1}{2} L'_{ma} \frac{di_m}{dt} - \frac{1}{2} L_{mb} \frac{d}{dt} i_{br} - \\
& i_{br} \frac{1}{2} L'_{mb} \frac{di_m}{dt} + L_{sr} \cos\left(\theta - \frac{2\pi}{3}\right) \frac{d}{dt} i_{as} + i_{as} L'_{sr} \frac{di_m}{dt} \cos\left(\theta - \frac{2\pi}{3}\right) - \\
& i_{as} L_{sr} \sin\left(\theta - \frac{2\pi}{3}\right) \omega_r + L_{sr} \cos\left(\theta + \frac{2\pi}{3}\right) \frac{d}{dt} i_{bs} + i_{bs} L'_{sr} \frac{di_m}{dt} \cos\left(\theta + \frac{2\pi}{3}\right) - \\
& i_{bs} L_{sr} \sin\left(\theta + \frac{2\pi}{3}\right) \omega_r + L_{sr} \cos(\theta) \frac{d}{dt} i_{cs} + i_{cs} L'_{sr} \frac{di_m}{dt} \cos(\theta) - \\
& i_{cs} L_{sr} \sin(\theta) \omega_r] \tag{3.42}
\end{aligned}$$

These equations can be written in a matrix form as follows:

$$\begin{bmatrix} v_{as} \\ v_{bs} \\ v_{cs} \\ v_{ar} \\ v_{br} \\ v_{cr} \end{bmatrix} = \begin{bmatrix} r_{as} & 0 & 0 & 0 & 0 & 0 \\ 0 & r_{bs} & 0 & 0 & 0 & 0 \\ 0 & 0 & r_{cs} & 0 & 0 & 0 \\ 0 & 0 & 0 & r_{ar} & 0 & 0 \\ 0 & 0 & 0 & 0 & r_{br} & 0 \\ 0 & 0 & 0 & 0 & 0 & r_{cr} \end{bmatrix} \begin{bmatrix} i_{as} \\ i_{bs} \\ i_{cs} \\ i_{ar} \\ i_{br} \\ i_{cr} \end{bmatrix} +$$

$$\begin{bmatrix} L_{sa} & -0.5L_{mb} & -0.5L_{mc} & L_{sr} a_1 & L_{sr} a_2 & L_{sr} a_3 \\ -0.5L_{ma} & L_{sb} & -0.5L_{mc} & L_{sr} a_3 & L_{sr} a_1 & L_{sr} a_2 \\ -0.5L_{ma} & -0.5L_{mb} & L_{sc} & L_{sr} a_2 & L_{sr} a_3 & L_{sr} a_1 \\ L_{sr} a_1 & L_{sr} a_3 & L_{sr} a_2 & L_{ra} & -0.5L_{mb} & -0.5L_{mc} \\ L_{sr} a_2 & L_{sr} a_1 & L_{sr} a_3 & -0.5L_{ma} & L_{rb} & -0.5L_{mc} \\ L_{sr} a_3 & L_{sr} a_2 & L_{sr} a_1 & -0.5L_{ma} & -0.5L_{mb} & L_{rc} \end{bmatrix} \begin{bmatrix} \frac{di_{as}}{dt} \\ \frac{di_{bs}}{dt} \\ \frac{di_{cs}}{dt} \\ \frac{di_{ar}}{dt} \\ \frac{di_{br}}{dt} \\ \frac{di_{cr}}{dt} \end{bmatrix}$$

$$-\omega_r \begin{bmatrix} 0 & 0 & 0 & L_{sr} b_1 & L_{sr} b_2 & L_{sr} b_3 \\ 0 & 0 & 0 & L_{sr} b_3 & L_{sr} b_1 & L_{sr} b_2 \\ 0 & 0 & 0 & L_{sr} b_2 & L_{sr} b_3 & L_{sr} b_1 \\ L_{sr} b_1 & L_{sr} b_3 & L_{sr} b_2 & 0 & 0 & 0 \\ L_{sr} b_2 & L_{sr} b_1 & L_{sr} b_3 & 0 & 0 & 0 \\ L_{sr} b_3 & L_{sr} b_2 & L_{sr} b_1 & 0 & 0 & 0 \end{bmatrix} \begin{bmatrix} i_{as} \\ i_{bs} \\ i_{cs} \\ i_{ar} \\ i_{br} \\ i_{cr} \end{bmatrix} +$$

$$\frac{di_m}{dt} \begin{bmatrix} L'_{sa} & -0.5L'_{mb} & -0.5L'_{mc} & L'_{sr} a_1 & L'_{sr} a_2 & L'_{sr} a_3 \\ -0.5L'_{ma} & L'_{sb} & -0.5L'_{mc} & L'_{sr} a_3 & L'_{sr} a_1 & L'_{sr} a_2 \\ -0.5L'_{ma} & -0.5L'_{mb} & L'_{sc} & L'_{sr} a_2 & L'_{sr} a_3 & L'_{sr} a_1 \\ L'_{sr} a_1 & L'_{sr} a_3 & L'_{sr} a_2 & L'_{ra} & -0.5L'_{mb} & -0.5L'_{mc} \\ L'_{sr} a_2 & L'_{sr} a_1 & L'_{sr} a_3 & -0.5L'_{ma} & L'_{rb} & -0.5L'_{mc} \\ L'_{sr} a_3 & L'_{sr} a_2 & L'_{sr} a_1 & -0.5L'_{ma} & -0.5L'_{mb} & L'_{rc} \end{bmatrix} \begin{bmatrix} i_{as} \\ i_{bs} \\ i_{cs} \\ i_{ar} \\ i_{br} \\ i_{cr} \end{bmatrix}$$

(3.43)

It can easily be noted that the difference between the conventional model in the previous section and this model is the last term in the above equation, which represents the term  $\frac{\partial[L]}{\partial i_m} \frac{\partial i_m}{\partial t} [i]$  in equation 3.29. For digital simulation purposes, equation 3.43 represented in state variable form so that the currents are state variables:

$$\begin{aligned} \frac{d}{dt} i_{as} = & \frac{1}{L_s} [v_{as} - r_{as} i_{as} - i_{as} L'_m \frac{di_m}{dt} + \frac{1}{2} L_m \frac{d}{dt} i_{bs} + i_{bs} \frac{1}{2} L'_m \frac{di_m}{dt} + \frac{1}{2} L_m \frac{d}{dt} i_{cs} + \\ & i_{cs} \frac{1}{2} L'_m \frac{di_m}{dt} - L_m \cos(\theta) \frac{d}{dt} i_{ar} - i_{ar} L'_m \frac{di_m}{dt} \cos(\theta) + i_{ar} L_m \sin(\theta) \omega_r - \\ & L_m \cos\left(\theta + \frac{2\pi}{3}\right) \frac{d}{dt} i_{br} - i_{br} L'_m \frac{di_m}{dt} \cos\left(\theta + \frac{2\pi}{3}\right) + i_{br} L_m \sin\left(\theta + \frac{2\pi}{3}\right) \omega_r - \\ & L_m \cos\left(\theta - \frac{2\pi}{3}\right) \frac{d}{dt} i_{cr} - i_{cr} L'_m \frac{di_m}{dt} \cos\left(\theta - \frac{2\pi}{3}\right) + i_{cr} L_m \sin\left(\theta - \frac{2\pi}{3}\right) \omega_r] \end{aligned} \quad (3.44)$$

These equations can be written in a matrix form as follows:

$$\begin{bmatrix} \frac{di_{as}}{dt} \\ \frac{di_{bs}}{dt} \\ \frac{di_{cs}}{dt} \\ \frac{di_{ar}}{dt} \\ \frac{di_{br}}{dt} \\ \frac{di_{cr}}{dt} \end{bmatrix} = \begin{bmatrix} \frac{1}{L_s} & 0 & 0 & 0 & 0 & 0 \\ L_s & \frac{1}{L_s} & 0 & 0 & 0 & 0 \\ 0 & L_s & \frac{1}{L_s} & 0 & 0 & 0 \\ 0 & 0 & L_s & \frac{1}{L_r} & 0 & 0 \\ 0 & 0 & 0 & L_r & \frac{1}{L_r} & 0 \\ 0 & 0 & 0 & 0 & L_r & \frac{1}{L_r} \end{bmatrix} \begin{Bmatrix} v_{as} \\ v_{bs} \\ v_{cs} \\ v_{ar} \\ v_{br} \\ v_{cr} \end{Bmatrix} - \begin{bmatrix} r_{as} & 0 & 0 & 0 & 0 & 0 \\ 0 & r_{bs} & 0 & 0 & 0 & 0 \\ 0 & 0 & r_{cs} & 0 & 0 & 0 \\ 0 & 0 & 0 & r_{ar} & 0 & 0 \\ 0 & 0 & 0 & 0 & r_{br} & 0 \\ 0 & 0 & 0 & 0 & 0 & r_{cr} \end{bmatrix} \begin{bmatrix} i_{as} \\ i_{bs} \\ i_{cs} \\ i_{ar} \\ i_{br} \\ i_{cr} \end{bmatrix}$$

$$- \begin{bmatrix} 0 & -0.5L_m & -0.5L_m & L_{sr} a_1 & L_{sr} a_2 & L_{sr} a_3 \\ -0.5L_m & 0 & -0.5L_m & L_{sr} a_3 & L_{sr} a_1 & L_{sr} a_2 \\ -0.5L_m & -0.5L_m & 0 & L_{sr} a_2 & L_{sr} a_3 & L_{sr} a_1 \\ L_{sr} a_1 & L_{sr} a_3 & L_{sr} a_2 & 0 & -0.5L_m & -0.5L_m \\ L_{sr} a_2 & L_{sr} a_1 & L_{sr} a_3 & -0.5L_m & 0 & -0.5L_m \\ L_{sr} a_3 & L_{sr} a_2 & L_{sr} a_1 & -0.5L_m & -0.5L_m & 0 \end{bmatrix} \begin{bmatrix} \frac{di_{as}}{dt} \\ \frac{di_{bs}}{dt} \\ \frac{di_{cs}}{dt} \\ \frac{di_{ar}}{dt} \\ \frac{di_{br}}{dt} \\ \frac{di_{cr}}{dt} \end{bmatrix}$$

$$+ \begin{bmatrix} 0 & 0 & 0 & L_{sr} b_1 \omega_r & L_{sr} b_2 \omega_r & L_{sr} b_3 \omega_r \\ 0 & 0 & 0 & L_{sr} b_3 \omega_r & L_{sr} b_1 \omega_r & L_{sr} b_2 \omega_r \\ 0 & 0 & 0 & L_{sr} b_2 \omega_r & L_{sr} b_3 \omega_r & L_{sr} b_1 \omega_r \\ L_{sr} b_1 \omega_r & L_{sr} b_3 \omega_r & L_{sr} b_2 \omega_r & 0 & 0 & 0 \\ L_{sr} b_2 \omega_r & L_{sr} b_1 \omega_r & L_{sr} b_3 \omega_r & 0 & 0 & 0 \\ L_{sr} b_3 \omega_r & L_{sr} b_2 \omega_r & L_{sr} b_1 \omega_r & 0 & 0 & 0 \end{bmatrix} \begin{bmatrix} i_{as} \\ i_{bs} \\ i_{cs} \\ i_{ar} \\ i_{br} \\ i_{cr} \end{bmatrix}$$

$$\begin{aligned}
& - \begin{bmatrix} L'_s \frac{di_m}{dt} & -0.5L'_m \frac{di_m}{dt} & -0.5L'_m \frac{di_m}{dt} & L'_{sr} a_1 \frac{di_m}{dt} & L'_{sr} a_2 \frac{di_m}{dt} & L'_{sr} a_3 \frac{di_m}{dt} \\ -0.5L'_m \frac{di_m}{dt} & L'_s \frac{di_m}{dt} & -0.5L'_m \frac{di_m}{dt} & L'_{sr} a_3 \frac{di_m}{dt} & L'_{sr} a_1 \frac{di_m}{dt} & L'_{sr} a_2 \frac{di_m}{dt} \\ -0.5L'_m \frac{di_m}{dt} & -0.5L'_m \frac{di_m}{dt} & L'_s \frac{di_m}{dt} & L'_{sr} a_2 \frac{di_m}{dt} & L'_{sr} a_3 \frac{di_m}{dt} & L'_{sr} a_1 \frac{di_m}{dt} \\ L'_{sr} a_1 \frac{di_m}{dt} & L'_{sr} a_3 \frac{di_m}{dt} & L'_{sr} a_2 \frac{di_m}{dt} & L'_r \frac{di_m}{dt} & -0.5L'_m \frac{di_m}{dt} & -0.5L'_m \frac{di_m}{dt} \\ L'_{sr} a_2 \frac{di_m}{dt} & L'_{sr} a_1 \frac{di_m}{dt} & L'_{sr} a_3 \frac{di_m}{dt} & -0.5L'_m \frac{di_m}{dt} & L'_r \frac{di_m}{dt} & -0.5L'_m \frac{di_m}{dt} \\ L'_{sr} a_3 \frac{di_m}{dt} & L'_{sr} a_2 \frac{di_m}{dt} & L'_{sr} a_1 \frac{di_m}{dt} & -0.5L'_m \frac{di_m}{dt} & -0.5L'_m \frac{di_m}{dt} & L'_r \frac{di_m}{dt} \end{bmatrix} \begin{bmatrix} i_{as} \\ i_{bs} \\ i_{cs} \\ i_{ar} \\ i_{br} \\ i_{cr} \end{bmatrix} \\
& \hspace{25em} (3.45)
\end{aligned}$$

The effects of the last term in the equation (3.45) is termed the dynamic matrix (or dynamic effects) in this study.

### 3.4 Flux linkage model of SEIGs

From section 3.2, it can be deduced that the total flux in each winding is given by the sum of its proper flux (linked by the inductance  $L_s$ , for a stator flux) with three rotor coupling fluxes (linked by a mutual inductance variable according to rotor position). For a stator flux and rotor flux, we then obtain:

$$\begin{bmatrix} \lambda_{as} \\ \lambda_{bs} \\ \lambda_{cs} \\ \lambda_{ar} \\ \lambda_{br} \\ \lambda_{cr} \end{bmatrix} = \begin{bmatrix} L_{sa} & -0.5L_{mb} & -0.5L_{mc} & L_{sr} a_1 & L_{sr} a_2 & L_{sr} a_3 \\ -0.5L_{ma} & L_{sb} & -0.5L_{mc} & L_{sr} a_3 & L_{sr} a_1 & L_{sr} a_2 \\ -0.5L_{ma} & -0.5L_{mb} & L_{sc} & L_{sr} a_2 & L_{sr} a_3 & L_{sr} a_1 \\ L_{sr} a_1 & L_{sr} a_3 & L_{sr} a_2 & L_{ra} & -0.5L_{mb} & -0.5L_{mc} \\ L_{sr} a_2 & L_{sr} a_1 & L_{sr} a_3 & -0.5L_{ma} & L_{rb} & -0.5L_{mc} \\ L_{sr} a_3 & L_{sr} a_2 & L_{sr} a_1 & -0.5L_{ma} & -0.5L_{mb} & L_{rc} \end{bmatrix} \begin{bmatrix} i_{as} \\ i_{bs} \\ i_{cs} \\ i_{ar} \\ i_{br} \\ i_{cr} \end{bmatrix} \quad 33.46)$$

### 3.5 Electromagnetic torque equation of SEIGs

To evaluate the energy stored in the coupling field, the following equation may be used [53]:

$$w_f(i_1, \dots, i_j, x) = \frac{1}{2} \sum_{p=1}^J \sum_{q=1}^J L_{pq} i_p i_q$$

The yield is:

$$w_f = \frac{1}{2} [i_s]_{abc}^T (L_s - L_{ls} I) [i_s]_{abc} + [i_s]_{abc}^T L_{sr} [i_r]_{abc} + \frac{1}{2} [i_r]_{abc}^T$$

$$(L_r - L_{lr} I) [i_r]_{abc} \quad (3.47)$$

the electromagnetic torque can be evaluated by [53]:

$$T_e(i_j, \theta_r) = \frac{P}{2} \frac{\partial W(i_j, \theta_r)}{\partial \theta_r} \quad (3.48)$$

assuming that  $L_s$  and  $L_r$  are not functions of  $\theta_r$  substituting  $w_f$  from equation 3.47 into equation 3.48 yields electromagnetic torque in Newton meters (N.m).

$$T_e = \left(\frac{P}{2}\right) [i_s]_{abc}^T \frac{\partial}{\partial \theta_r} [L_{sr}] [i_r]_{abc} \quad (3.49)$$

where,

$$\frac{\partial}{\partial \theta_r} [L_{sr}] = -L_{sr} \begin{bmatrix} b_1 & b_2 & b_3 \\ b_3 & b_1 & b_2 \\ b_2 & b_3 & b_1 \end{bmatrix} \quad (3.50)$$

$$\frac{\partial}{\partial \theta_r} [L_{sr}] [i_r]_{abc} = -L_{sr} \begin{bmatrix} i_{ra} b_1 + & i_{rb} b_2 + & i_{rc} b_3 \\ i_{ra} b_3 + & i_{rb} b_1 + & i_{rc} b_2 \\ i_{ra} b_2 + & i_{rb} b_3 + & i_{rc} b_1 \end{bmatrix} \quad (3.51)$$

expanding the electromagnetic torque equation yields:

$$\begin{aligned} T_e = & -L_{sr} \left( \frac{P}{2} \right) \left[ i_{ra} \sin(\theta) + i_{rb} \sin\left(\theta + \frac{2\pi}{3}\right) + i_{rc} \sin\left(\theta - \frac{2\pi}{3}\right) \right] i_{sa} \\ & -L_{sr} \left( \frac{P}{2} \right) \left[ i_{ra} \sin\left(\theta - \frac{2\pi}{3}\right) + i_{rb} \sin(\theta) + i_{rc} \sin\left(\theta + \frac{2\pi}{3}\right) \right] i_{sb} \\ & -L_{sr} \left( \frac{P}{2} \right) \left[ i_{ra} \sin\left(\theta + \frac{2\pi}{3}\right) + i_{rb} \sin\left(\theta - \frac{2\pi}{3}\right) + i_{rc} \sin(\theta) \right] i_{sc} \end{aligned} \quad (3.52)$$

but from trigonometry we know:

$$\sin\left(\theta + \frac{2\pi}{3}\right) = -\frac{1}{2} \sin(\theta) - \frac{\sqrt{3}}{2} \cos \theta$$

$$\sin\left(\theta - \frac{2\pi}{3}\right) = -\frac{1}{2} \sin(\theta) + \frac{\sqrt{3}}{2} \cos \theta$$

Therefore,

$$T_e = i_{sa} i_{ra} \sin(\theta) - \frac{1}{2} i_{sa} i_{rb} \sin(\theta) + \frac{\sqrt{3}}{2} i_{sa} i_{rb} \cos \theta - \frac{1}{2} i_{sa} i_{rc} \sin(\theta) -$$

$$\begin{aligned}
& \frac{\sqrt{3}}{2} i_{sa} i_{rc} \cos \theta - \frac{1}{2} i_{sb} i_{ra} \sin(\theta) - \frac{\sqrt{3}}{2} i_{sb} i_{ra} \cos \theta - i_{sb} i_{rb} \sin(\theta) - \\
& \frac{1}{2} i_{sb} i_{rc} \sin(\theta) + \frac{\sqrt{3}}{2} i_{sb} i_{rc} \cos \theta - \frac{1}{2} i_{sc} i_{ra} \sin(\theta) + \frac{\sqrt{3}}{2} i_{sc} i_{ra} \cos \theta - \\
& \frac{1}{2} i_{sc} i_{rb} \sin(\theta) - \frac{\sqrt{3}}{2} i_{sc} i_{rb} \cos \theta + i_{sc} i_{rc} \sin(\theta)
\end{aligned} \tag{3.53}$$

or,

$$\begin{aligned}
T_e = & -Lsr \left( \frac{P}{2} \right) \left\{ \left[ \left( i_{ra} - \frac{1}{2} i_{rb} - \frac{1}{2} i_{rc} \right) i_{sa} + \left( i_{rb} - \frac{1}{2} i_{ra} - \frac{1}{2} i_{rc} \right) i_{sb} + \right. \right. \\
& \left. \left( i_{rc} - \frac{1}{2} i_{ra} - \frac{1}{2} i_{rb} \right) i_{sc} \right] \sin(\theta) + \frac{\sqrt{3}}{2} \left[ (i_{rb} - i_{rc}) i_{sa} + (i_{rc} - i_{ra}) i_{sb} \right. \\
& \left. \left. + (i_{ra} - i_{rb}) i_{sc} \right] \cos \theta \right\}
\end{aligned} \tag{3.54}$$

### 3.6 Mechanical torque equation of SEIGs

The mechanical torque equation can be written as follows [53]:

$$T_L = T_e - J \left( \frac{2}{P} \right) \frac{\partial \omega_{mec}}{\partial t} - B_m \omega_{mec} \tag{3.55}$$

where,

$J$  is the moment of inertia of the rotor and has the unit  $\text{Kg.m}^2$

$B_m$  is a damping coefficient associated with the rotational system of the machine and has the unit  $\text{Nms / rad}$

$T_L$  is the mechanical torque in  $\text{Nm}$

### 3.7 Mathematical model of the load and excitation capacitors

The load is one of the main components of an SEIG system, and hence it is important to model it accurately. The SEIG is tested under a resistive load connected in star connection, and an inductive load parallel with a resistive load both connected in the star arrangement. The following two sections shows how this configuration is modelled mathematically.

#### 3.7.1 Resistive load

The layout of the system when the resistive load is connected is shown in the following Figure 3.3 . From the single-phase diagram of the system under study illustrated in Figure 3.4, it can be found that:

$$i_{as} = i_{al} + i_{ac}$$

or:

$$i_{as} = i_{al} + c \frac{dv_{ac}}{dt}$$

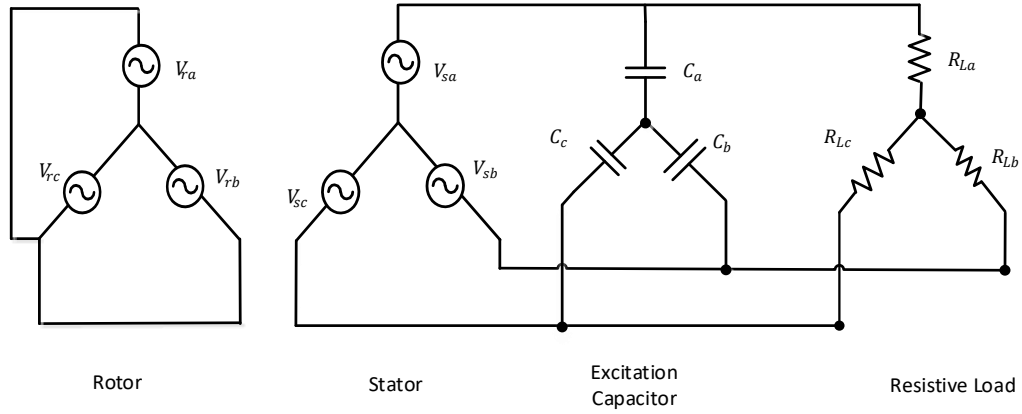


**Figure 3.3** Configuration of the system when a resistive load is connected.

From Figure 3.4 it can be observed that  $v_{as} = v_{al} = v_{ac}$ , and therefore:

$$\frac{dv_{as}}{dt} = \frac{1}{C_a} [i_{as} - i_{al}]$$

Thus, we can model the current of the excitation capacitors and load resistors in the three phases by using the following matrix equations:

$$\begin{bmatrix} \frac{dv_{as}}{dt} \\ \frac{dv_{bs}}{dt} \\ \frac{dv_{cs}}{dt} \end{bmatrix} = \begin{bmatrix} \frac{1}{C_a} & 0 & 0 \\ 0 & \frac{1}{C_b} & 0 \\ 0 & 0 & \frac{1}{C_c} \end{bmatrix} \begin{bmatrix} i_{as} - i_{al} \\ i_{bs} - i_{bl} \\ i_{cs} - i_{cl} \end{bmatrix} \quad (3.56)$$

and

$$\begin{bmatrix} v_{as} \\ v_{bs} \\ v_{cs} \end{bmatrix} = \begin{bmatrix} R_{al} & 0 & 0 \\ 0 & R_{bl} & 0 \\ 0 & 0 & R_{cl} \end{bmatrix} \begin{bmatrix} i_{al} \\ i_{bl} \\ i_{cl} \end{bmatrix} \quad (3.57)$$

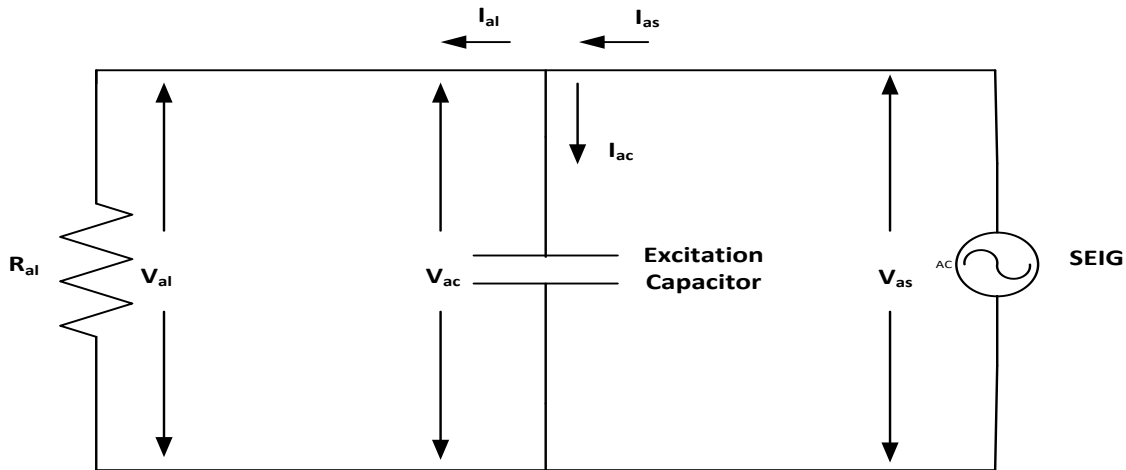


*Figure 3.4 Single-phase diagram of the system under study.*

These equations can be rearranged in the form of a state-space representation and solved numerically for the stator currents and voltages to obtain all other machine quantities.

### **3.7.2 Inductive and resistive load**

The inductive and resistive load are both connected in the star arrangement such that the inductive load is parallel to the resistive load as shown in Figure 3.5. Since the reactive power is shared by the load and the induction generator, and to meet the demands of reactive power by the inductive load in addition to the demand by the induction generator for excitation, the value of the excitation capacitance value should be increased to be  $37 \mu\text{F}$  instead of  $30 \mu\text{F}$  when the load is a resistive load.

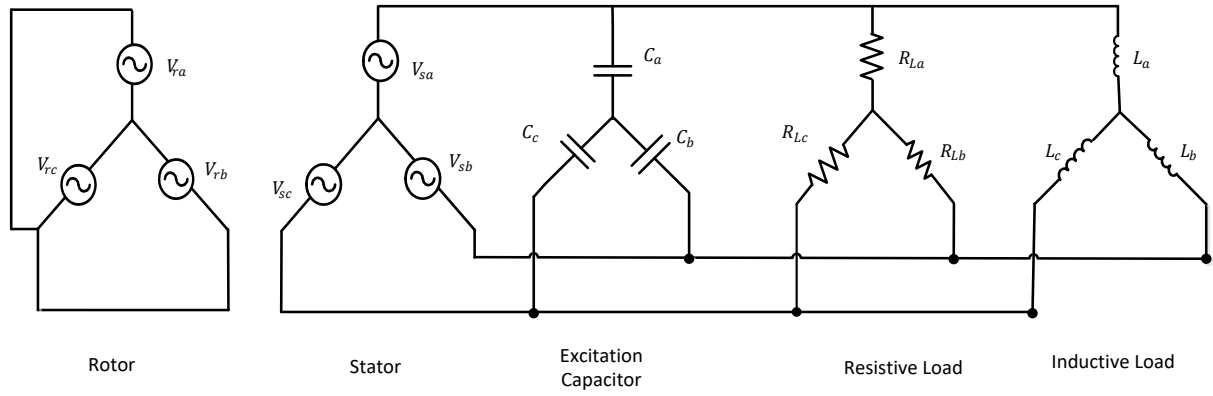


**Figure 3.5** Configuration of the system under study when R-L load is connected.

Based on the configuration of the system depicted in Figure 3.5 the equations that relate to the currents passing in the excitation capacitors and the parallel combination of resistive and inductive loads can be expressed as follows:

$$i_{as} = i_{ac} + i_{aR} + i_{aL}$$

or:

$$[i_c]_{abc} = [i_s]_{abc} - [i_R]_{abc} - [i_l]_{abc} \quad (3.58)$$

$$i_{as} = c \frac{dv_{ac}}{dt} + i_{aR} + \frac{1}{L} \int v_{aL} dt$$

then:

$$\frac{dv_{as}}{dt} = \frac{1}{C_a} \left[ i_{as} - \frac{v_{as}}{R_{al}} - \frac{1}{L} \int v_{aL} dt \right]$$

Thus, we can model the current of the excitation capacitors and load resistors in the three phases by using the following matrix equation:

$$\begin{bmatrix} \frac{dv_{as}}{dt} \\ \frac{dv_{bs}}{dt} \\ \frac{dv_{cs}}{dt} \end{bmatrix} = \begin{bmatrix} \frac{1}{C_a} & 0 & 0 \\ 0 & \frac{1}{C_b} & 0 \\ 0 & 0 & \frac{1}{C_c} \end{bmatrix} \begin{bmatrix} i_{as} \\ i_{bs} \\ i_{cs} \end{bmatrix} - \begin{bmatrix} \frac{1}{R_{al}} & 0 & 0 \\ 0 & \frac{1}{R_{bl}} & 0 \\ 0 & 0 & \frac{1}{R_{cl}} \end{bmatrix} \begin{bmatrix} v_{as} \\ v_{bs} \\ v_{cs} \end{bmatrix} - \int \begin{bmatrix} \frac{1}{L_a} & 0 & 0 \\ 0 & \frac{1}{L_b} & 0 \\ 0 & 0 & \frac{1}{L_c} \end{bmatrix} \begin{bmatrix} v_{as} \\ v_{bs} \\ v_{cs} \end{bmatrix} \quad (3.59)$$

### 3.8 Modelling the residual flux of SEIGs

In chapter 2, it was mentioned that the self-excitation process of the SEIG can take place if there is sufficient residual magnetic flux in the rotor [11] or if an initial voltage is imposed across the terminals of the excitation capacitors. This is also true in the simulation implemented in the Matlab Simulink environment. For this reason, the residual flux should be simulated. To simulate the remnant EMF, a voltage source has a frequency which is a function of rotor speed. The value of this voltage was measured at the terminals of the induction machine at no-load conditions while the generator was running at a synchronous speed. In this study, a small phase voltage value was measured at stator terminals ( $V_s$  is 7 rms volt), therefore the residual flux can be modelled as follows:

$$E_{res} = \sqrt{2}V_s \sin\omega_r t$$

where  $E_{res}$  is voltage produced by the residual flux and  $\omega_r$  is the angular frequency of the rotor in rad/sec.

### 3.9 Magnetizing current equation for SEIGs

The magnetizing current is important in this study, and in order to determine the value of magnetizing inductance this current can be defined as:

$$i_m = i_s + i_r$$

The stator and rotor currents can be found by solving the equation 3.45. Stable operation of SEIG can only occur with a reasonable degree of saturation in its magnetic circuit [56]. The effect of such saturation can be simulated by a corresponding change in the value of  $L_m$  estimated at the end of each integration step and used in the next step. The rms magnetizing current ( $I_m$ ) is calculated as [16]:

$$I_m = \sqrt{\frac{1}{3}\{(i_{sa} - i_{ra})^2 + (i_{sb} - i_{rb})^2 + (i_{sc} - i_{rc})^2\}} \quad (3.60)$$

Another method to estimate the equivalent instantaneous magnetizing current is to be achieved by project the stator and rotor phase currents into stationary orthogonal d-q axes. If we assume the d-axis coincides with the phase a-axis, hence the rms magnetizing current ( $I_m$ ) is calculated [8] as:

$$i_{sd} = i_{sa} \quad (3.61)$$

$$i_{sq} = (i_{sb} - i_{sc})/\sqrt{3} \quad (3.62)$$

$$i_{rd} = \frac{2}{3}\left(i_{ra} \cos \theta + i_{rb} \cos\left(\theta + \frac{2\pi}{3}\right) + i_{rc} \cos\left(\theta - \frac{2\pi}{3}\right)\right) \quad (3.63)$$

$$i_{rq} = \frac{2}{3}\left(i_{ra} \sin \theta + i_{rb} \sin\left(\theta + \frac{2\pi}{3}\right) + i_{rc} \sin\left(\theta - \frac{2\pi}{3}\right)\right) \quad (3.64)$$

This can be written in a matrix form as:

$$\begin{bmatrix} i_{ds} \\ i_{qs} \end{bmatrix} = \begin{bmatrix} 1 & 0 & 0 \\ 0 & \frac{1}{\sqrt{3}} & \frac{-1}{\sqrt{3}} \end{bmatrix} \begin{bmatrix} i_{sa} \\ i_{sb} \\ i_{sc} \end{bmatrix} \quad (3.65)$$

$$\begin{bmatrix} i_{ds} \\ i_{qs} \end{bmatrix} = \frac{2}{3} \begin{bmatrix} \cos \theta & \cos(\theta + \frac{2\pi}{3}) & \cos(\theta - \frac{2\pi}{3}) \\ \sin \theta & \sin(\theta + \frac{2\pi}{3}) & \sin(\theta - \frac{2\pi}{3}) \end{bmatrix} \begin{bmatrix} i_{ra} \\ i_{rb} \\ i_{rc} \end{bmatrix} \quad (3.66)$$

$$i_m = \frac{1}{\sqrt{2}} \sqrt{(i_{ds} + i_{dr})^2 + (i_{qs} + i_{qr})^2} \quad (3.67)$$

### 3.10 Conclusion

In this chapter, a new three-phase analytical model of the three-phase induction generator is derived which accounts for the main path saturation effects and the mutual saturation between the three phase stator windings as well as the mutual saturation between the rotor three phase windings. This model is used to investigate the behaviour and the performance of a three-phase SEIG under various circumstances. It can be observed that the difference between the new proposed model presented in section 3.3 and the conventional model presented in section 3.2 is the last matrix in equation 3.45, which represents the saturation effects. The saturation effects were taken into account by assuming that the magnetizing inductance is a variable and not a constant, and so it is considered as a function not only of rotor displacement but also of the magnetizing current. Hence, the model is developed taking into account the derivative of the magnetizing inductance with respect to the magnetizing current in order to be able to accurately predict the performance of the induction generator at balanced and unbalanced dynamic response. However, all studies employed the models developed in the natural ABC/abc reference frame to predict the SEIG performance described in chapter 2, neglect these dynamic effects. This will support the model in being able to predict the performance of the isolated induction generator during transient operation. Developing the model in the natural ABC/abc reference frame means that is applicable under various unbalanced operating conditions, and

it is also suitable for studying even a complex unbalanced state. In addition, the resistive and inductive load, linkage flux, residual flux, electromagnetic torque and mechanical torque have been modelled mathematically in this chapter.

# Chapter 4. Representation of variation in magnetizing inductance

---

## 4.1 Introduction

In the previous chapter, a new model of the SEIG has been presented taking into consideration the saturation effects. However, the method used to calculate the value of magnetizing inductance, which varies as the magnetizing current varies, was not shown. In this chapter, variation in magnetizing inductance is approximated by an exponential function derived by Simoes [99], which has not yet been tested in practice.

A T-model consisting of two resistances and three inductances is traditionally used to model the induction machine. For simple simulation, parameters are considered to have constant values in this approach. However, due to magnetic saturation in the induction machine, the magnetizing inductances vary as a function of the operating point. Several authors have modeled induction machines by assuming that effects of magnetizing inductance are negligible [41-43]. In this method of analysis, the value of magnetizing inductance is considered a constant, and thus  $L_m$  does not vary with the magnetizing current. However, others have reported that saturation significantly affects the stability and dynamic states of an induction machine [60, 103, 104].

It has been reported that it is unsatisfactory in induction machine modelling and analysis to assume that the circuit is linear in many transient conditions such as switching on and off the load [73]. The value of the voltage operating point reached after the self-excitation process in a SEIG is initiated can be attributed to magnetic saturation, which balances the excitation capacitance and the machine voltage [22]. The steady state operation of the SEIG take place at the point of the intersection of the magnetizing curve and the capacitor voltage line. The rated operating point on the magnetizing curve is always in the saturated region [23, 60]. Figure 4.1

shows that, as the excitation capacitor value increase the operating voltage increases and the magnetizing current also increases.

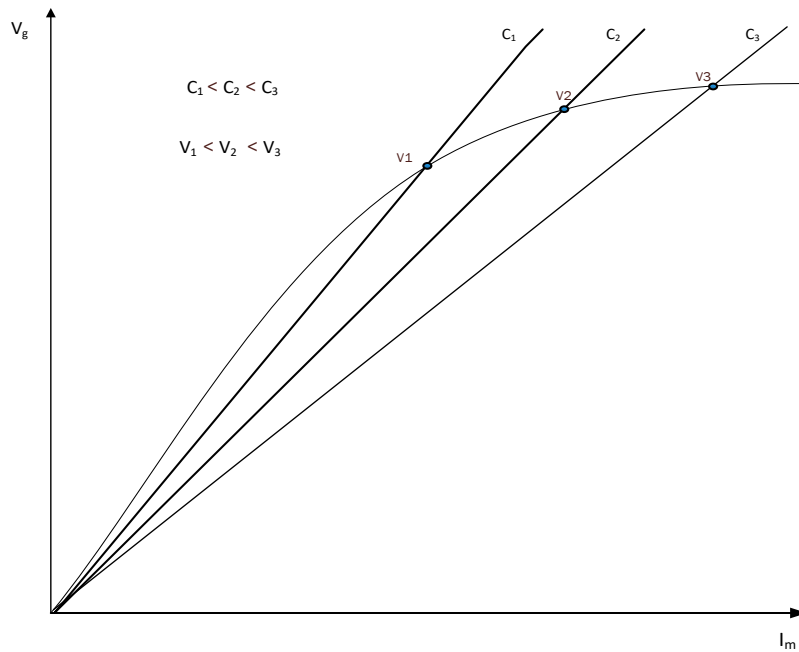


**Figure 4.1** Determination of stable operation of self-excited induction generator.

## 4.2 Methods used to model magnetizing inductance

The relationship between the air-gap voltage, which is the voltage across the magnetizing inductance (or the magnetizing current) and magnetizing inductance has been discussed by several authors. Generally speaking, the two main methods which are used to represent the variation between the magnetizing inductance and magnetizing current use a linear piecewise or a polynomial function. A linear piecewise association within the range of magnetizing current is used to approximate variations in magnetizing inductance, and several authors have applied this method [9, 16, 86]. Both of these methods rely on a fitting technique to approximate the value of magnetizing inductance as a function of  $I_m$ , and both also depend on the curve of

magnetizing characteristics which is obtained experimentally.

Complex and lengthy measurements are needed in the traditional method which requires the measured no-load curve to be obtained experimentally. This may threaten the integrity of the induction machine when the test is conducted and so alternative methods to determine the magnetizing inductance have been proposed [94, 98, 99].

Another method used to represent the nonlinear relationship between air-gap voltage and magnetizing current is a polynomial function to express magnetising inductance with respect to magnetising current  $i_m$ . The higher degree used the higher accuracy results is achieved. The coefficient of the polynomial function can be obtained experimentally. For better results in representing variation in magnetizing inductance, a polynomial function has been used in many studies [44, 50, 56].

### 4.3 The exponential method to represent the magnetizing inductance

This section shows the relationship between the magnetizing inductance and magnetizing current ( $I_m$ ) through the following nonlinear exponential equation [99]:

$$V_g = FI_m (K_1 e^{K_2 I_m^2} + K_3) \quad (4.1)$$

where  $F$  is the per unit frequency ( $f/f_{\text{base}}$ ) and  $f_{\text{base}}$  is the reference frequency used in the test to obtain the excitation curve.  $K_1$ ,  $K_2$ , and  $K_3$  are constants that can be calculated from the following equations:

$$K_1 = (c - K_3) \left( \frac{a - b}{b - c} \right)^{49/24} \quad (4.2)$$

$$K_2 = \frac{49 \ln \left( \frac{b-c}{a-b} \right)}{24 I_{m3}^2} \quad (4.3)$$

$$K_3 = \frac{b^2 - ac}{2b - (a + c)} \quad (4.4)$$

where, a, b and c in the above equations can be calculated using only three points of the magnetizing curve  $[(I_{m1}, V_{g1}), (I_{m2}, V_{g2}) \text{ and } (I_{m3}, V_{g3})]$ :

$$a = \frac{V_{g1}}{I_{m1}}, \quad b = \frac{V_{g2}}{I_{m2}} \quad \text{and} \quad c = \frac{V_{g2}}{I_{m2}}$$

where  $I_{m3}$  is the maximum magnetising current that could be safely measured. The values of  $I_{m1}$  and  $I_{m2}$  are then determined from  $I_{m2} = 0.7143I_{m3}$  and  $I_{m1} = 0.1428I_{m3}$ . The magnetizing reactance can be expressed as:

$$X_m = \omega L_m = \frac{V_g}{I_m} = F (K_1 e^{K_2 I_m^2} + K_3) \quad (4.5)$$

and the variation in magnetizing reactance is obtained as:

$$X'_m = \omega L'_m = \frac{dV_g}{dI_m} = F K_1 e^{K_2 I_m^2} (1 + 2K_2 I_m^2) + F K_3 \quad (4.6)$$

More details of how those equations are derived can be found in appendix A.

Figure 4.2 shows the calculated magnetization curve of the induction machine used as an induction generator in this study. The exponential function is used to predict this curve using three measured points to implement the calculation as follows: (0.578 A, 58.77 V), (2.896, 279.9 V) and (4.05, 325.32 V) as shown in the figure. The comparison between the calculate magnetization curve produced using the exponential function and the curve generated experimentally is depicted in Figure 4.3. It is clear that there is a high level of agreement between the calculated and measured curve. Hence, it can be concluded that the exponential method used to predict the magnetization curve using three measured points is not only simple but also gives very good accuracy.

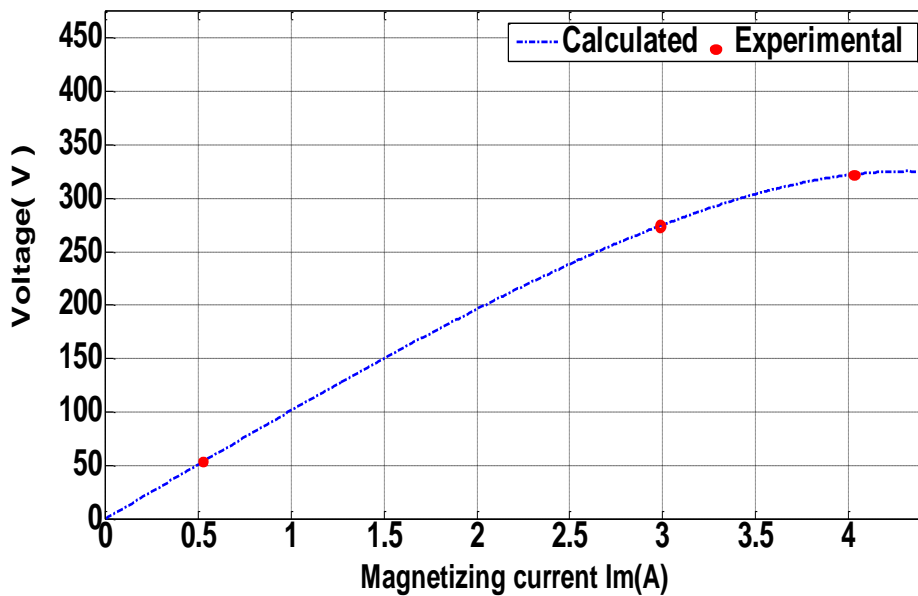


*Figure 4.2 Calculated induction machine magnetization curve.*

To find the magnetizing curve of the induction machine, the open circuit test is employed, and stator current and stator voltage are measured. To find the value of  $L_m$  in this test, the following equation is used:

$$L_m = \frac{V_{sa}}{\omega I_{sa}}$$

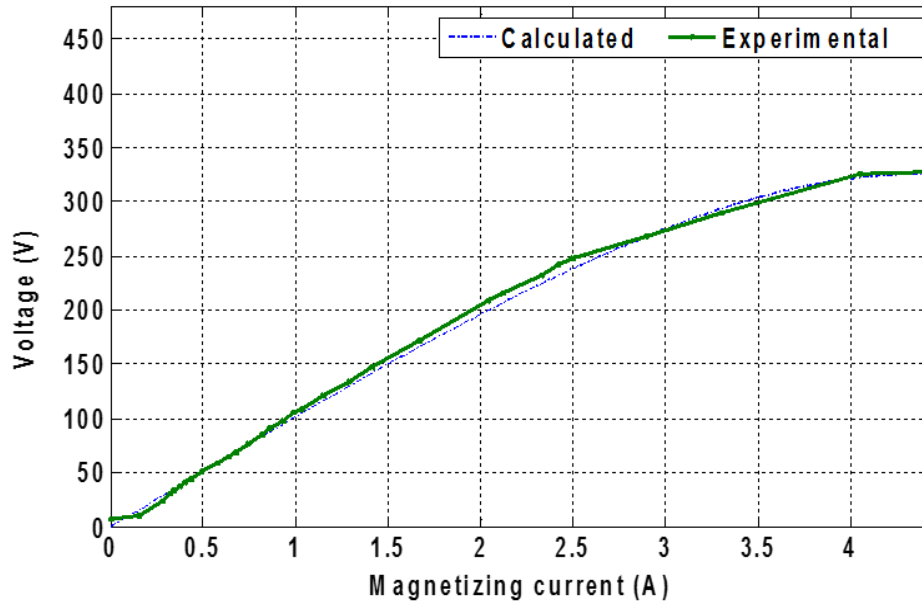


**Figure 4.3** Induction machine magnetization curve.

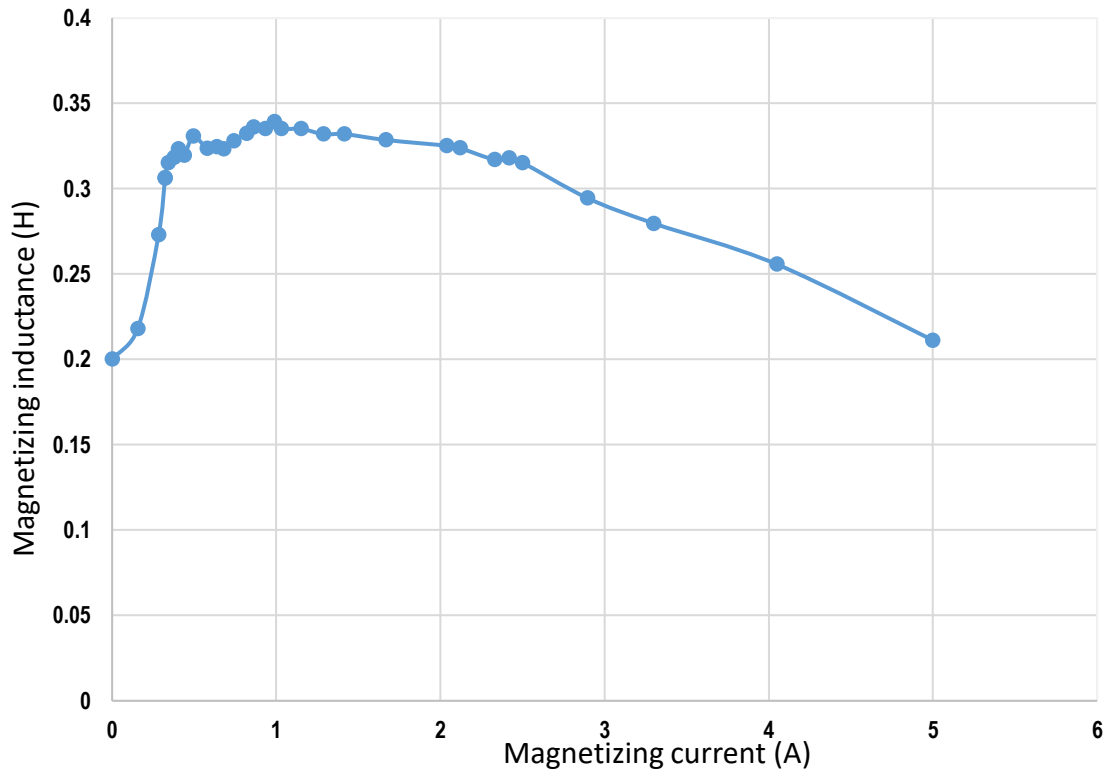
However, this method is not sufficient to obtain accurate results. The voltage shown in

Figure 4.3 is the air-gap voltage, which is the voltage across the magnetizing inductance and not the voltage across the stator terminals. If the stator voltage is measured, then the air-gap voltage can be calculated using the following equation:

$$V_g = \left( \sqrt{\frac{V_{sa}^2}{I_{sa}^2} - R_{sa}^2 - X_{ls}} \right) I_{sa} \quad (4.7)$$

where,  $V_g$  is the air-gap voltage across the magnetizing inductance;  $V_{sa}$  is the phase voltage measured across the stator terminals; and  $I_{sa}$  is the current measured in the stator windings.

Figure 4.4 shows the magnetizing inductance versus the magnetizing current. As can be noted that the magnetizing inductance begins with a small value then increases to reach a peak value before decreasing again as magnetizing current increases. The performance evaluation sequence is illustrated in the flowchart shown in Figure 4.5.



*Figure 4.4 Magnetizing characteristics of the induction machine under study.*

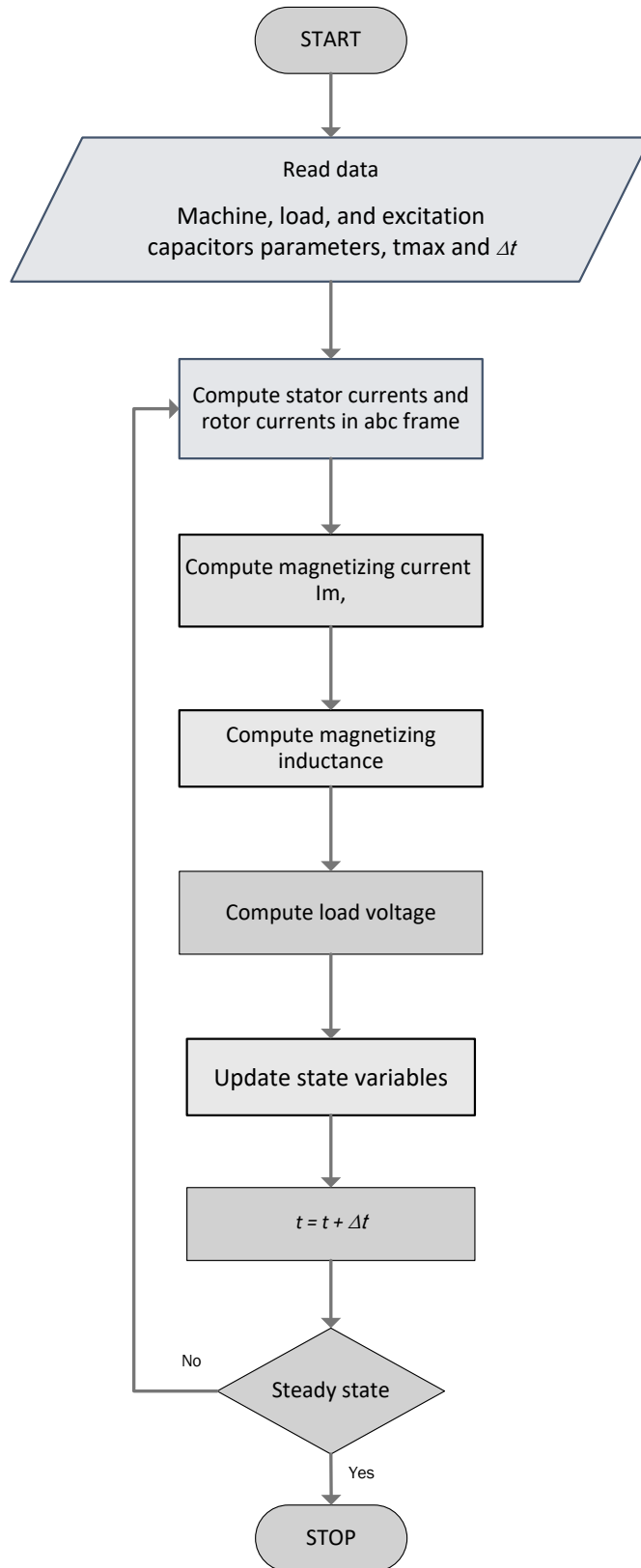


**Figure 4.5** Flow chart describing the performance evaluation.

#### 4.4 Conclusion

The saturation effects were taken by means of a variable magnetizing inductance. In other words, the magnetizing inductance is considered to be a function of the magnetizing current besides the displacement of the rotor. Hence, at each sampling step, the value of the magnetic inductance is adjusted according to the magnetizing current. To avoid the lengthy measurement process required in the conventional method of determining magnetizing inductance and to overcome the risk to machine integrity, an exponential function is employed to express the relationship between magnetizing inductance and magnetizing current. Very good agreement has been found between the calculated induction machine magnetization curve and the curve obtained experimentally.

# Chapter 5. The experimental system

## 5.1 Introduction

The three phase isolated induction generator system in this study is constructed of four main components: the prime mover, the induction machine (a 7.5kW, 415V, 50Hz, 4 pole, three-phase cage induction machine), the bank of excitation capacitors, and the load. The layout of the system under study is illustrated in Figure 5.1. The prime mover in this study is emulated by a DC motor which is coupled mechanically to the induction generator as shown in Figure 5.2.

The verification of the results obtained by the proposed model is a crucial process. The calculations resulting from the simulation implemented using the MATLAB–Simulink of Mathworks are then compared and validated against experimental results with the SEIG is running under different conditions such as no load and when it is loaded with a resistive load and/or an inductive load, or in steady state operation, load perturbation or in fault conditions.

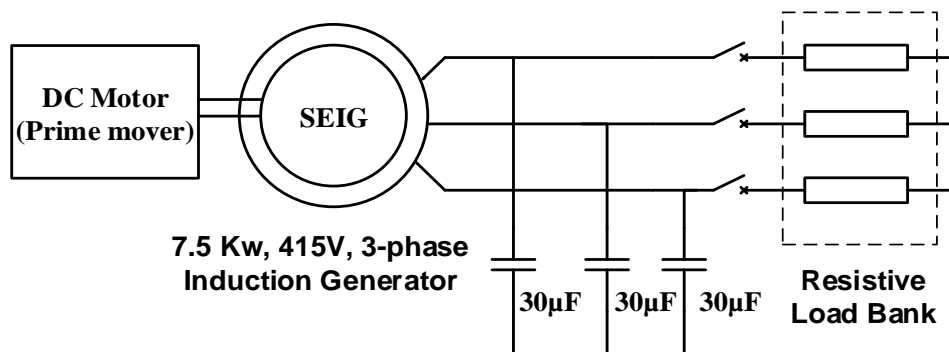


*Figure 5.1* Circuit diagram of the experimental setup.

A 7.5 kW, 415, V 50 Hz, 4-pole squirrel-cage induction machine with star connected windings, manufactured by Brook Hansen, is used as a self-excited induction generator.

The main objective of this chapter is to give an overview of the SEIG experimental test bench and its components, the devices used, the equipment mounted on the bench to construct this test rig and how it was set up. Additionally, the types and conditions in each test carried out in order to study the behaviour of SEIG and to validate the results obtained by simulation are described in this chapter.

The parameters of the induction machine under study are also identified and the procedures used in each test are clearly described. Popular and standard tests are employed to determine the parameters: a DC test, a no load test and a locked rotor test. The parameters of the induction machine are given in Table 5.4.

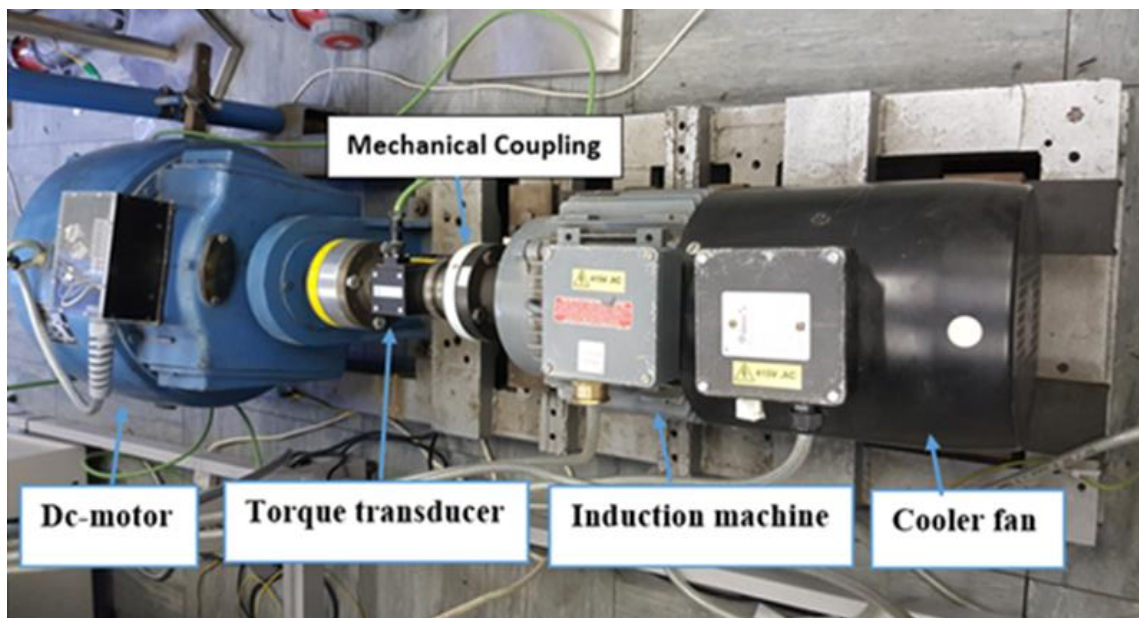


**Figure 5.2** Mechanical coupling between the SEIG and a DC motor for the system under study.

The magnetizing characteristics of the induction machine are among the most important parameters, and these are described clearly by explaining the aims and conditions of each test. The tests were carried out in the Power Electronic Machines and Drives Laboratory at Newcastle University.

## 5.2 The experimental system under study

The three-phase, star-connected squirrel-cage induction generator 7.5kW, 415V, 50Hz, 4 poles, used in this study is driven by a small wind/hydro turbine through a gearbox. The output terminals of the generator are connected to a star-connected capacitor bank for excitation purposes. The three-phase excitation capacitors are connected in parallel with a three-phase resistive load, and in parallel with an inductive load in some cases. Both the resistive and the inductive loads are star-connected. The configuration of this system under study was depicted in Figure 3.1.

Three-phase capacitors are connected to the stator terminals of the induction generator for excitation purposes. Variable capacitor values can be selected from the capacitor bank such that the minimum value shown on the nameplate is 5 $\mu$ F then 10  $\mu$ F, 20  $\mu$ F, 30  $\mu$ F per phase. An LCR meter is used in this study to measure the actual value of the capacitor. The experimental bench shown in Figure 5.3 is used in this study to test the SEIG model proposed in chapter 3 and to verify its accuracy. The induction generator is driven by a DC motor, 9 kW, 240 V, 37.5 A, maximum RPM 1800 rpm, armature: 240 V, 15 A, fields: 240 V, 0.6/0.16.

A DC-motor was coupled mechanically to the induction machine as shown in Figure 5.2 in order to emulate wind/hydro turbine operation. The speed of the DC motor (prime mover) was controlled by a DC-drive converter to run the generator at a constant speed, and to vary the speed if needed. In this work, it is assumed that the machine is symmetrical with sinusoidal flux. Therefore,  $L_{ms} = L_{mr} = L_{sr} = L_m$ , and the machine parameters are the same for all three phases.

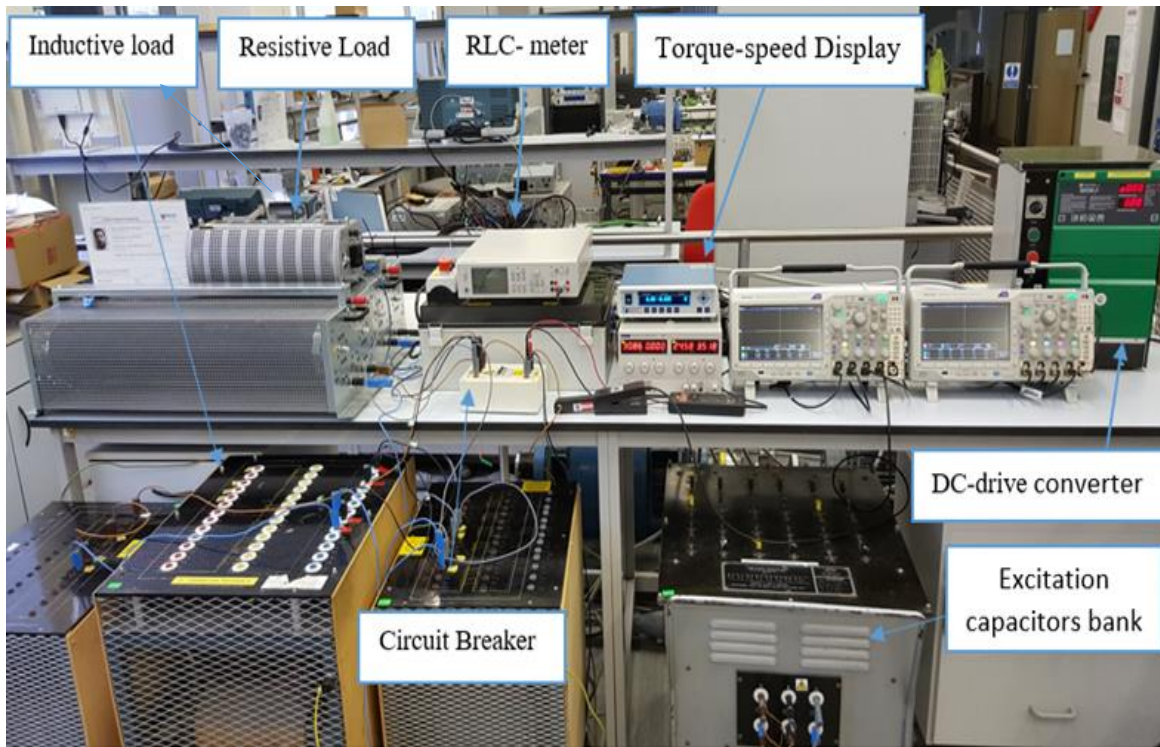


*Figure 5.3 Experimental bench for the system.*

The minimum value of the excitation capacitor which can trigger the process of the build-up voltage at no-load has been found using two mathematical methods. Using the first method [35] (equation 2.1), it was found that the minimum value in the no load condition is equal to approximately  $30 \mu\text{F}$ , whereas the minimum value given by the second method [69] (as shown in appendix B) is equal to  $25 \mu\text{F}$ . In the laboratory, the nameplate for the minimum excitation capacitor value in the no load condition is  $25 \mu\text{F}$ , but the actual value measured by the LCR meter was  $27 \mu\text{F}$  (where minimum tab value possible in the lab is  $5 \mu\text{F}$ ). In our case, it is clear that the second method is more accurate.

It is recommended that a capacitor value more than the critical value should be used. For this reason,  $30 \mu\text{F}$  has been used for the resistive load, while  $37 \mu\text{F}$  is used for the L-R Load.

### 5.3 Determination of induction machine parameters

The identification of the parameters of the induction machine is important in this study in order to represent accurately all of the characteristics of the physical machine in the Matlab-Simulink environment. The most common ways to experimentally obtain the equivalent circuit parameters for induction machine are to use a standard DC test, a no load test, and a locked rotor test. These tests were carried out according to IEEE standards [105]. The objective of the DC test is to obtain the stator resistance value, and the objective of the no load test is to calculate the core losses and magnetising inductance, while the stator and rotor resistance and stator and rotor leakage inductances are obtained from the locked rotor test. The following sections give details of the results obtained using these tests.

#### 5.3.1 DC test

This test is used to obtain the stator resistance which represents the copper losses in the stator. This test can be conducted when the motor is at standstill, and the DC voltage supply  $V_{dc}$  is applied until a current flows in the induction machine windings. The readings are then taken when the current reaches approximately the rated value.

Voltage (v)	I (A)	$R_s$ ( $\Omega$ )
59.49	12.55	2.330
59.52	12.50	2.380
59.48	13.30	2.236
59.10	12.45	2.373
The average value of $R_s$		2.330

**Table 5.1** Results of the DC test.

The stator resistance per phase can be calculated as  $R_1 = \frac{V_{dc}}{2I_{dc}}$ , because the connection of the stator is star-connected. The test should be implemented when the machine has heated up. The

results of this test is shown in Table 5.1.

### 5.3.2 Locked rotor test

The aim of this test is to determine the value of rotor winding resistance,  $R_r$ , stator leakage reactance  $X_s$  and rotor leakage reactance  $X_r$  when the rotor is locked ( $n_r = 0$ ), and so the slip is equal to unity ( $s = \frac{n_s - n_r}{n_s} = \frac{n_s - 0}{n_s} = 1$ ). Since the excitation current is very small compared to  $I_r$ , the shunt branch in the equivalent circuit of the induction machine which represents magnetization is neglected. Hence, the equivalent circuit is as shown as in Figure 5.4. According to the IEEE standard test procedure [105], this test should be conducted at 25% of the rated frequency using an ET system variable voltage, variable frequency three-phase AC power supply,  $3 \times 2000\text{VA}$ ,  $3 \times 0 \sim 270\text{V}$ ,  $3 \times 15\text{A}$ .

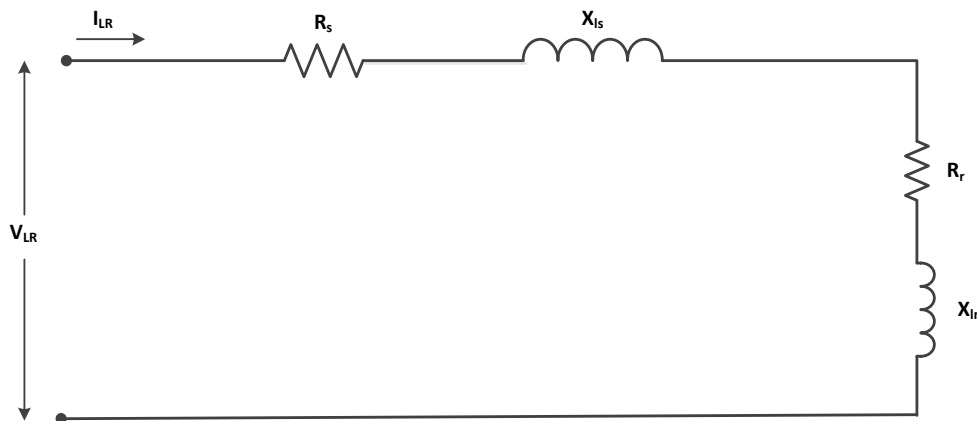


**Figure 5.4** Approximate equivalent circuit for the locked rotor test.

Reading 1

$P_1 = 1345 \text{ Watt}$        $P_2 = 715 \text{ Watt}$       @  $f = 12.55 \text{ Hz}$

$V_{L-L} = 106.2\text{V}$        $I_{L-L} = 12.46 \text{ A}$

$$P_T = P_1 + P_2 = 1345 + 715 = 2065 \text{ Watt}$$

$$R_{L0} = \frac{P_T}{3I_L^2} = 2065 / (3 \times 12.46^2) = 4.433 \Omega$$

$$R_2 = R_{L0} - R_1 = 4.433 - 2.33 = 2.11 \Omega$$

$$Z = \frac{V_{PH}}{I_L} = \frac{106.2/\sqrt{3}}{12.46} = 4.921 \Omega$$

$$X_{L12.5\text{HZ}} = \sqrt{Z^2 - R_{L0}^2} = \sqrt{4.92^2 - 4.433^2} = 2.136 \Omega$$

$$X_{L12.5\text{HZ}} = X_{L12.5\text{HZ}} \times \frac{50}{12.55} = 8.513 \Omega = X_1 + X_2$$

$$\text{So } X_1 = 4.2565 \Omega = X_2$$

$$\text{And } L_1 = \frac{4.2565}{2 \times \pi \times 50} = 13.5487 \text{ mH} = L_2$$

$$P_1 = 1345 \text{ Watt} \quad P_2 = 715 \text{ Watt} \quad @ f = 12.55 \text{ Hz}$$

$$V_{L-L} = 106.2 \text{ V} \quad I_{L-L} = 12.46 \text{ A}$$

where  $P_1$  and  $P_2$  are the readings of Wattmeters number 1 and 2 respectively. Table 5.2 shows the other readings:

Reading	$P_1$ (Watt)	$P_2$ (Watt)	$I_{L-L}$ (A)	$V_{L-L}$ (V)	F (Hz)	$R_2$ ( $\Omega$ )	$L_1$ (mH)	$L_2$ (mH)
1	1345	715	12.46	106.2	12.55	2.11	13.54	13.54
2	1298	759	12.54	105.63	12.55	2.03	13.37	13.37
3	1309	718	12.20	106.36	12.50	2.21	13.8	13.8
4	1420	730	12.86	107	12.5	2.00	13.2	13.2
The average value for the above readings						2.1	13.5	13.5

**Table 5.2:** Results of the locked rotor test.

### 5.3.3 No load test

The no load test is used to find the magnetising reactance,  $X_m$  and the stator core losses due to hysteresis and eddy current. This test was conducted by applying a balanced poly-phase rated voltage and the rated frequency on the stator. The speed of the rotor is almost equal to the synchronous speed ( $n_r \approx n_s = 1500$  rpm) because the rotor is allowed to rotate at no load and so the slip will be very small ( $s = (n_s - n_r) / n_s \approx 0$ ). As a result, the rotor branch in the equivalent circuit can be omitted; i.e. an open circuit. Consequently, the equivalent circuit for the no load test can be approximated as shown in Figure 5.5. Thereafter, the values of current, voltage and power were measured at the stator terminals, and these measurements are shown below in detail.

$$P_1 = 480 \text{ Watt} \qquad P_2 = 325 \text{ Watt} \qquad @ f = 50 \text{ Hz}$$

$$I_{L-L} = 2.01 \text{ A} \qquad V_{L-L} = 415 \text{ V}$$

$$P_T = P_1 + P_2 = 805 \text{ Watt}$$

$$S = \sqrt{3} IV = \sqrt{3} \times 2.01 \times 415 = 1444.79 \text{ VA}$$

$$Q_{3\text{ph}} = \sqrt{S^2 - P^2} = \sqrt{1444.79^2 - 805^2} = 1199.747 \text{ VARs} \quad \text{or} \quad Q_{1\text{ph}} = 399.9157 \text{ VARs}$$

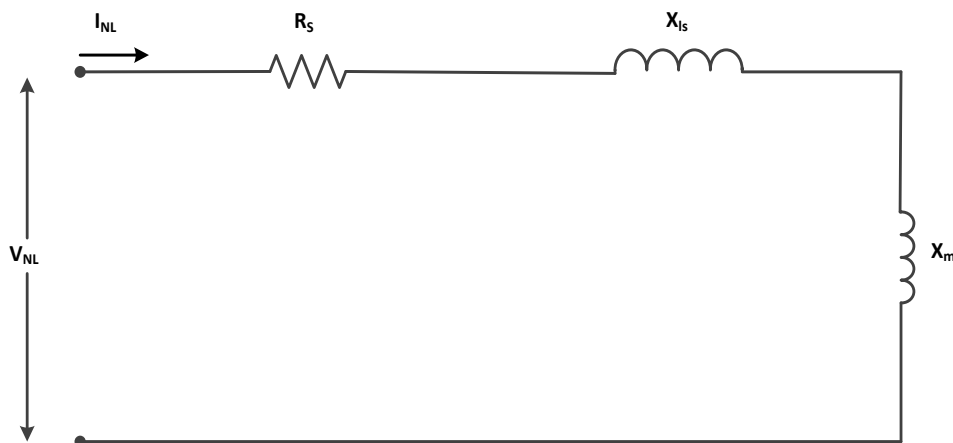


*Figure 5.5 Approximate equivalent circuit for no load test.*

From:

$$Q = I^2 X_{nl}$$

$$X_{nl} = \frac{Q}{I^2} = \frac{399.916}{2.01^2} = 98.9866 \Omega$$

$$X_{nl} = X_1 + X_m$$

$$X_m = X_{nl} - X_1 = 98.9866 - 4.2565 = 94.7301 \Omega/\text{Phase}$$

Or :

$$L_m = \frac{X_m}{2\pi 50} = 301.535 \text{ mH}$$

Reading	P <sub>1</sub> (Watt)	P <sub>2</sub> (Watt)	I <sub>L-L</sub> (A)	V <sub>L-L</sub> (V)	F (Hz)	L <sub>m</sub> (mH)	R <sub>c</sub> (Ω)
1	480	325	2.01	415	50	301.535	64.1
2	530	320	1.90	415	50	301.37	76.15
3	525	320	1.94	415	50	298.85	72.51
Average						300.585	70.92

**Table 5.3:** Results of the no load test.

From the above tests the parameters of the induction machine can be given as shown in Table 5.4.

<i>Machine parameter</i>	<i>Value</i>
$R_{sa}, R_{sb}, R_{sc}$	$2.33 \Omega$
$R_{ra}, R_{rb}, R_{rc}$	$2.11 \Omega$
$L_{lsa}, L_{lsb}, L_{lsc}$	$13.54 \text{ mH}$
$L_{lra}, L_{lrb}, L_{lrc}$	$13.54 \text{ mH}$
$L_m$	$300.58 \text{ mH}$

**Table 5.4:** Induction machine parameters.

#### 5.4 Magnetizing characteristics

The saturation curve of the induction machine can be obtained by driving the rotor of the induction machine at a constant speed corresponding to the synchronised speed of the machine at 50 Hz using a DC motor, while a variable sinusoidal voltage at 50 Hz is applied to its stator terminals [59]. To provide the induction machine with a three-phase variable voltage, a three-phase autotransformer is used as a variable voltage source with maximum winding current of 20 A and maximum winding voltage 270V. This is not like the open circuit test used to find the machine parameters, and the induction machine should be driven at the synchronised speed so that the slip will be very small (almost zero), which implies that the rotor branch in the equivalent circuit (EC) of the induction machine can be neglected. As a result, the rotor current will be zero, since the magnetising current is the difference between the stator current and the rotor current referred to the stator. Therefore, the magnetising current will equal the stator current if the core losses are ignored. To maintain the rotor speed at synchronise speed is in practice quite difficult, especially when high values of current are reached. In practice, it is not only difficult to obtain accurate results at this stage but also the machine becomes unstable and its integrity may be effected [99].

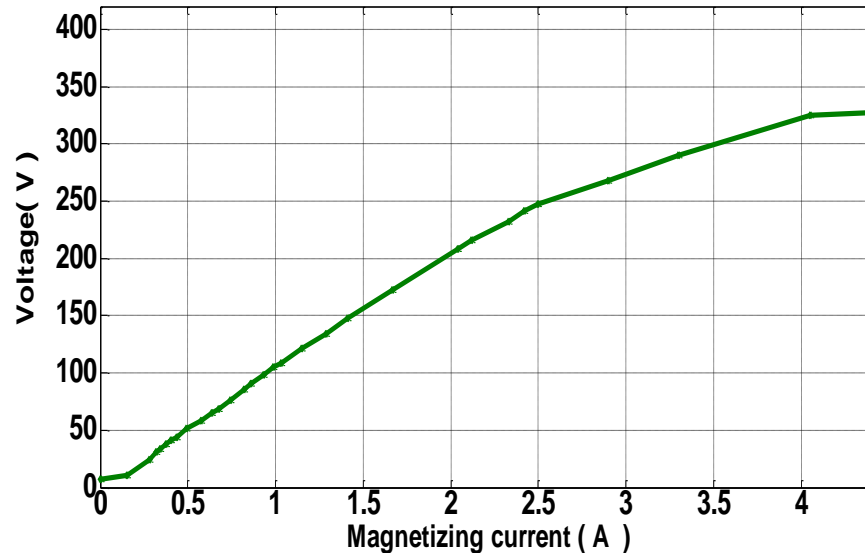


*Figure 5.6 Magnetization characteristics for the 7.5 kW induction machine.*

### 5.5 Speed measurements

The speed of the DC motor used to emulate the prime mover in this study was controlled by a DC-drive converter, 1.5 kW, Mentor II (more details are shown in appendix C) to emulate wind/hydro turbine operation at a constant speed. This speed is measured using an encoder and torque display model number TM 210, TORQUEMASTER Vibro-Meter with rated torque 50 N.m and a pulse wheel of 30 pulses/Rev. The shaft speed was measured and used as the input speed vector in the simulation model in order to account for any small vibrations around the average constant speed caused by the DC drive harmonics or the mechanical vibration of the test induction generator. If the variable speed or a sudden change in the speed was required to be emulated, a DC-drive converter could be employed to achieve this manually.

### 5.6 Conclusion

The experimental bench components and layout have been described in this chapter. The methods and procedures for identifying the parameters of the induction machine have been explained. The parameters of the EC for the induction machine have been found by carrying out the traditional DC test, open load, and locked rotor tests. The magnetizing characteristic of

the induction machine under study have been identified. The calculated results from simulation implemented in Matlab-Simulink rely on this identification. Therefore, error in the results obtained in the laboratory can lead to error in the simulation results. Hence, it is necessary to determine these parameters as accurately as possible. So the IEEE standards have been followed in conducting these experiments.

# Chapter 6. Simulation results and experimental validation

---

## 6.1 Introduction

A numerical simulation using Matlab-Simulink has been developed in order to solve the proposed mathematical model presented in chapter 3. More than fifty parameters are required for the simulation (for instance, the stator and rotor winding resistances in the three phases, the mutual inductance between the three-phase stator winding and rotor winding, and so on). In addition, many differential equations used to simulate the induction machine, load, and excitation capacitors need to be modelled and solved. In such a complex environment, it is likely that mistakes can be made. Hence, it is important to validate the results accomplished using Matlab-Simulink against the results achieved in the lab. Additionally, the experimental results will be used as a reference to verify the accuracy of the mathematical representation of the SEIG.

The simulation is used to investigate the performance of the SEIG in the no-load condition and when the generator is loaded with a pure resistive load and resistive and inductive loads at steady-state and during transient behaviour when the load is balanced, and unbalanced. Furthermore, in order to show the capability of the new model in predicting the performance of the self-excited induction generator under very stressful conditions, its performance is investigated in the presence of different types of faults, the decay of the terminal voltages with heavy loads and with different levels of load perturbation. The values of capacitance, resistive load, and inductive load were chosen based on the rated values of the induction machine, the minimum value of the capacitors required to ensure self-excitation and the limitations in the laboratory, for instance, the maximum load current allowed to pass in the resistor and the rated voltage that can be applied to the inductive load. The root mean square error ( $RMS_e$ ) will be used to measure the difference (the error) between values predicted by the proposed model and values obtained by experiment as follows:

$$RMS_e = \sqrt{\frac{1}{n} \sum_{i=1}^n (x_i - y_i)^2} \quad (6.1)$$

where,

x is the results obtained experimentally.

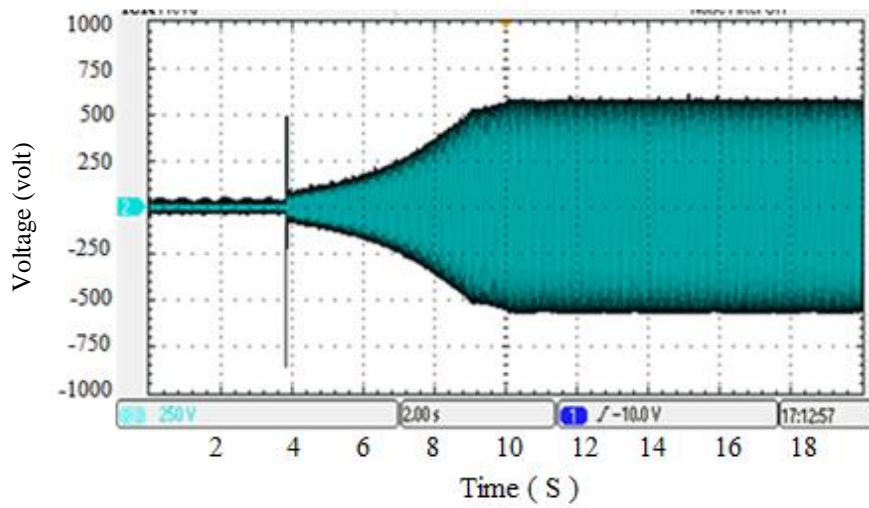
y is the results predicted by the mathematical model.

## 6.2 No-load results

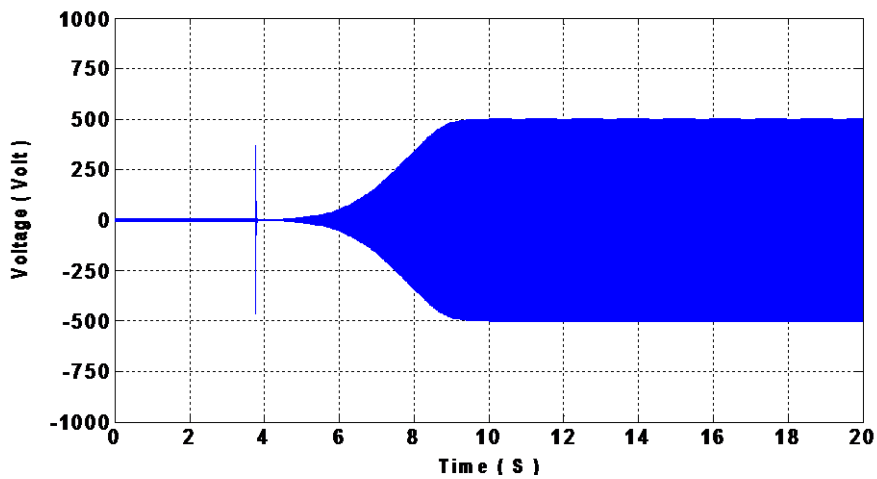
The waveforms of the stator output voltages, stator currents, flux and other parameters are obtained, in this case, when the SEIG is in the no-load condition. In this state, only the excitation capacitors are connected to the terminals of the induction generator. The excitation capacitors are connected to the generator through a three-phase circuit breaker, to be switched when the SEIG reaches the steady state and is running at the required speed.

For the induction machine used in this investigation, the minimum per phase excitation capacitance for the successful build-up of the SEIG's voltage was calculated to be 25 $\mu$ F at no load. A capacitor of 30 $\mu$ F was used in the load tests described in this study in order to give the reactive power needed by the generator in the case of only a resistive load is used. If an inductive load is added, the excitation capacitor should be increased to 37 $\mu$ F to cover the increase in demand for reactive power. The speed of the DC motor/prime mover was controlled by a DC-drive converter to emulate wind/hydro turbine operation at constant speed.

Figure 6.1 shows the measured and simulated voltage build-up process of the induction machine (for phase a) when the excitation capacitors are switched on ( $C_a=C_b=C_c= 30 \mu$ F) at  $t=1.8$  sec while the SEIG is running at no-load at a speed of 1450 rpm (with this speed being determined by the choice of available power capacitors at the time of carrying out these experiments), The experimental result is shown in Figure 6.1 a, while the predicted behaviour of the stator terminal voltage is depicted in Figure 6.1 b. As shown, a good agreement is achieved between the model results and the measurements in terms of the value of terminal voltage ( $RMS_e= 35.61$ ) and the time taken to complete the process.



(a)

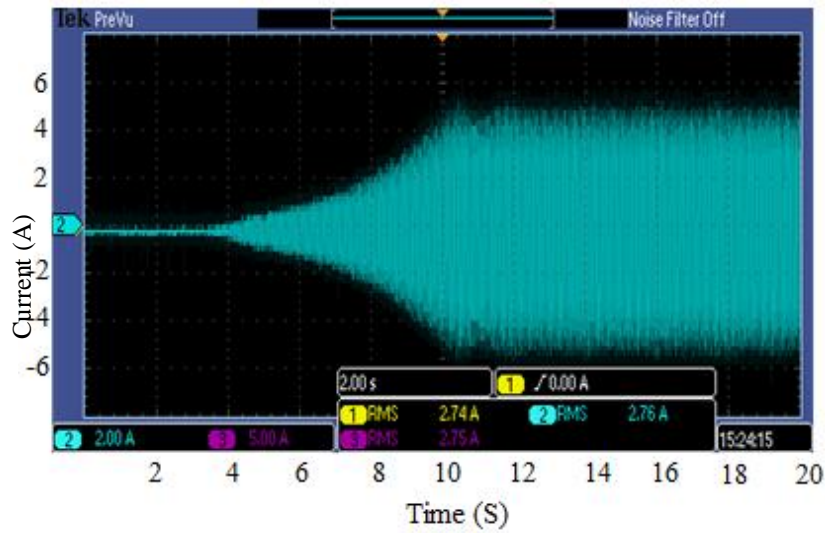


(b)

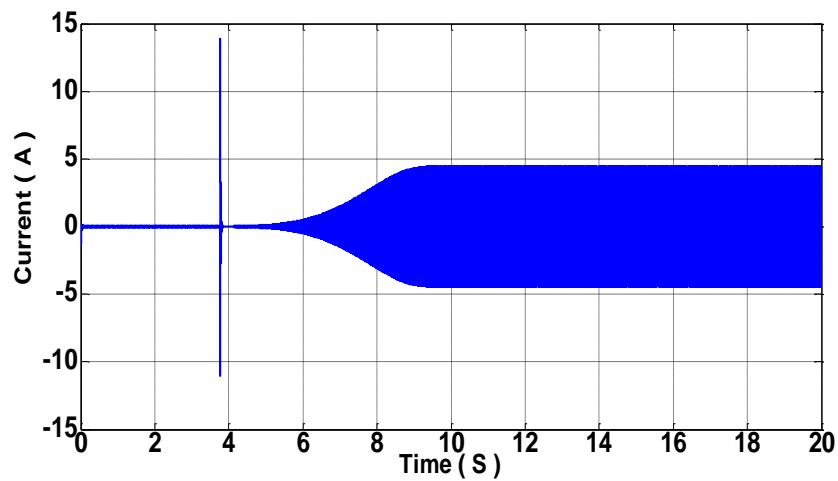
**Figure 6.1** Measured phase voltage (a); calculated phase voltage (b), during the build-up process of the SEIG at  $C = 30 \mu\text{F}$  per phase and 1450 rpm.

The experimental and simulated build-up process of the phase current of the SEIG for the above considered case is shown in Figure 6.2 a and Figure 6.2 b respectively. As shown, a high level of agreement is apparent between the experimental and calculated results ( $RMS_e =$

0.2121).



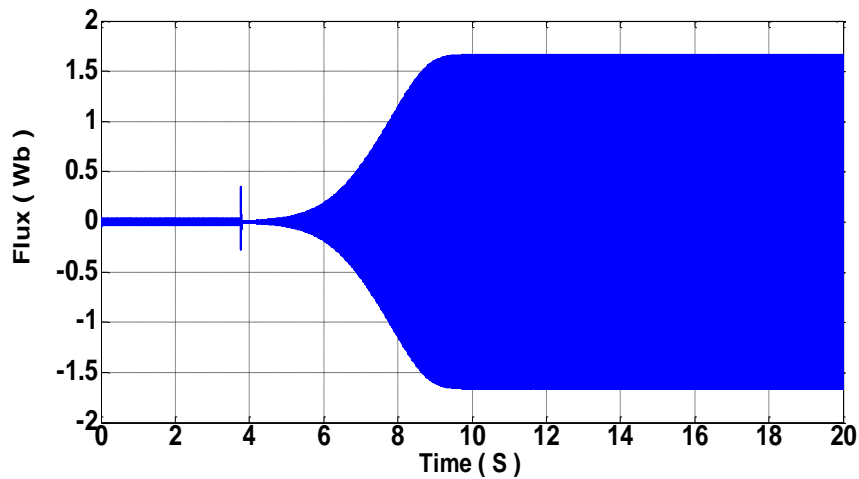
(a)



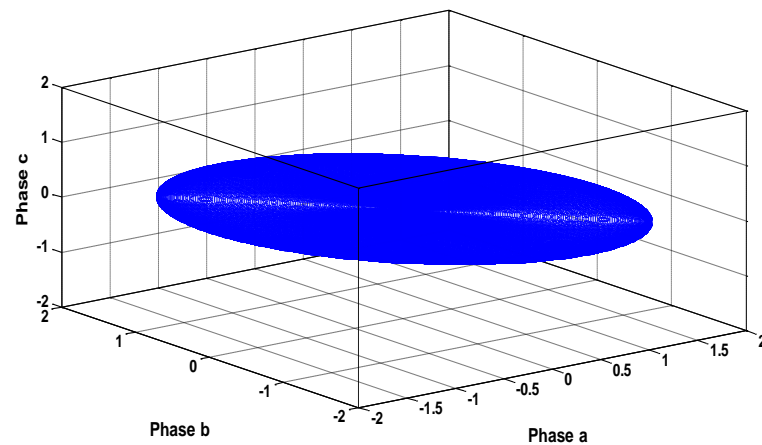
(b)

**Figure 6.2** Measured phase voltage (a) and calculated phase current (b), during the build-up process of the SEIG at  $C = 30 \mu\text{F}$  per phase and 1450 rpm.

The variation in the calculated flux in the stator winding phase-a during the build-up process under the same conditions is shown in Figure 6.3 a. It can be seen that the flux acts in the same way as the voltage and current during the build-up process as well as taking the same time to reach the steady state condition. The waveform of the flux of the three-phase stator winding is illustrated in Figure 6.3 b. It can be observed that the flux is rotating since the machine is in a balanced condition which means its magnitude value is constant whereas its phase angle is rotates as the rotor displacement changes.



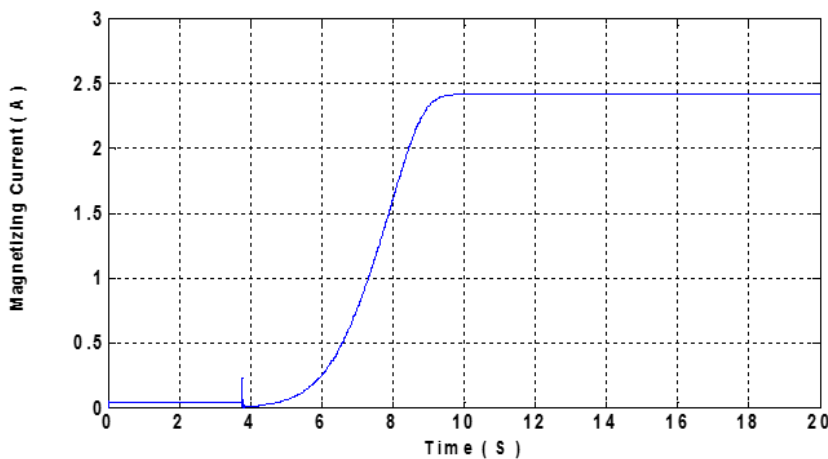
(a)



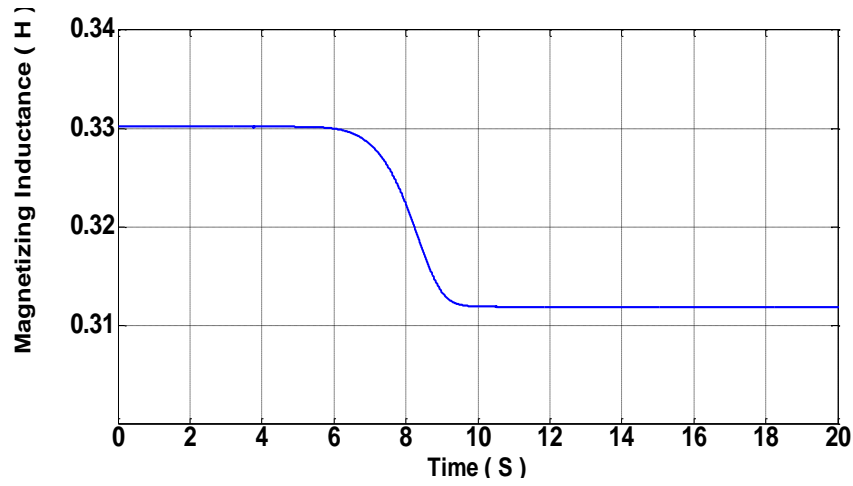
(b)

**Figure 6.3** The variation of the flux in the stator windings during the build-up process of the SEIG at  $C = 30 \mu F$  per phase and 1450 rpm: (a) phase a (b) in a three-dimension (abc frame).

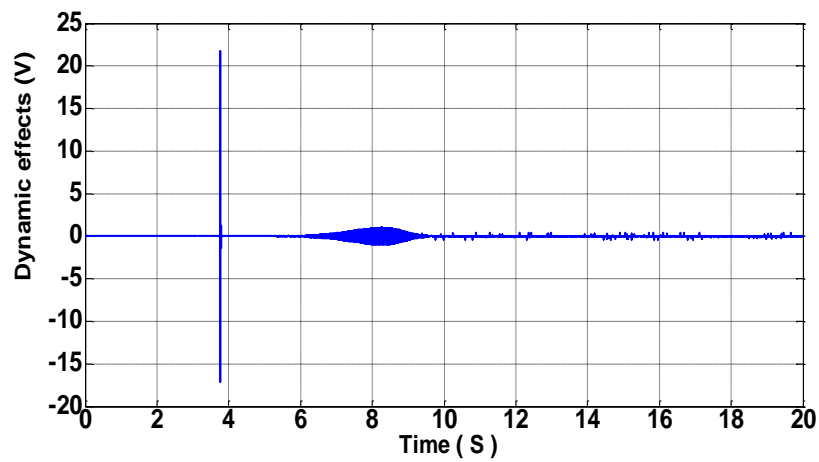
The variation in the magnetizing current during the voltage build-up processes is shown in Figure 6.4 a, whereas the change in the magnetic inductance with time during the self-excitation process is illustrated in Figure 6.4 b. From both graphs, it can be observed that the magnetizing inductance decreases as the magnetizing current increases, which agrees with the results presented in chapter 4 (section 4.3, Figure 4.4). In addition, it can be seen from Figure 6.4 a that the magnetizing current acts in the same way as the voltage, current and flux during the build-up process. Changes in the derivative of the magnetizing inductance with respect to the magnetizing current (i.e., the dynamic inductance) for the stator and the rotor are shown in Figure 6.4 c, and 6.3 d respectively. The waveform in Figure 6.4 c is produced by the first row in the dynamic matrix in equation 3.45 (in Chapter 3), whereas the waveform in Figure 6.4 d is produced by the fourth row of the same matrix. Both waveforms clearly demonstrate that the dynamic inductance does not have any significant effect on the steady-state operation of the induction generator. However, its effect during the dynamic response when the induction generator is building up its output voltage is considerable.



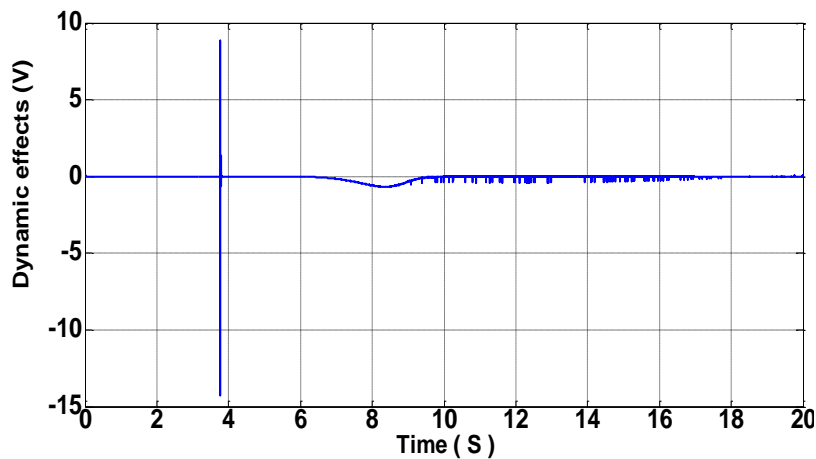
(a)



(b)



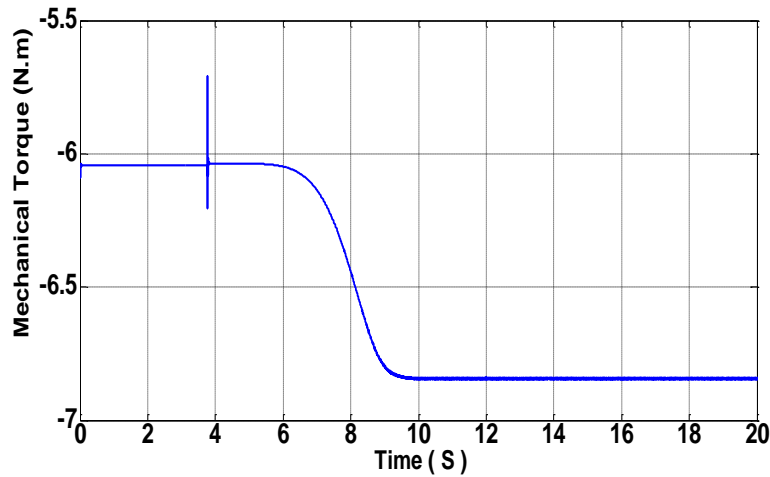
(c)



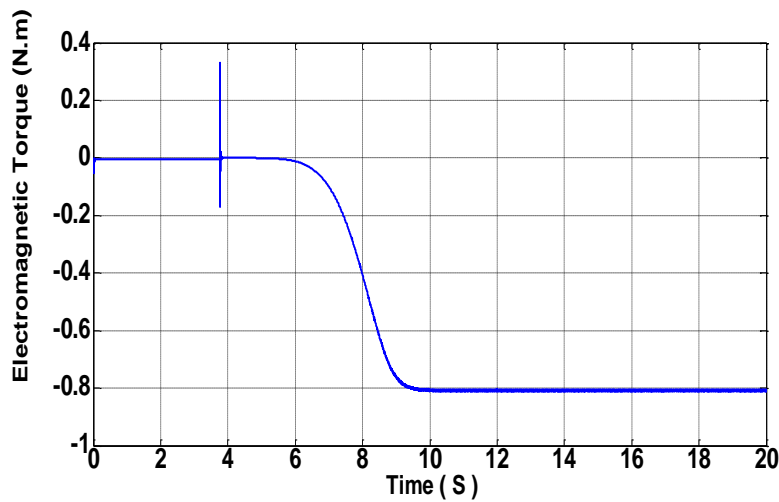
(d)

**Figure 6.4** Variation in: (a) magnetizing current; (b) magnetizing inductance; (c) dynamic inductance in stator phase a; (d) dynamic inductance in the rotor phase a, during the build-up process of the SEIG at  $C = 30 \mu\text{F}$  per phase and 1450 rpm.

The behaviour of the mechanical and electromagnetic torque of the SEIG during the build-up process with a phase voltage at  $C= 30 \mu F$  per phase and 1450 rpm is shown in Figure 6.5. It is clear that both types of torque act in a similar way.



(a)



(b)

**Figure 6.5** Variation in: (a) mechanical torque and (b) electromagnetic torque during the build-up process of the phase of the voltage of the SEIG at  $C= 30 \mu F$  per phase and 1450 rpm.

Figure 6.6 shows the measured steady-state stator generated voltage and current waveforms at a rotor speed of 1450 rpm together with the simulation results obtained from the proposed model. Excellent agreement can be observed between the calculated and measured waveforms ( $RMS_e = 0.1850$ ). According to the experimental work carried out in this study, the load should stay disconnected during the self-excitation process until the generator reaches the steady state condition in order to ensure a successful and smoothly build-up process of a SEIG.

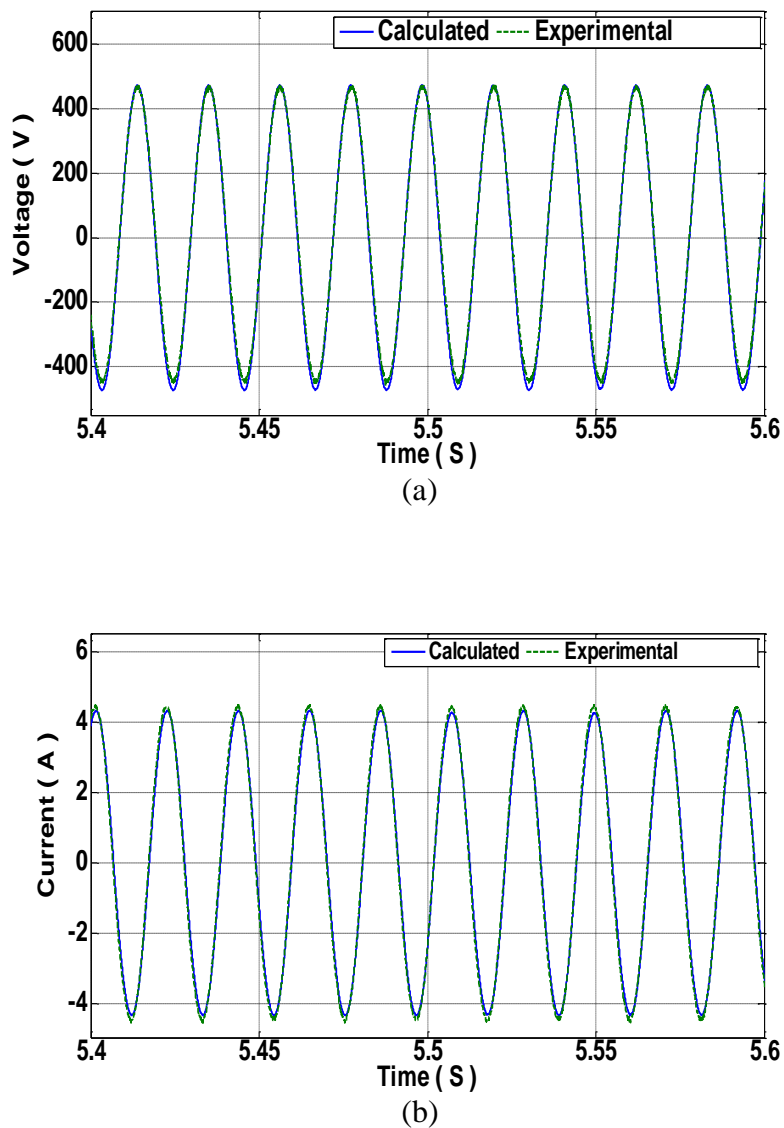
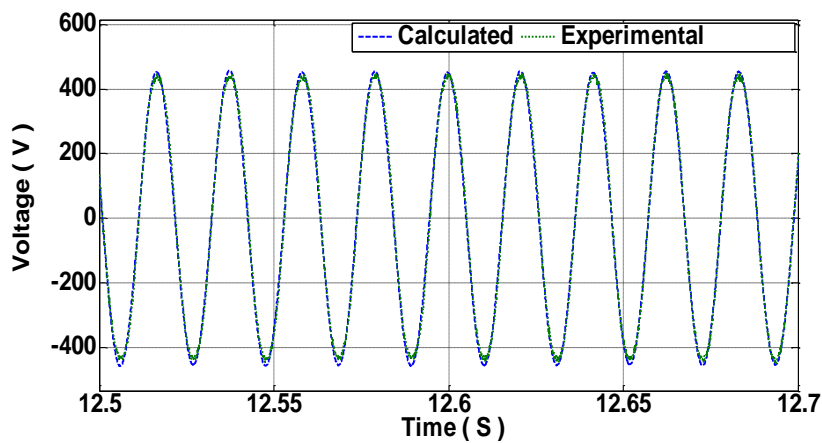


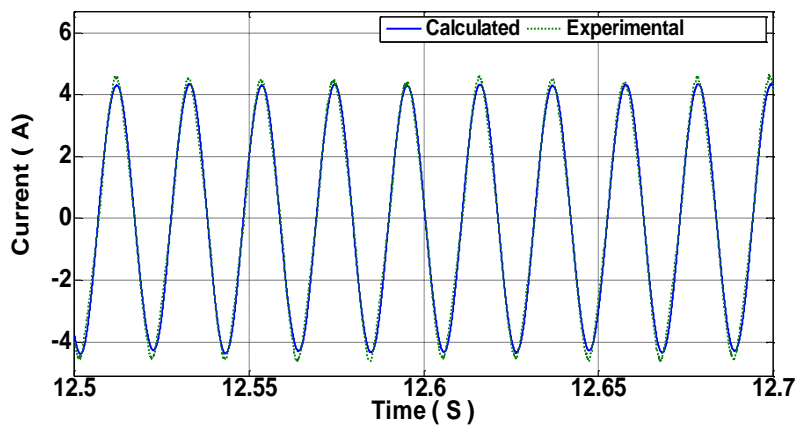
**Figure 6.6** No-load generated voltage and current waveforms at 1450 rpm;  $C=30\mu F$  per phase.

### 6.3 Balanced load results

Steady-state stator voltage and current waveforms when the SEIG is loaded with  $500\ \Omega$  per phase and running at a rotor speed of 1450 rpm and with excitation capacitance of  $30\ \mu\text{F}$  per phase are shown in Figure 6.7. Excellent agreement is demonstrated between the experimental measurements and the results obtained from the proposed model in terms of both magnitude and frequency ( $RMS_e = 0.2632$ ).



(a)

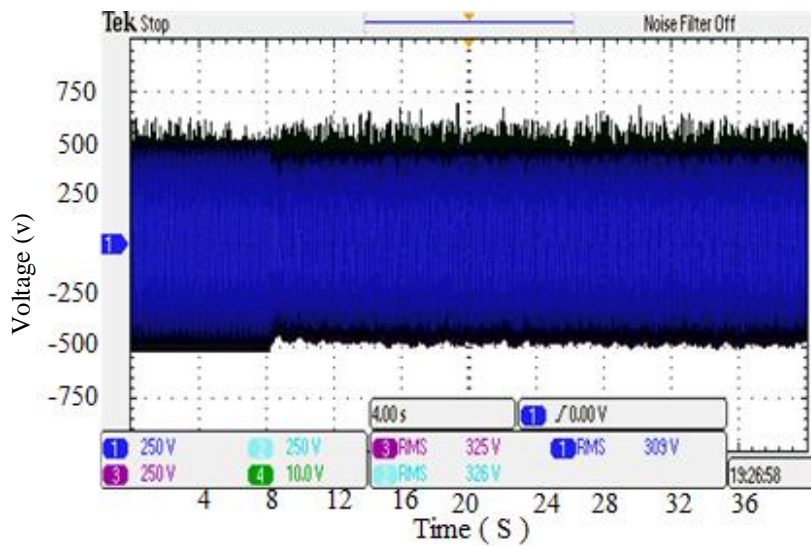


(b)

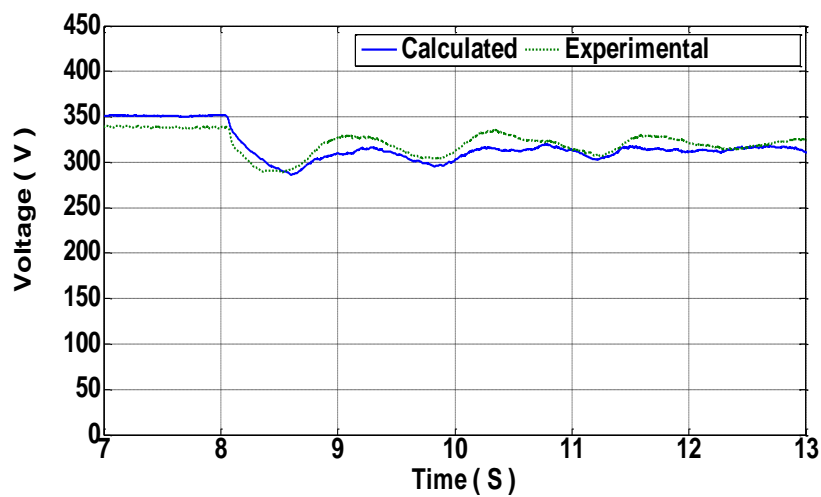
**Figure 6.7** Steady-state generated voltage (a) and current (b) waveforms with a balanced resistive load of  $500\ \Omega$  per phase,  $C = 30\ \mu\text{F}$  per phase.

To examine the transient performance of the SEIG when loaded, a balanced three-phase, star-connected resistor-load ( $500\Omega$  per phase) was connected to the stator terminals while operating at no load. The SEIG remains excited; however, it may suffer from de-excitation if excessive load is added as demonstrated later in section 6.5.

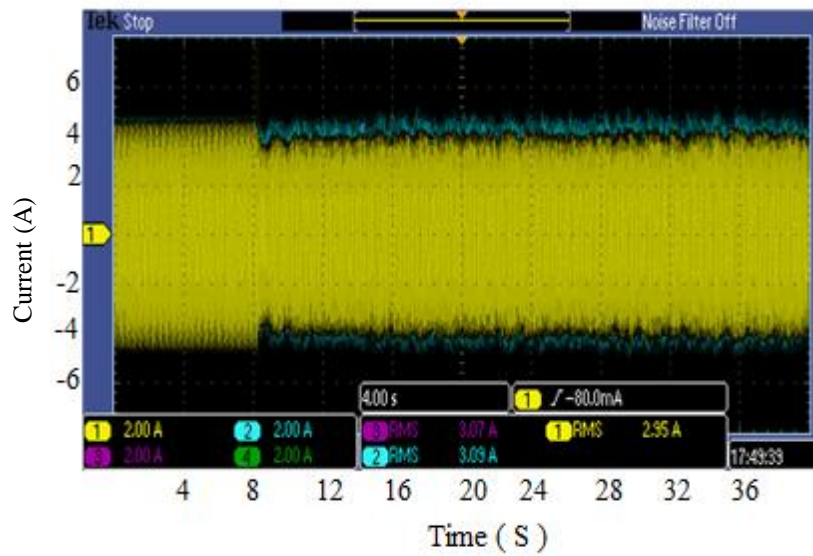
Figure 6.8 shows the rms values of the generated voltage and current, illustrating the transient response of the SEIG following the sudden connection of the load resistors. It can be observed that the proposed model accurately predicts the behaviour of the induction generator during the dynamic response with ( $RMS_e = 0.2778$ )



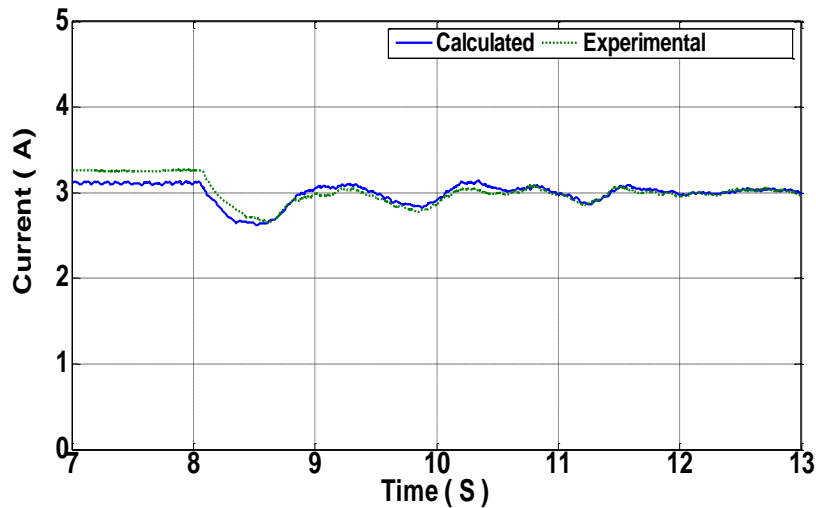
(a)



(b)



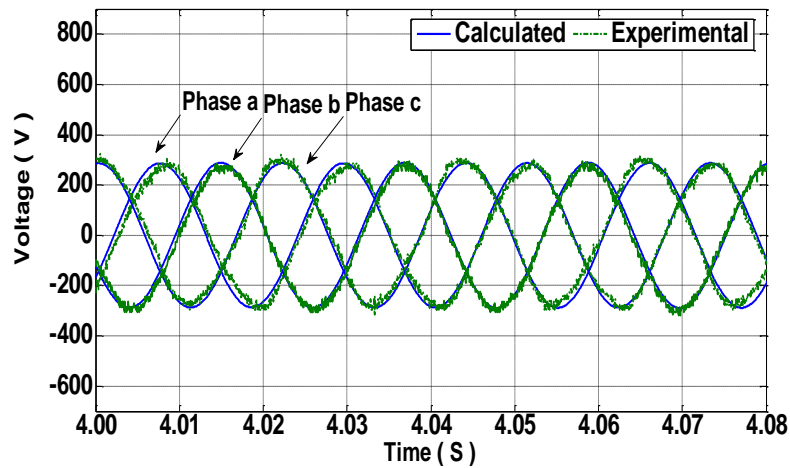
(c)



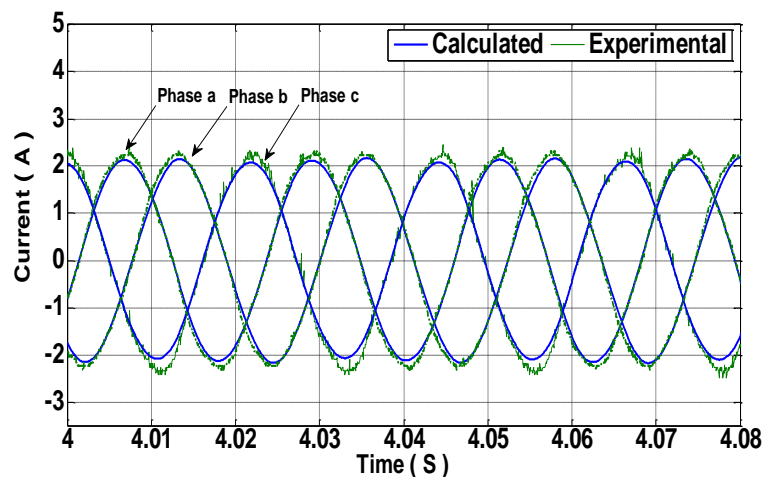
(d)

**Figure 6.8** Waveforms of phase voltage (oscilloscope screenshot) (a); phase voltage (rms) (b); phase current (oscilloscope screenshot) (c) and phase current (rms) (d) during switching on a balanced load at 8.1 seconds;  $R=500\Omega$  per phase.

Further results for a balanced load are shown in Figure 6.9. This time, the load is an R-L load such that  $R=365\Omega$  per phase and  $L=1\text{ H}$  per phase and both are connected in a star connection as shown in Figure 6.10. In addition, the excitation capacitance is increased to  $37\text{ }\mu\text{F}$  in order to cover the reactive power consumed by the inductive load besides the demand by the induction generator for excitation. The calculated steady-state generated voltage and current waveforms give good agreement with those obtained experimentally ( $RMS_e=0.0961$ ).

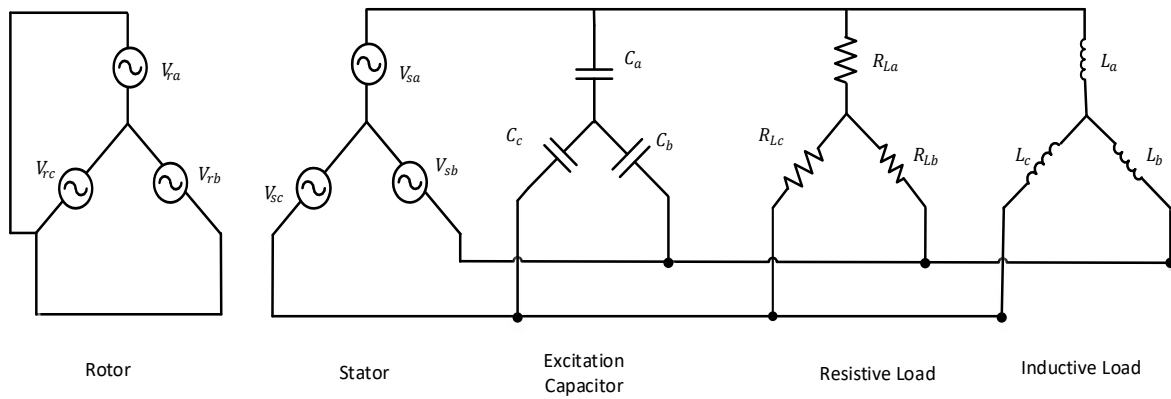


(a)



(b)

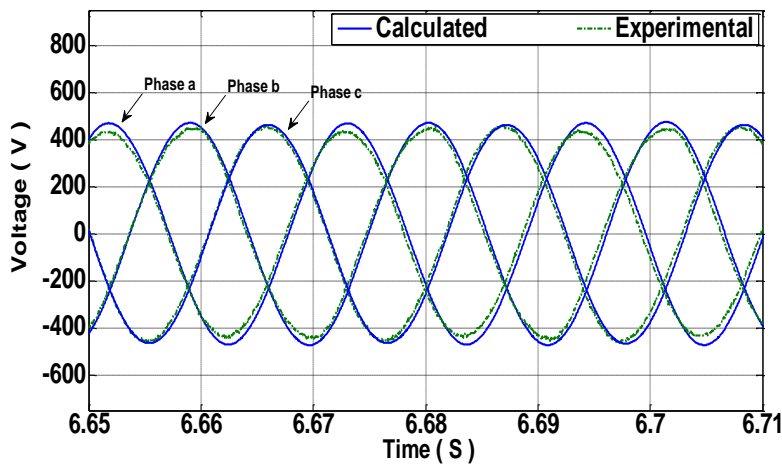
**Figure 6.9** Steady-state generated voltage (a) and current (b) waveforms with a balanced R-L load,  $R=365\Omega$  per phase,  $L=1\text{H}$  per phase,  $C=37\mu\text{F}$  per phase.

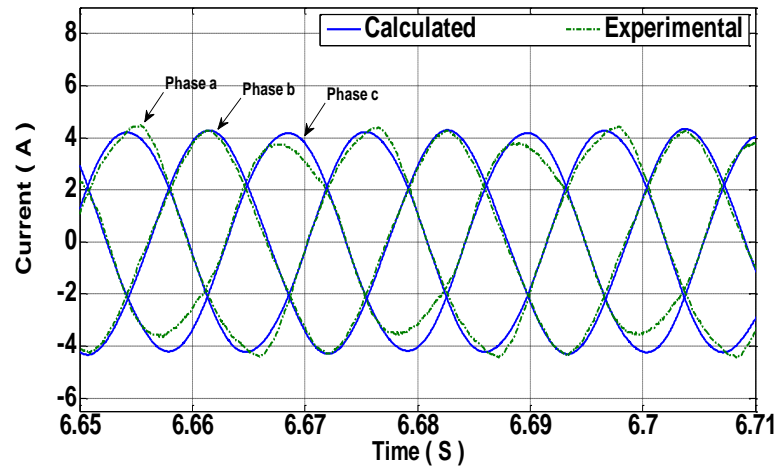


**Figure 6.10** Configuration of the system under study when R-L load is connected.

#### 6.4 Unbalanced-load results

In this section, the performance of the SEIG during operation with an unbalanced load is tested and demonstrated. Operation with an unbalanced load is shown in Figure 6.11. In this test, an unbalanced resistive load ( $R_{la} = R_{lb} = 620\Omega$  and  $R_{lc} = 500\Omega$ ) is applied at the SEIG generator terminals. Excellent prediction performance is achieved here for both current and voltage.

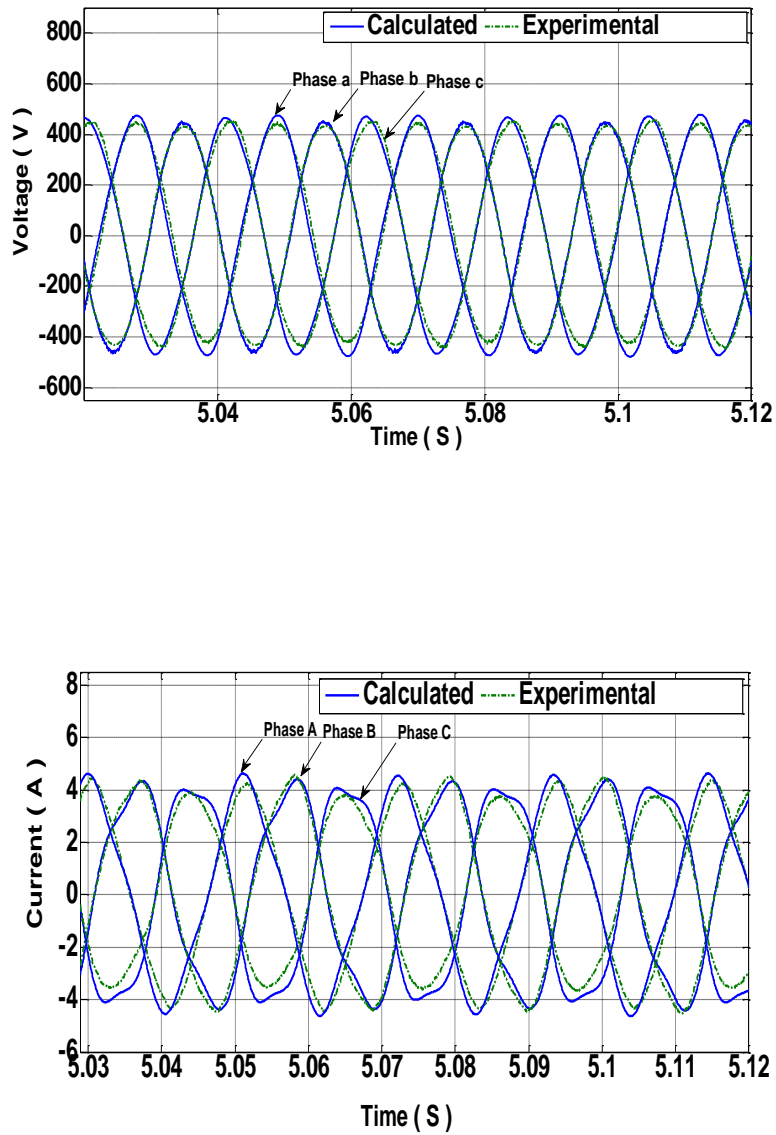




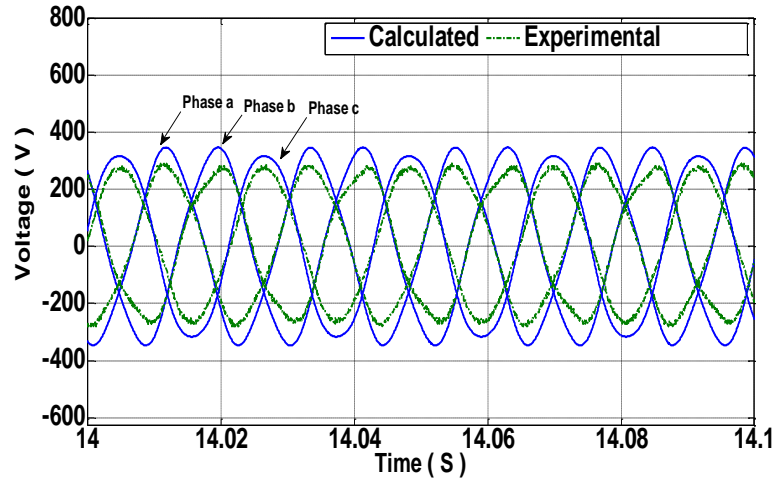
**Figure 6.11** Steady-state generated voltage and current waveforms; unbalanced resistive load ( $R_{la} = R_{lb} = 620\Omega$  and  $R_{lc} = 500\Omega$ ),  $C = 30\mu F$  per phase.

Figure 6.12 shows the stator voltage and current waveforms for a more severely unbalanced loading condition where  $500\Omega$  load resistances are connected to phases b and c while phase a is left as an open circuit. As in the previous tests, the results of the proposed model show very good agreement with the experimental results even in the presence of severely unbalanced loading conditions.

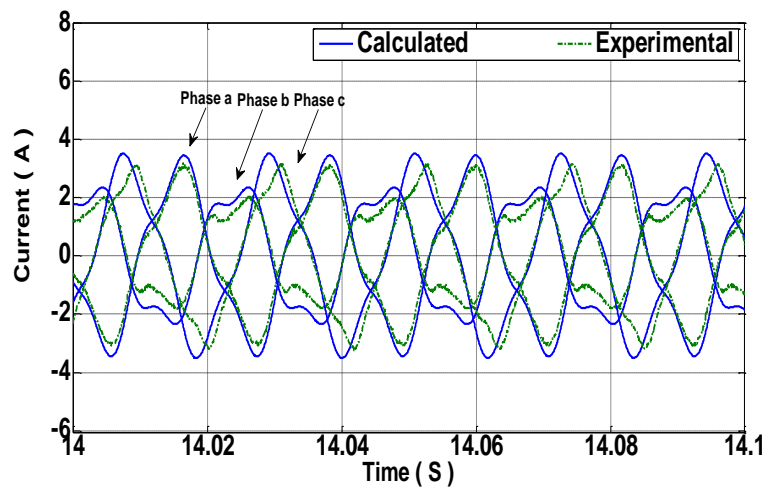
Figure 6.13 shows the generator voltage and current waveforms when an unbalanced R-L load is connected across the stator terminals ( $L_a=1.4H$ ,  $L_b=0.6H$ ,  $L_c=1.54H$ ,  $R_a=R_b=R_c=365\Omega$ ,  $C_a=C_b=C_c=37\mu F$ ). It is clear that the developed model is not only able to match the magnitude value but it also able to follow the shape of the experimental waveform even if the waveform is not pure sinusoidal, but instead is distorted. Machine waveforms are no longer sinusoidal because of the distortion of the flux waveform because the flux is not rotating flux.



**Figure 6.12** Generated voltage and current waveforms;  $500\Omega$  resistive load connected to phases b and c while phase a is open circuited;  $C = 30\mu F$  per phase.



(a)



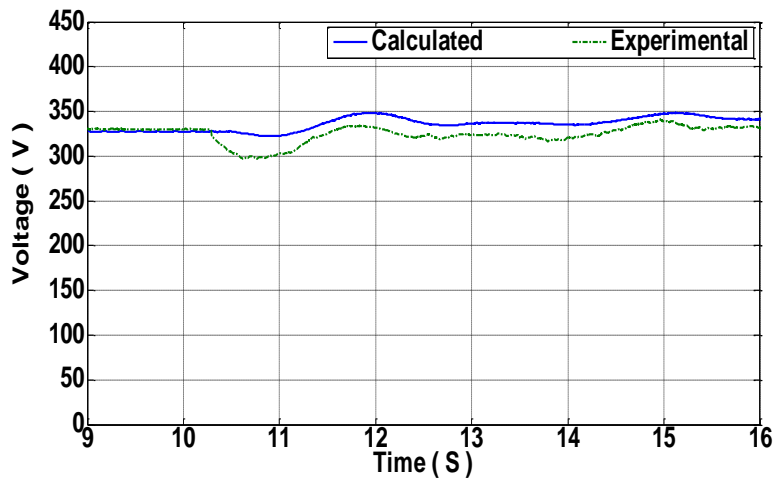
(b)

**Figure 6.13** Steady-state of voltage (a) and current(b) waveforms; unbalance R-L load,  $C = 37\mu\text{F}$  per phase, 1400 rpm.

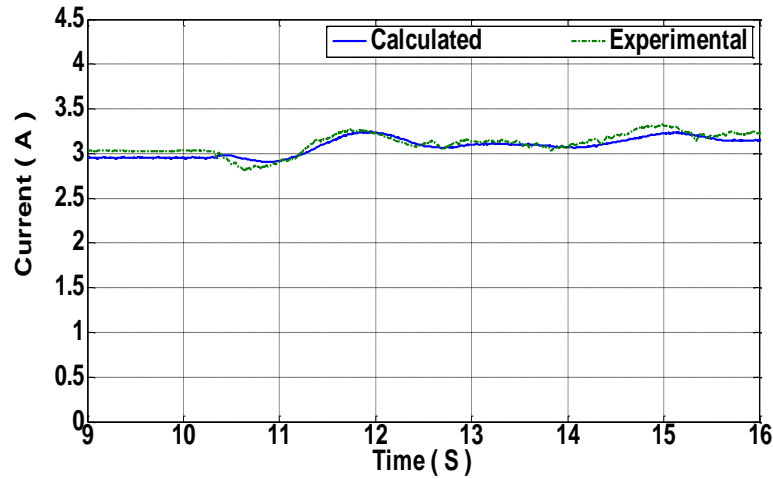
## 6.5 Load perturbation results

The SEIG was then exposed to more severe conditions due to a sharp and sudden change in voltage and current in order to investigate the capability of the proposed model in predicting the performance of the induction generator under balanced and unbalanced load perturbation such as sudden load application or load rejection.

The dynamic response of the SEIG following a sudden three-phase resistive load rejection is demonstrated in Figure 6.14. This transient was applied in order to examine the performance of the proposed model in predicting the behaviour of the SEIG during load perturbation. With the generator operating with a balanced three-phase, star-connected resistor-load ( $500\Omega$  per phase), a sudden disconnection of the three-phase resistive load occurred. Figure 6.14 shows the rms values of the generated voltage and current, illustrating very good prediction produced by the proposed model for the transient response of the SEIG following the sudden disconnection of the load resistors.



(a)

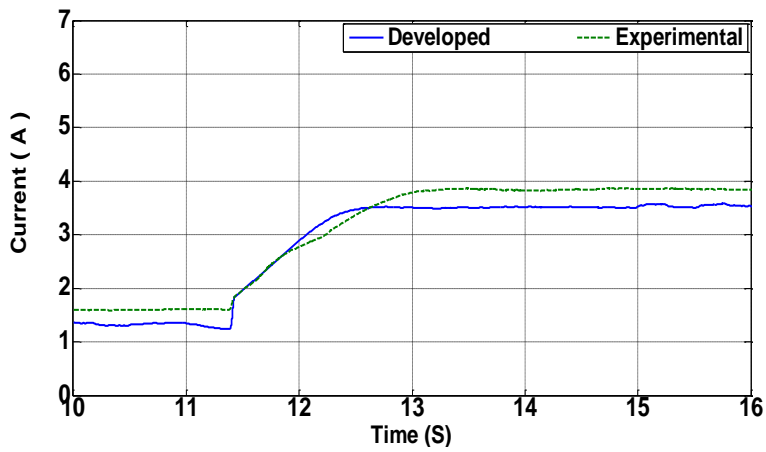
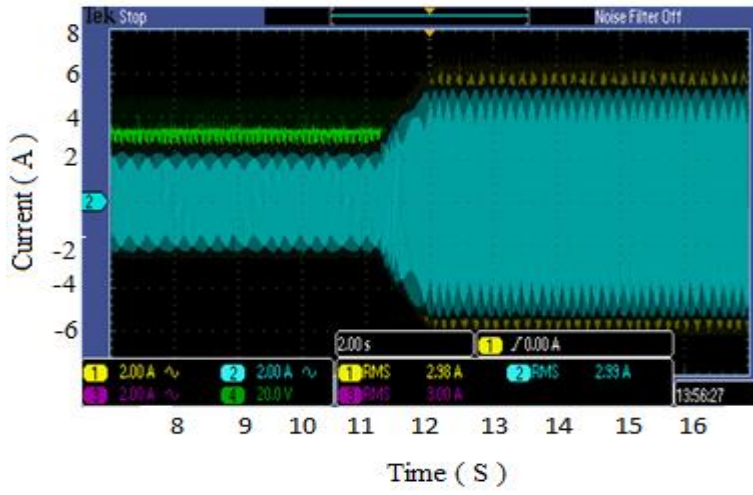


(b)

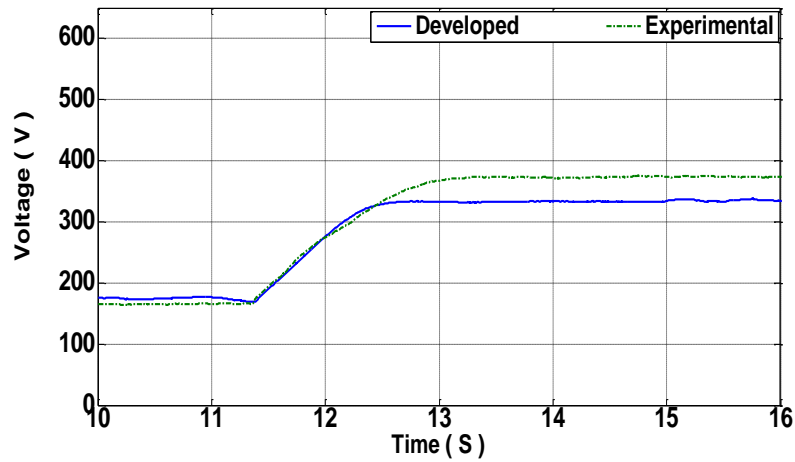
**Figure 6.14** Waveforms of phase voltage (a), phase current (b), during switching of a balanced load at 10.3 seconds;  $R=500\Omega$  per phase.

With the generator operating with a balanced three-phase, star-connected R-L load ( $L_a=1.0\text{H}$ ,  $L_b=1.0\text{H}$ ,  $L_c=1.0\text{H}$ ,  $R_a=R_b=R_c=365\Omega$ ,  $C_a=C_b=C_c=37\mu\text{F}$ ), a three-phase load rejection was applied to examine the performance of the SEIG during load perturbation. Figure 6.15 shows the rms values of the generated voltage and current, illustrating the transient response of the SEIG following sudden disconnection of the three-phase R-L load suddenly at 11.4 seconds. The calculated voltage and current waveforms give good agreement with those obtained experimentally ( $RMS_e=0.2776$ ).

It can be observed easily that the phase voltage and current increase significantly by more than 200 % of its steady state value. This increase can be attributed to a sudden increase in the excitation power after load rejection. Hence, a schematic protection is required for conditions such as these in order to protect the generator and the excitation capacitors as well as maintenance staff.



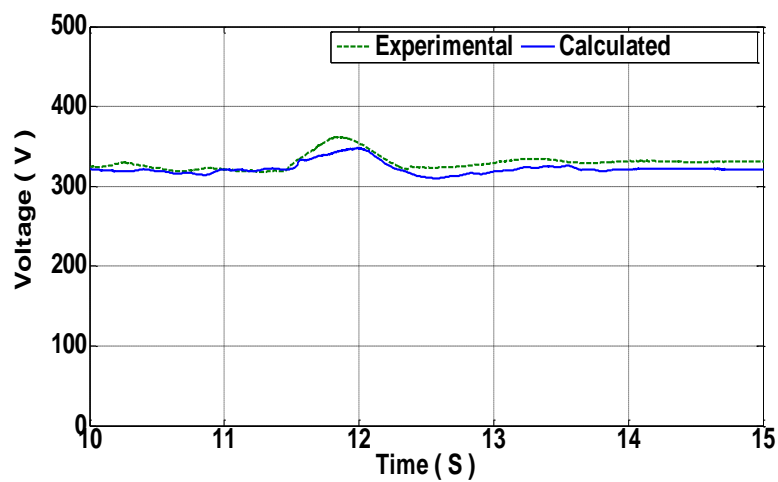
(a)



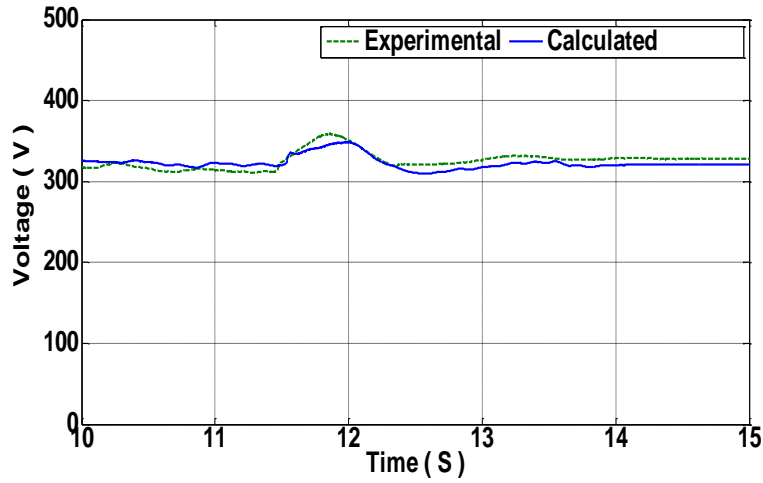
(b)

**Figure 6.15** Waveforms of: (a) phase voltage; (b) phase current, during the removal of a balanced load;  $R=365\Omega$  per phase,  $L=1H$  per phase,  $C=37\mu F$  per phase.

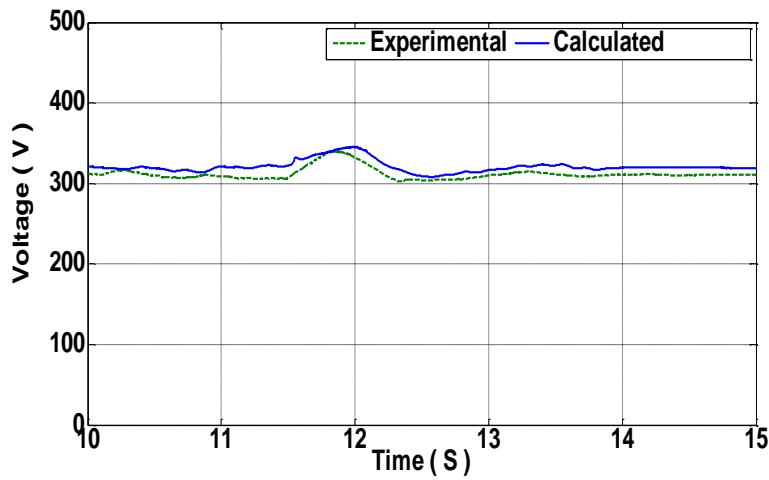
Figure 6.16 and Figure 6.17 show that, after the steady state was attained with an unbalanced resistive load ( $R_a = R_b = 500\Omega$ ) while phase c is unloaded, a load rejection for phase-a and phase-b occurred at 11.5 sec. while the voltage and current for phase c remain almost constant. From the figure, it is clear that good agreement has been achieved between the measured and calculated results.



(a)

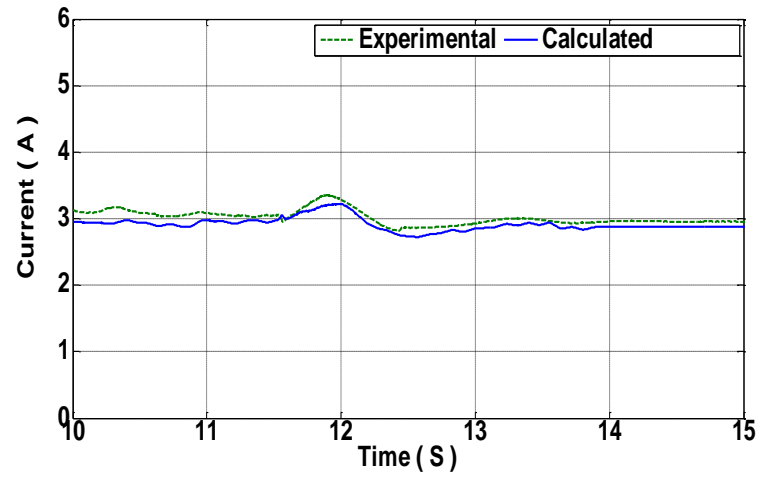


(b)

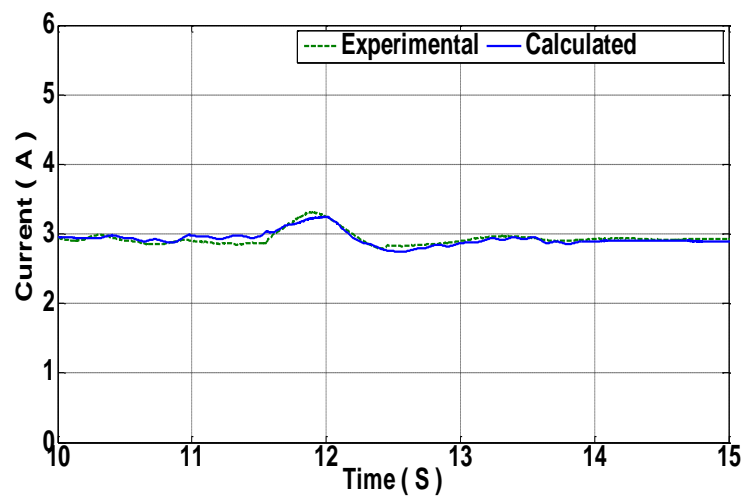


(c)

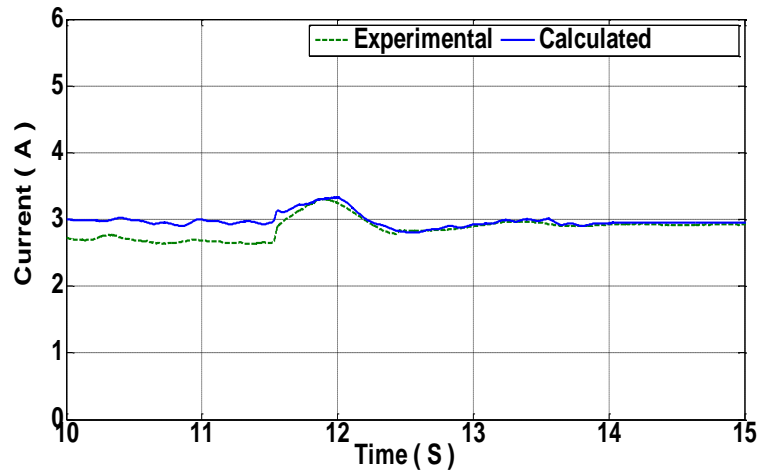
**Figure 6.16** Behaviour of phase voltage: (a) phase a; (b) phase b; (c) phase c, during load perturbation at unbalanced conditions with two phase load rejection,  $C = 30\mu\text{F}$  per phase, 1450 rpm.



(a)



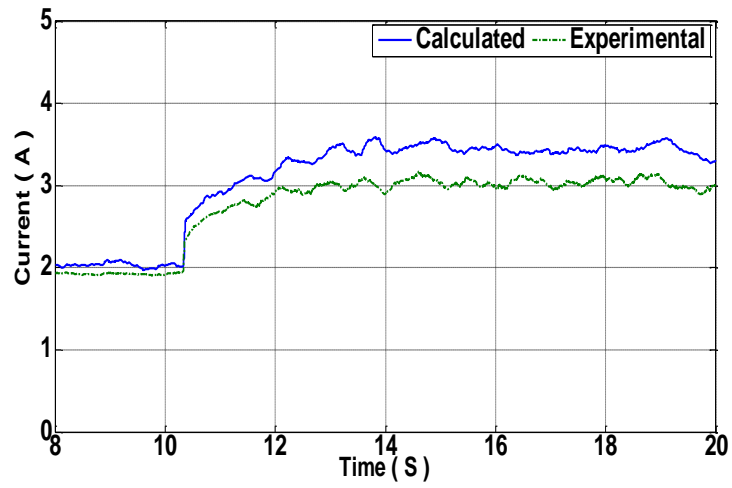
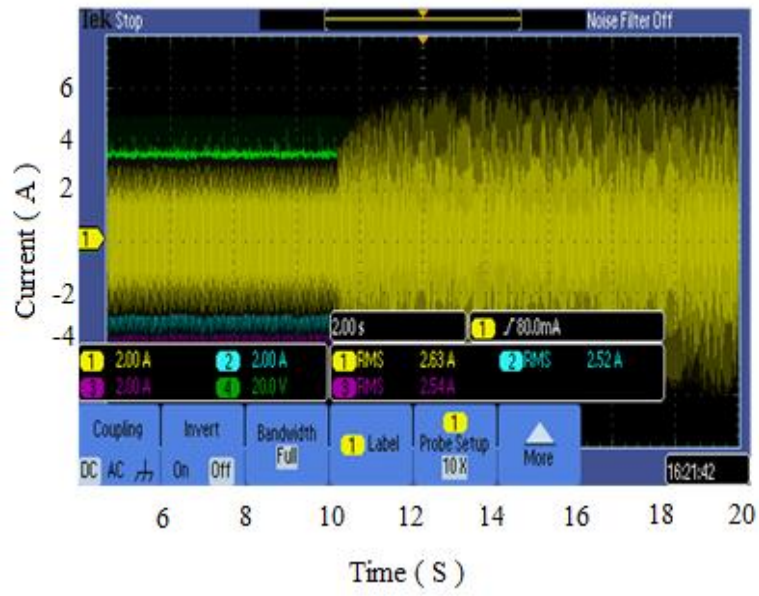
(b)



(c)

**Figure 6.17** Behaviour of the generated current (r.m.s): (a) phase a; (b) phase b; (c) phase c, during load perturbation at unbalanced conditions with two phase load rejection,  $C = 30\mu\text{F}$  per phase, 1450 rpm.

Figure 6.18 and Figure 6.19 show the performance of the induction generator was tested under conditions of unbalanced disturbance by applying an unbalanced load rejection such that, when the generator was running at a rotor speed of 1400 rpm and feeding R-L load ( $L_a=1\text{ H}$ ,  $L_b=1\text{ H}$ ,  $L_c=1\text{ H}$ ,  $R_a=R_b=R_c=365$ ,  $C_a=C_b=C_c=37\text{ }\mu\text{F}$ ), one phase (phase-a) of the R-L load was suddenly disconnected while the other two phases were still connected. A high level of agreement ( $RMS_e = 0.1020$  for phase b and c whereas phase a is 0.3551) between measured and calculated results for phase current and voltage is demonstrated in Figure 6.18 and Figure 6.19 respectively.



(a)

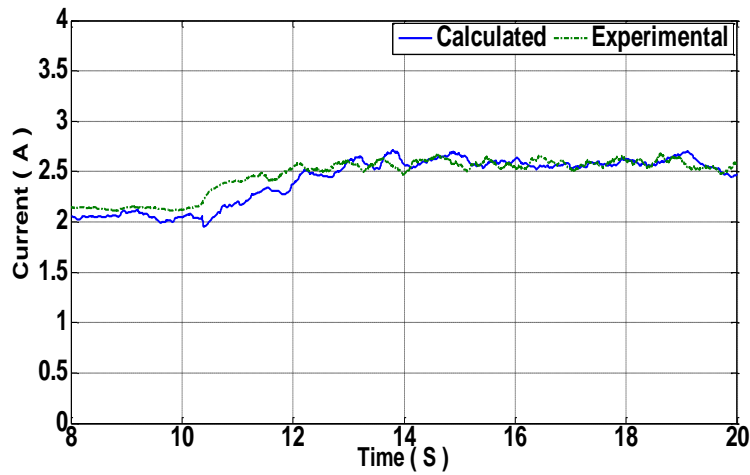
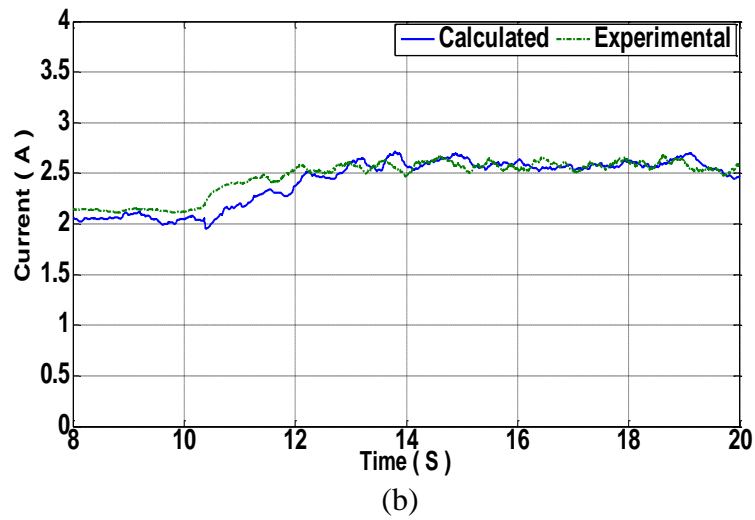
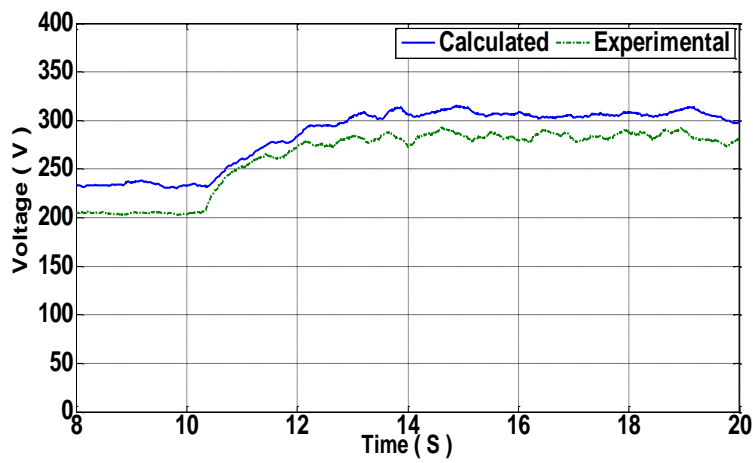
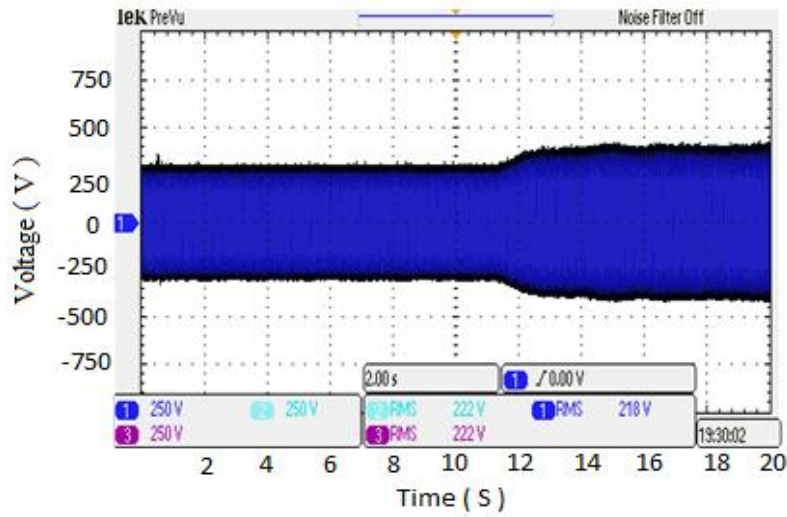
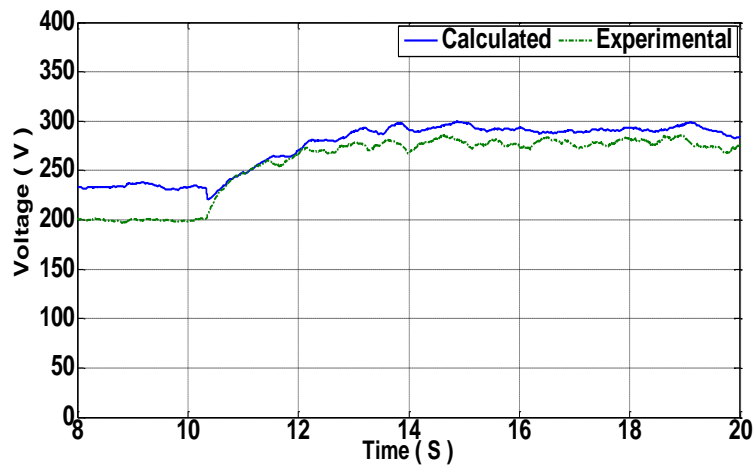


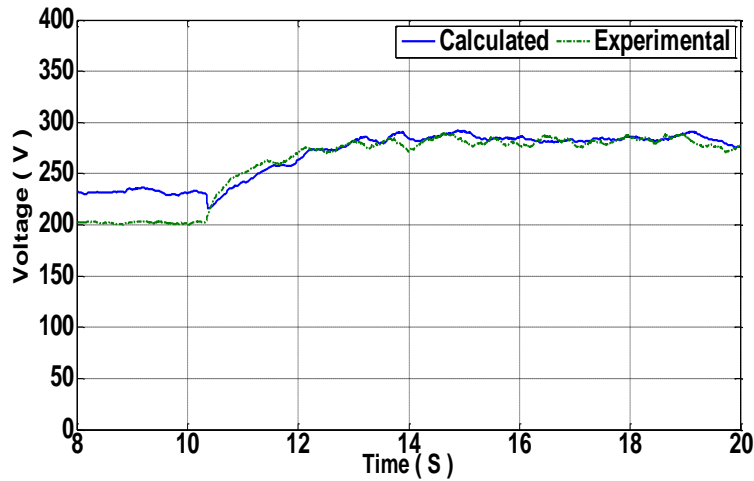
**Figure 6.18** Behaviour of the stator current: (a) phase a; (b) phase b; (c) phase c; of SEIG after removing one phase (phase a) of the load.



(a)



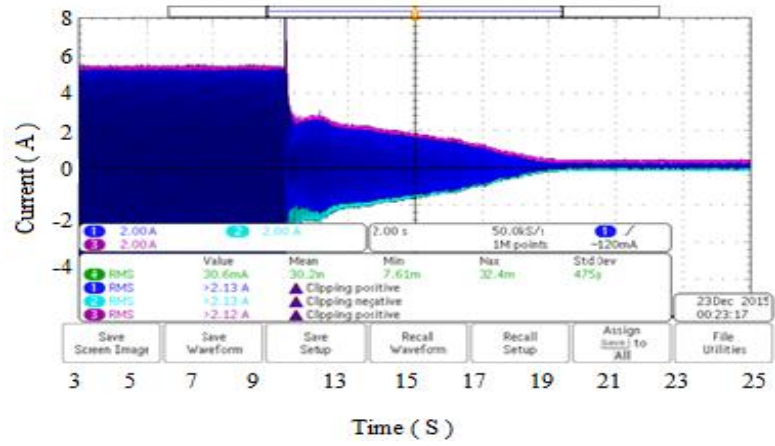
(b)



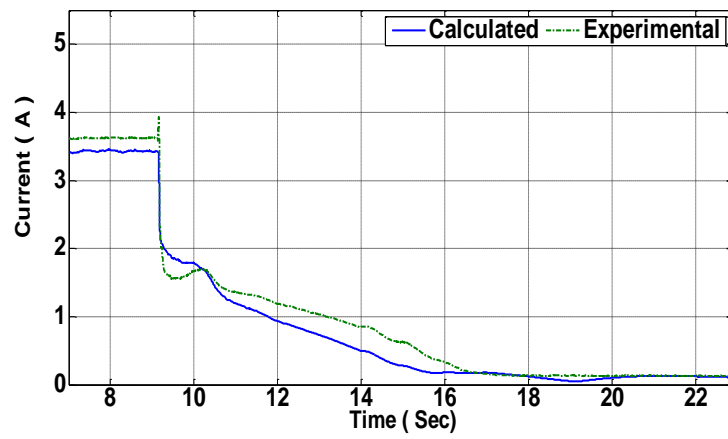
(c)

**Figure 6.19** The Behaviour of output voltage: (a) phase a; (b) phase b; (c) phase c, of SEIG after removing phase a of the load.

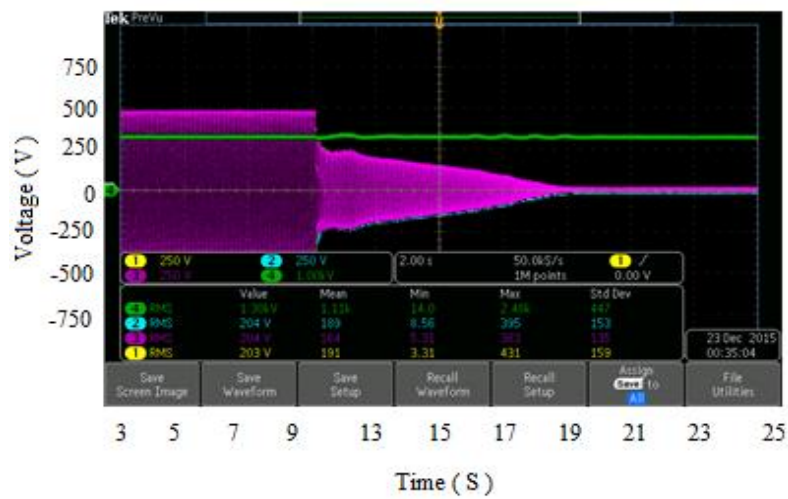
Figure 6.20 and Figure 6.21 show the performance of the SEIG when an excessive load was added suddenly when it was operating at a no-load condition at a speed of 1330 rpm (the load is considered as excessive in this case because the speed is less than it should be for this particular load; the speed would be expected to be 1400 rpm). It is clear that the voltage, current and flux all collapsed immediately following the application of the R-L load ( $L_a=L_b=L_c=1.0\text{H}$ ,  $R_a=R_b=R_c=365\Omega$ ), with the excitation capacitance at  $C_a=C_b=C_c=37\mu\text{F}$ , and the generator becoming de-excited. To avoid this de-excitation, either the value of excitation capacitance or shaft speed should be increased. In this case, the  $RMS_e=0.2145$ .



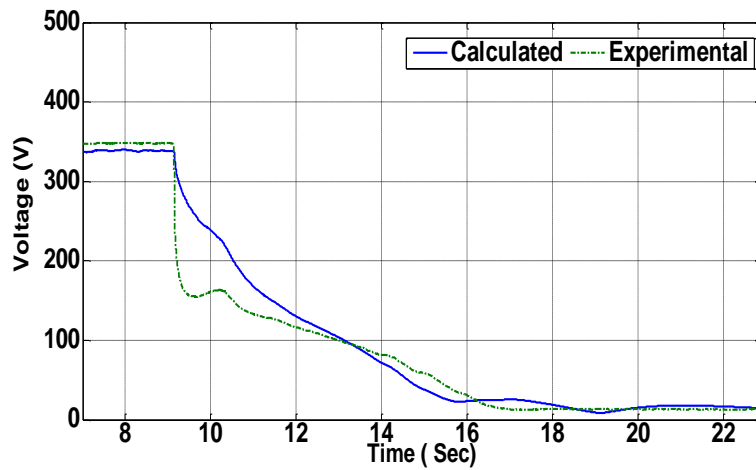
(a)



(b)

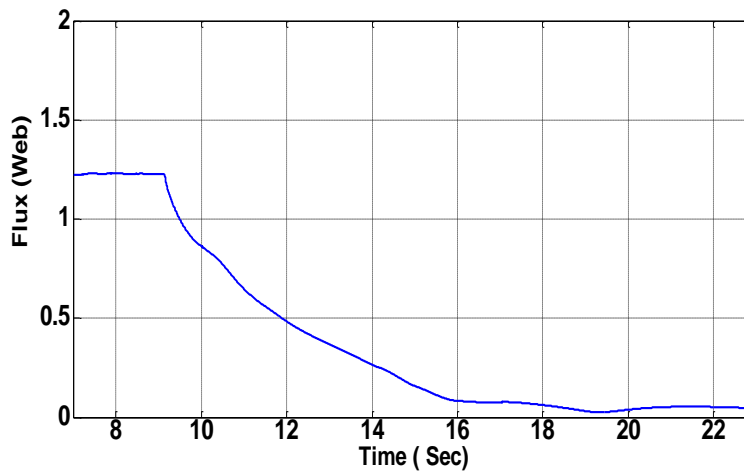


(c)

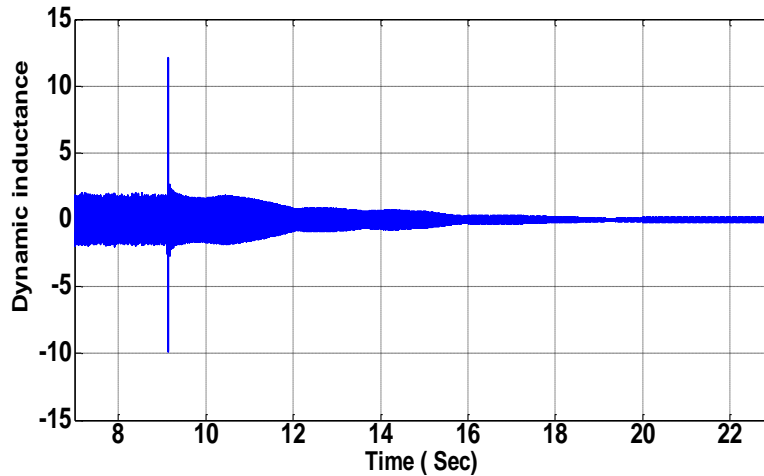


(d)

**Figure 6.20** SEIG performance after adding an excessive three-phase load when running at 1330rpm at no-load: (a) phase current (oscilloscope screenshot);(b)phase current (rms) (c) phase voltage (oscilloscope screenshot) (d) phase voltage (rms).



(a)



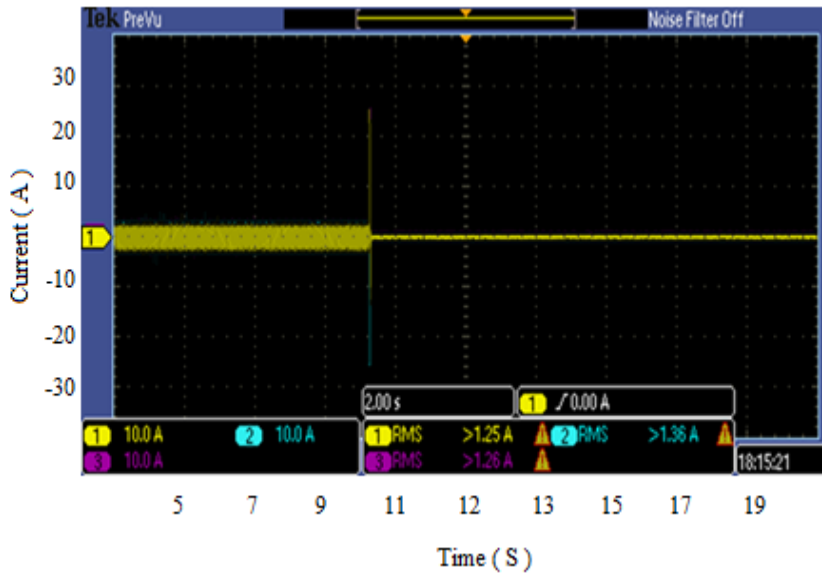
(b)

**Figure 6.21** SEIG performance after adding an excessive three-phase load when running at 1330rpm at no-load: (a) flux, (b) dynamic inductance.

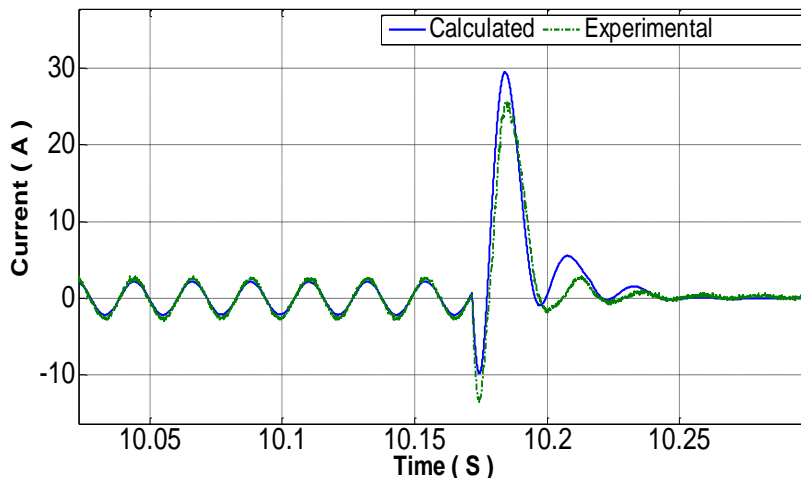
## 6.6 Fault response results

The fault responses of the SEIG calculated from the developed model and compared with experimental measurements are shown in Figure 6.22 and Figure 6.23, again showing excellent agreement. Figure 6.22 shows the behaviour of the induction generator following the introduction of a balanced three-phase fault (solid fault) at the stator terminals, while the response to a line-to-line fault on the system is shown in Figure 6.23. Both faults were introduced at the stator terminals while the generator was in steady-state operation feeding a balanced, three-phase  $R$ - $L$  load ( $R_{la}=R_{lb}=R_{lc}=365\Omega$ ,  $L_a=L_b=L_c=1\text{H}$ ,  $C_a=C_b=C_c=37\mu\text{F}$ ). The results demonstrate how the SEIG is a self-protected generator with the generated voltage and current dying quickly after the fault. This happens because the excitation capacitor is feeding the fault rather than feeding the generator. From both Figure 6.22 and Figure 6.23, it can easily be observed that the developed model is able to follow the phase and the magnitude of the experimental signal, even in the worst cases when there is a sharp and sudden change such as three-phase fault ( $RMS_e=1.80$ ) and line to line fault ( $RMS_e=1.21$ ).

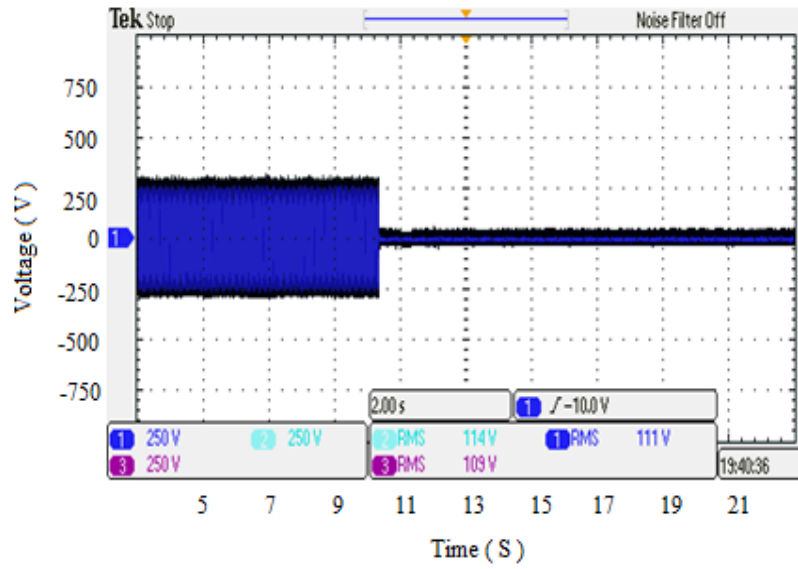
The shaft speed in rpm during the line-to-line fault is shown in Figure 6.24. This mechanical speed is almost constant at 1400 rpm apart from a small change during the Double line fault by approximately  $\pm 30$  rpm.



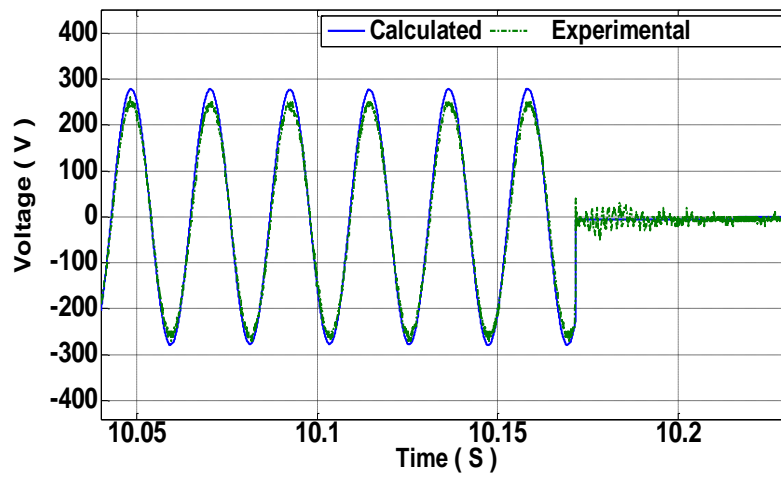
(a)



(b)

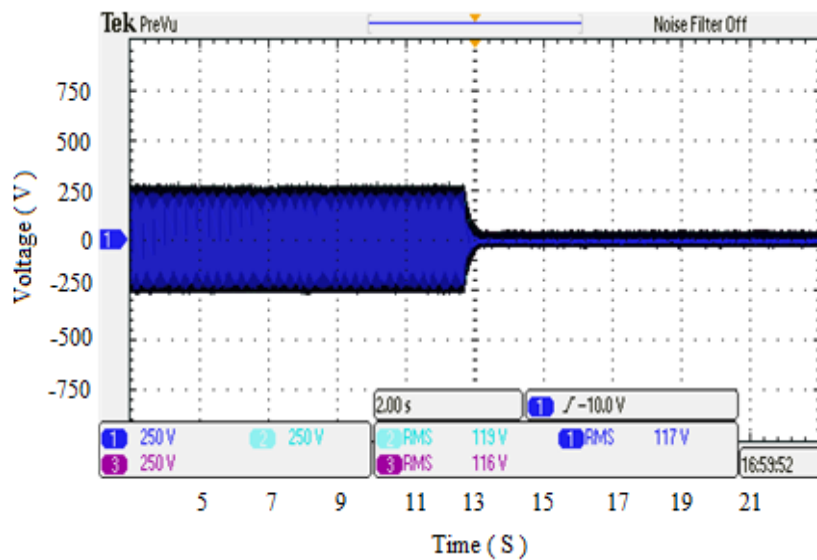
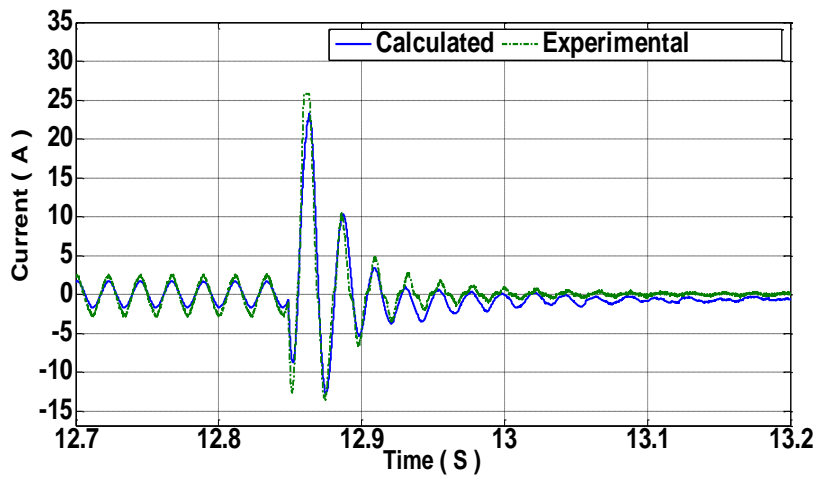
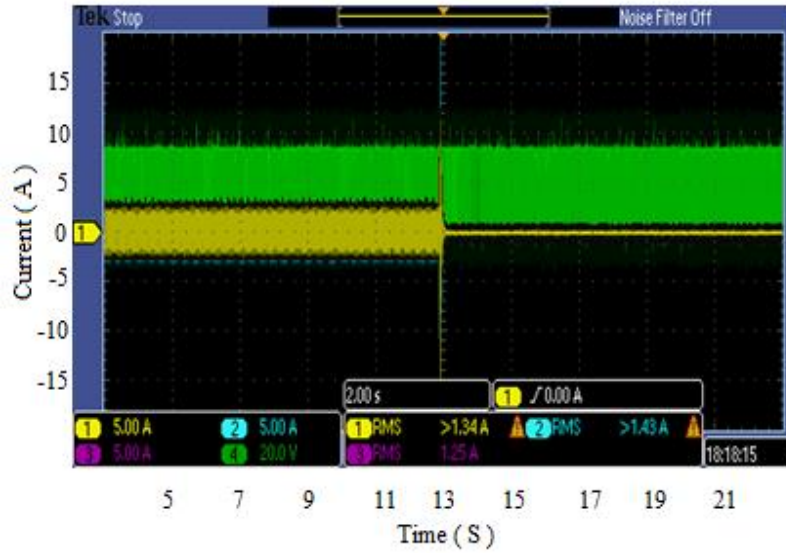


(c)



(d)

*Figure 6.22* Fault behavior of the SEIG with a three-phase fault at the generator terminals.



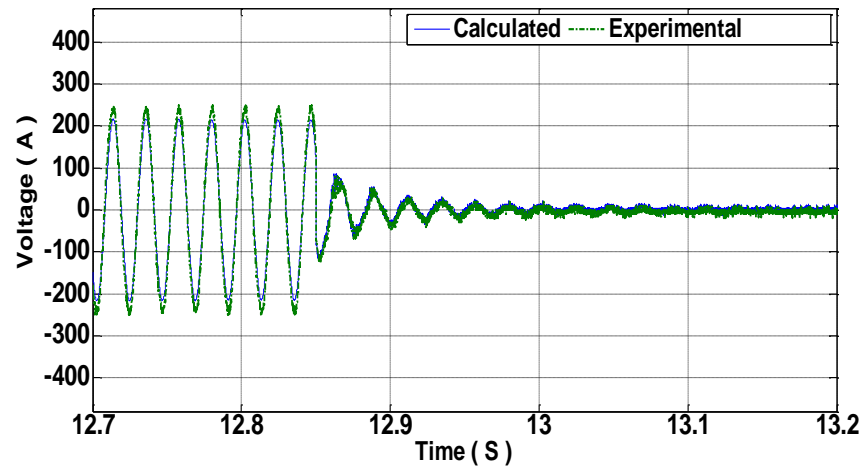


*Figure 6.23* Fault behaviour of the SEIG with a line-to-line fault at the generator terminals.

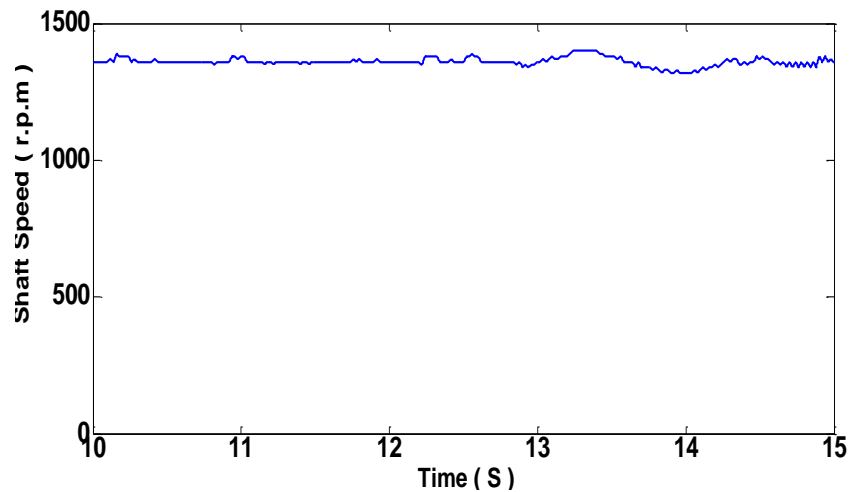


*Figure 6.24* Shaft speed of self-excited induction generator during a DL fault.

### 6.7 Sudden change in speed results

To investigate whether or not the proposed model can cope with a sudden change in the input speed, the shaft speed of the prime mover (DC motor) was varied using a DC-drive converter such

that the speed varied as shown in Figure 6.25 by applied a sharp change manually ( $\pm 150$  rpm.). Figure 6.26 and Figure 6.27 show the behaviour of the stator current and output phase voltage respectively as a result of a sudden sharp fluctuation in mechanical speed when the generator was loaded with a balanced R-L load such that  $L_a=L_b=L_c=1\text{H}$ ,  $R_a=R_b=R_c=365$ , and with excitation capacitance  $C_a=C_b=C_c=37\ \mu\text{F}$ . Although there was a sudden sharp drop and then a sharp increase in the shaft speed, the model successful coped with these variations in speed with error  $RMS_e=0.1732$  for the current whereas the error for voltage is  $RMS_e=26$ . It can be observed that the variation in voltage and current follow almost the same behaviour as the variation in mechanical speed; hence, it can be concluded that the developed model can be used for applications with a variable speed within a limited range. Figure 6.28 shows the effects of dynamic matrix produced by the last matrix in equation 3.45, it can be observed that the effects of the dynamic inductance is significant and change as the speed change.

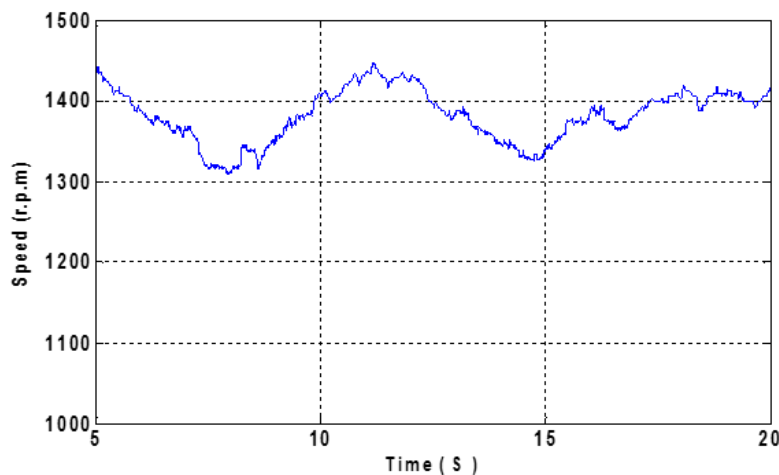
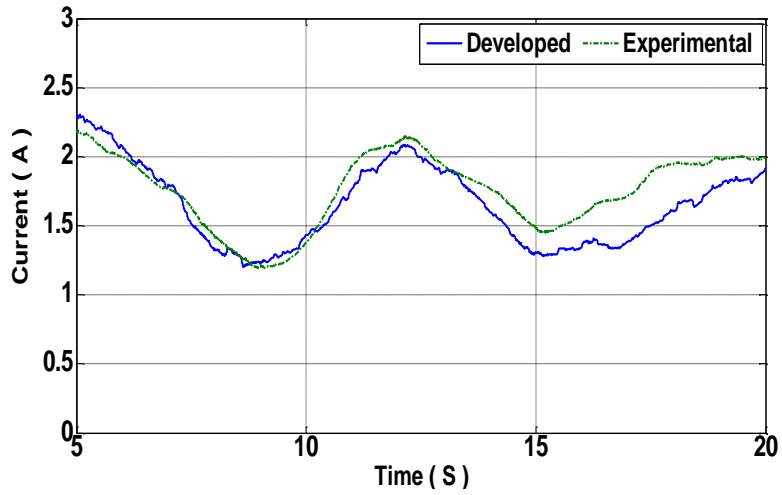
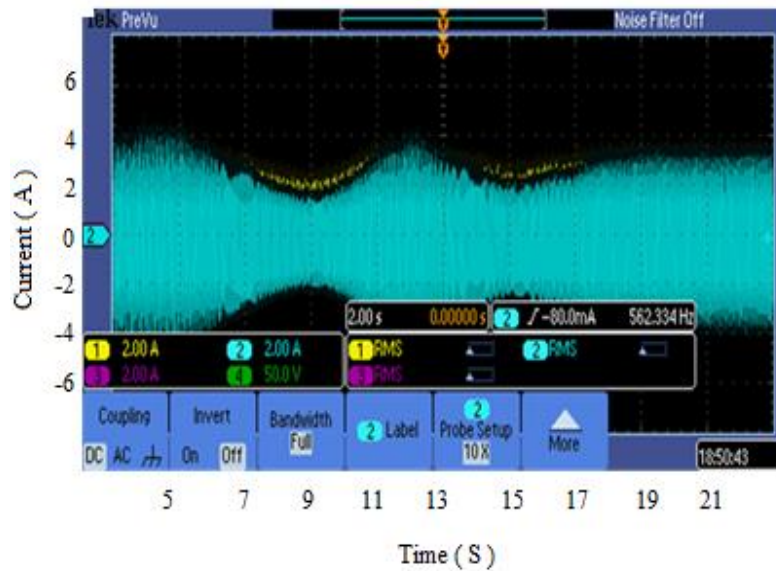


**Figure 6.25** Variation in shaft speed of the prime mover of the SEIG.

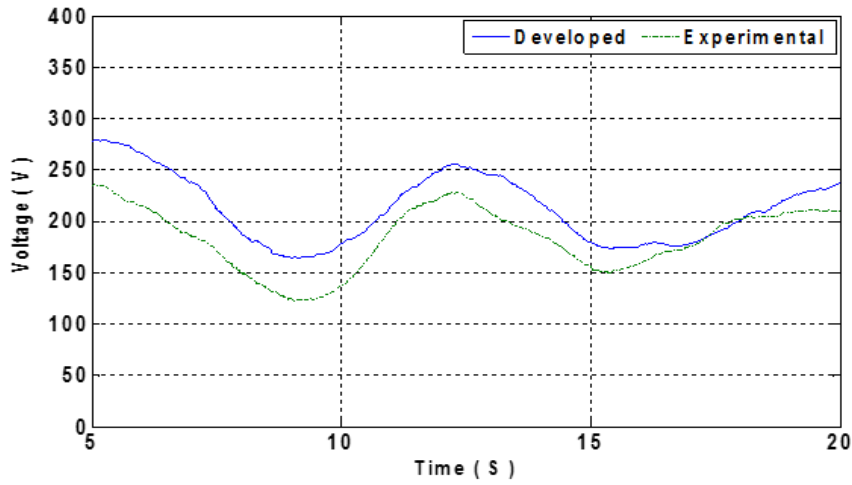


(a)

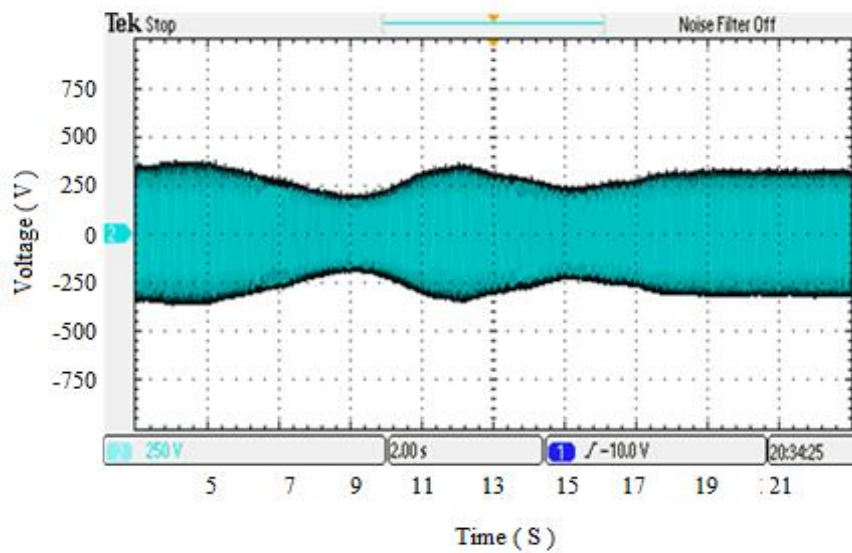


(b)

**Figure 6.26** Performance of the SEIG during a sudden change in rotor speed: (a) phase stator current; (b) screen shot of the oscilloscope of the phase current, with a balanced R-L load.

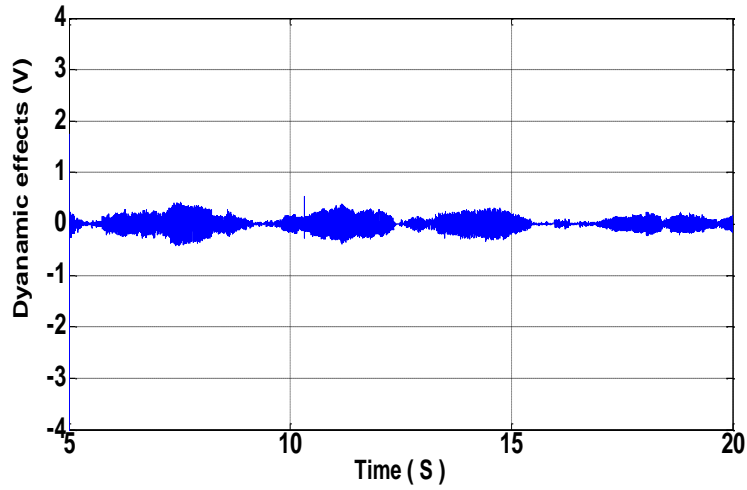


(a)

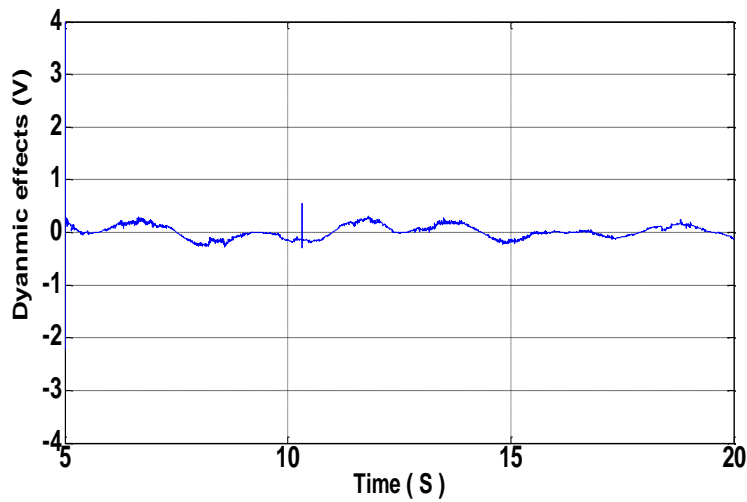


(b)

**Figure 6.27** Performance of the SEIG during a sudden change in rotor speed:(a) phase stator voltage; (b) screen shot of the oscilloscope of the phase voltage when a balanced R-L load was connected.



(a)



(b)

**Figure 6.28** Change in the dynamic inductance of phase-a in: (a) the stator; (b) the rotor, due to sudden change in speed.

## 6.8 Conclusion

In this chapter, a simple three-phase analytical model of the induction generator that accounts for the main path saturation effects and mutual saturation between the three-phase stator

windings as well as the mutual saturation between the rotor three-phase windings is employed to investigate the behaviour and performance of a three-phase SEIG under various circumstances. The saturation effects were taken into consideration by means of a variable magnetizing inductance. In other words, the magnetizing inductance is considered to be a function of the magnetizing current and the displacement of the rotor.

The proposed model is validated through comparison of the results calculated from the model with those measured experimentally under different conditions. The performance of the SEIG was tested in a variety of conditions such as no-load, build-up, an excessive load application, balanced, unbalanced, and balanced and unbalanced fault conditions. Some of these conditions considered are severe in order to examine the performance of the proposed model in predicting the behaviour of a self-excited induction generator in extreme cases. This validation shows a high level of agreement between calculated and measured results. The small differences observed between the measured and calculated results are likely related to neglected losses, leakage saturation, magnetization curve approximation and measurement error.

# Chapter 7. The effects of dynamic inductance

---

## 7.1 Introduction

Many authors have tended to employ simple machine models by considering machine parameters with constant values [39-43]. Such models are suitable to study the characteristics of an induction machine at specific operating points in the steady state condition. However, if the operating point varies the parameters will no longer remaining constant and this approach will not be sufficient since flux magnitudes and frequencies will vary.

Several recent studies have considered saturation effects [9, 16, 49], but although they investigate the performance of the SEIG during a dynamic response, they neglect the derivative of magnetizing inductance with respect to magnetizing current. Therefore, the effects of this derivative (that was already taken into account in Chapter 6) on the accuracy of representation of the non-linearity in a self-excited induction generator should be highlighted. In order to achieve this, a comparison need to be made between the performance of the analytical developed model and that of a conventional model that does not take such a derivative into account.

The variation in magnetizing inductance due to the saturation effect is represented in the conventional machine saturation model using the same exponential function used in the proposed model, without considering the derivative of magnetizing inductance with respect to the magnetizing current (i. e.,  $\frac{d[L]}{di_m}$  is neglected).

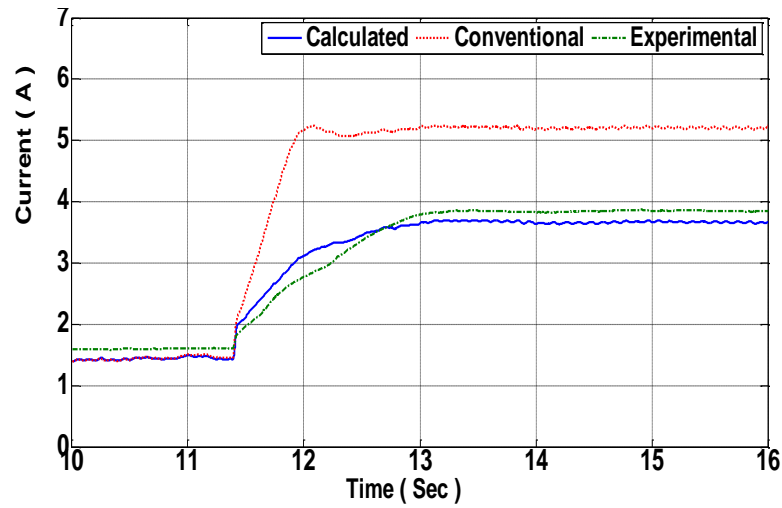
Hence, the conventional model is the same as the developed model except that the dynamic matrix which is modelled by the last matrix in equation (3.45) is omitted in this model.

The performance of both the proposed and the conventional models are examined under the same transient conditions such as load perturbation and faults, and validation against experimental results is conducted.

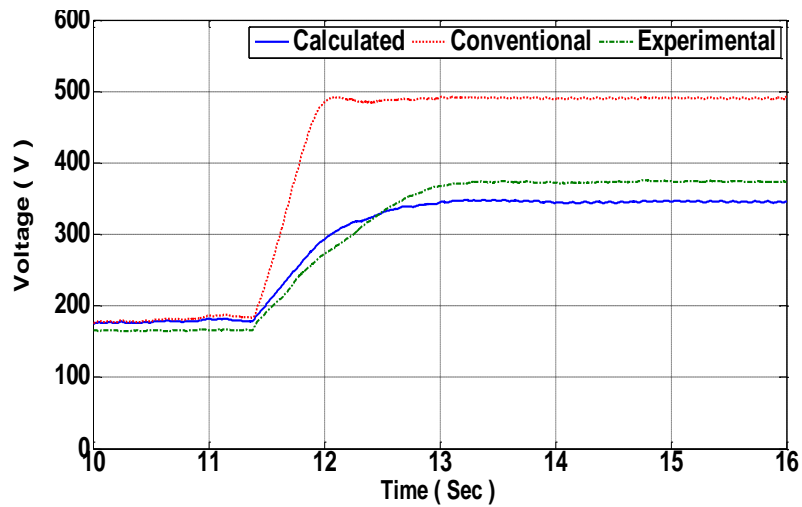
## 7.2 Results and discussion

The three curves in the following figures show a dashed grain line, which represents the results obtained in the laboratory, a blue solid line that represents the results obtained by the proposed model, and a red dotted line showing the results obtained by the conventional model. Some severe dynamic cases shown in chapter 6 are repeated here to show the effects of the derivative of magnetizing inductance with respect to magnetizing current.

In order to examine the dynamic response of the proposed model in predicting the behaviour of the SEIG during load perturbation, a sudden three-phase resistive load disconnection is applied while the generator is operating with a balanced three-phase, star-connected R-L load ( $L_a=1.0\text{H}$ ,  $L_b=1.0\text{H}$ ,  $L_c=1.0\text{H}$ ,  $R_a=R_b=R_c=365\Omega$ ,  $C_a=C_b=C_c=37\mu\text{F}$ ). Figure 7.1 shows the rms values of the generated voltage and current, illustrating no significant effects of the derivative of the magnetizing inductance with respect to magnetizing current during the steady state condition. In both values of the generated voltage and current the results produced by the conventional and proposed models are almost the same apart from a small difference which may be due to variation in speed or error in the numerical solution. However, a significant error in the results produced by the conventional model ( $RMS_e=1.24$ ) after load rejection occurs. This error can be observed in both the voltage and current generated, whereas the proposed model predicts the performance of the induction generator much more accurately ( $RMS_e=0.27$ ).



(a)

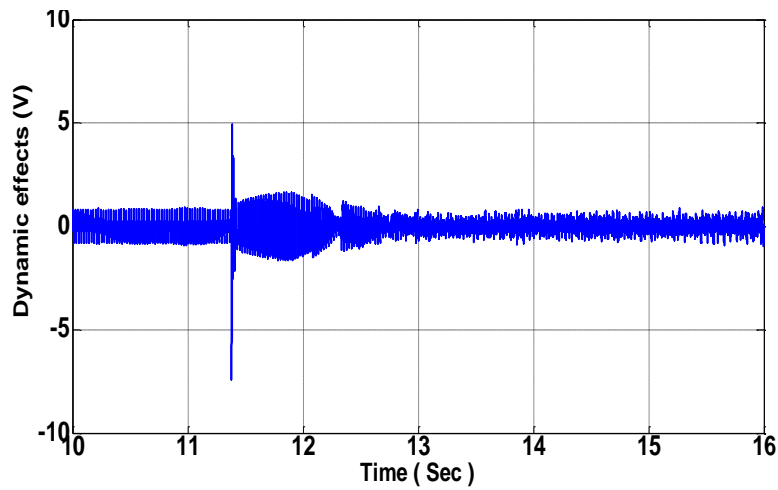


(b)

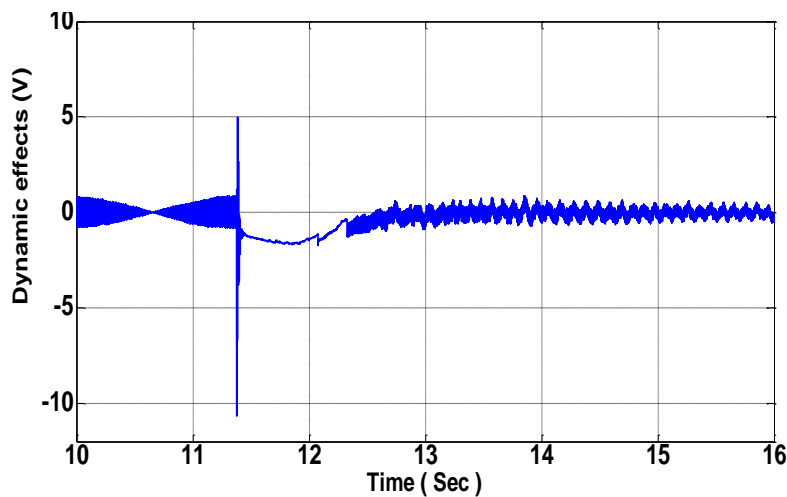
**Figure 7.1** Comparison of the performance of the proposed and conventional models following sudden disconnection of balanced three-phase R-L load,  $R=365\Omega$  per phase,  $L=1H$  per phase,  $C = 37\mu F$  per phase, 1400 rpm.

The effects of the derivative of the magnetizing inductance with respect to magnetizing current during this load perturbation are produced by the first row in the last matrix in equation 3.45

as demonstrated in Figure 7.2-a, whereas that produced by the forth row of the same matrix presented in Figure 7.2-b. At steady state, there is a small effect of the dynamic response. This effect can be attributed to the small variation in rotor speed during the steady state.



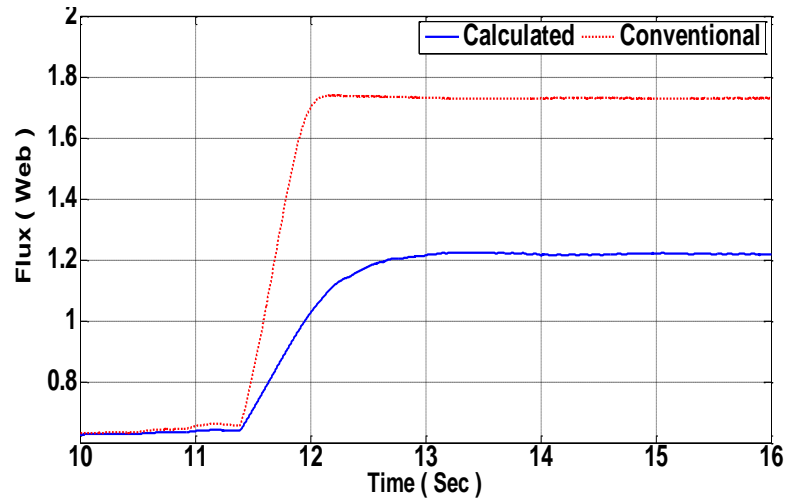
(a)



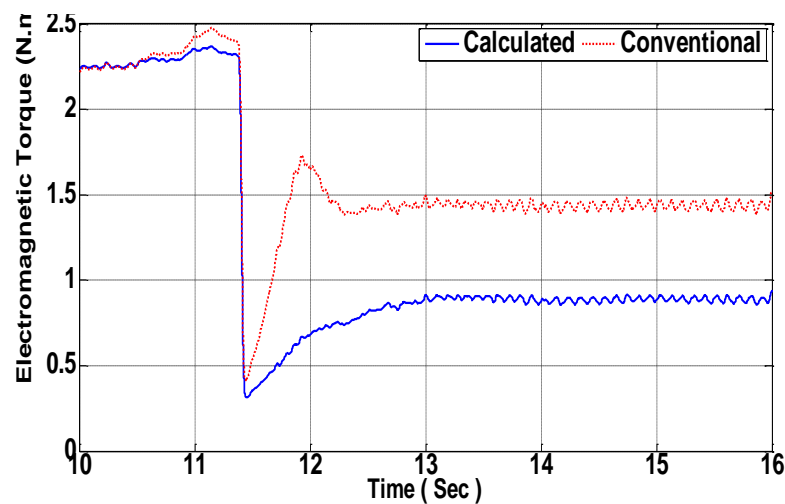
(b)

**Figure 7.2** Behaviour of the dynamic effects in the stator phase-a (a), and the rotor phase-a (b) for same case as figure 7.1.

From Figure 7.3 it can be observed that, in the steady state condition, the results produced by both proposed and conventional models are almost the same, while in the transient state the difference between them is considerable. From this, it can be deduced that the error is not present only in voltage and current values but can also extend to other parameters such as fluxes.



(a)

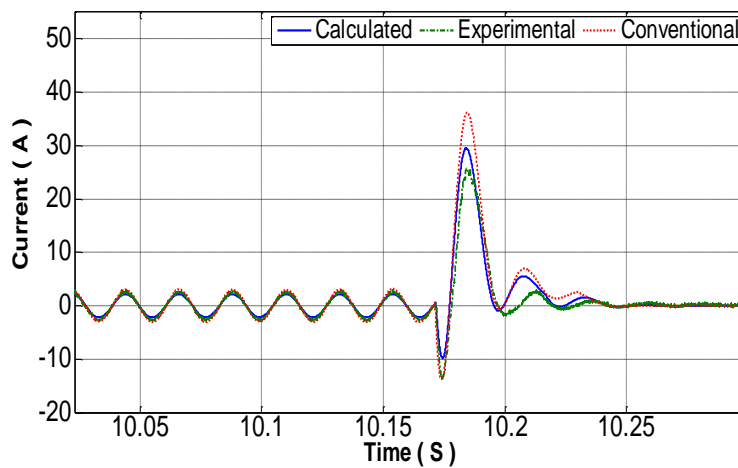


(b)

**Figure 7.3** Comparison of the behaviour of (a) the flux of stator windings in phase-a and (b) electromagnetic torque obtained by the proposed and conventional models during sudden removal of balanced three phase R-L load,  $R=365\Omega$  per phase,  $L=1H$  per phase,  $C = 37\mu F$  per phase, speed = 1400 rpm.

The fault responses of the SEIG calculated from the proposed and conventional models are shown in Figure 7.4 and Figure 7.5 and validated against measured results.

Figure 7.4 shows the behaviour of the machine following the introduction of a balanced three-phase fault at the stator terminals. The fault was introduced at the stator terminals while the generator was in steady-state operation feeding a balanced, three-phase R-L load ( $R_{la}=R_{lb}=R_{lc}=365\Omega$ ,  $L_a=L_b=L_c=1\text{H}$ ) with excitation capacitance ( $C_a=C_b=C_c=37\mu\text{F}$ ). The fault responses of the SEIG predicted by the conventional and proposed models are depicted in Figure 7.4 and compared with measurement results. The results produced by the proposed and conventional models produced results with almost the same level of accuracy in the steady state condition; on the other hand, after fault, an outstanding disparity between the measured and results obtained by the conventional model can be noted ( $RMS_e=2.75$ ), whereas the disparity between the measured and results produced by proposed model is small relatively ( $RMS_e=1.80$ ).



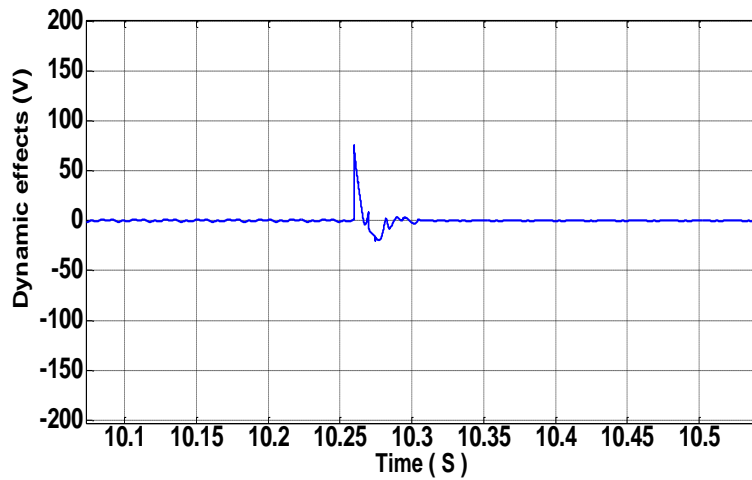
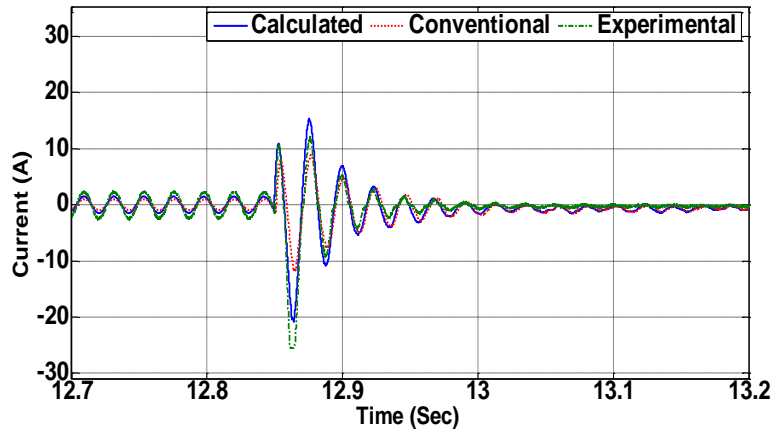
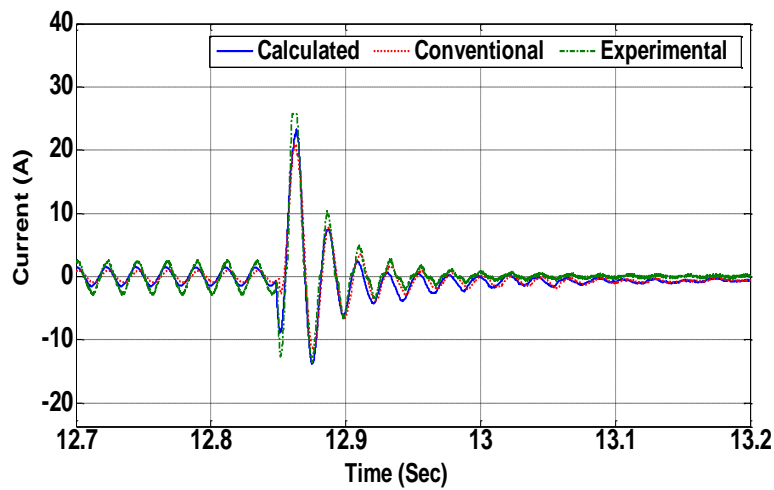


**Figure 7.4** Comparison of the proposed and conventional models during three-phase fault when parallel R-L load is connected,  $R=365\Omega$  per phase,  $L=1H$  per phase,  $C = 37\mu F$  per phase, 1400 rpm.

Predictions of the performance of the SEIG following the introduction of a line-to-line fault generated by the proposed and the conventional models are shown in Figure 7.5. The fault was introduced at the stator terminals while the generator was in steady-state operation feeding a balanced, three-phase R-L load ( $R_{la}=R_{lb}=R_{lc}=365\Omega$ ,  $L_a=L_b=L_c=1H$ ) with excitation capacitance ( $C_a=C_b=C_c=37\mu F$ ). The results produced by both analytical models compared with experimental measurements, again the results produced by the proposed model showing a good agreement ( $RMS_e=1.21$ ), whereas the results generated by the conventional model showing a noticeable error ( $RMS_e=1.63$ ) due to neglecting the effects of the dynamic response.



(a)



(b)

**Figure 7.5** Comparison of the stator current phase-a (a) and phase-b (b) produced by proposed and conventional models during line-to-line fault when parallel R-L load is connected,  $R=365\Omega$  per phase,  $L=1H$  per phase,  $C = 37\mu F$  per phase, 1400 rpm.

### 7.3 Conclusion

In this chapter, the importance of the derivative of the magnetizing inductance with respects to the magnetizing current has been clearly highlighted. This has been achieved by comparing the results obtained by the proposed model which includes the magnetizing inductance derivative with respect to the magnetizing current with those produced by the conventional model which neglects the dynamic response. In both models, variation of magnetizing inductance is simulated by the exponential function. It can be clearly concluded that the impact of dynamic inductance on the accuracy of predictions of the performance of the SEIG in terms of current, voltage, torque and flux is important. In particular, adding the effects of this derivative during the dynamic response can improve the accuracy of the result produced from the model. The small disparity between the predictions of the proposed and conventional models during the steady state conditions can be attributed to a very small variation in the measured shaft speed during the steady state.

# Chapter 8. The effects of leakage saturation

---

## 8.1 Introduction

Modelling the self-excited induction generator accurately is important in most applications such as electrical vehicles, small wind turbines and micro-hydro schemes where a grid connection is not available. The main path saturation of the self-excited induction generator is included in a wide range of previous studies; however, the leakage saturation of self-excited induction generators is neglected in previous studies.

The drop in voltage across the leakage inductance becomes prominent as the load increases [23]. Taking the leakage inductance saturation into consideration becomes imperative if the stator and rotor currents are very high [49]. The inclusion of the nonlinearity approach to modelling induction machines based on the saturation of leakage inductance is usually applied to motors with large inrush current conditions, in particular in high-power industrial motor drives [102].

In all papers mentioned which have focused on how to include saturation effects in models employed to predict the performance of the self-excited induction generator, the effects of leakage saturation have been neglected. The aim of this chapter is to determine whether or not this approximation may affect the accuracy of the simulation of induction generators at different conditions of operation, and in particular in terms of the dynamic response.

In this chapter, a generalized dynamic model of a three-phase self-excited induction generator (SEIG) in the natural three-phase  $abc$  reference frame is presented such that leakage saturation is taken into account (as it will be shown in section 8.3). Additionally, the effects of the derivative of leakage inductance with magnetizing current is included in this model. The variation in leakage inductance is approximated by a polynomial function.

## 8.2 Leakage inductance characteristic

The leakage saturation curve can be obtained using the locked rotor test explained in chapter 5. The method will be the same except that this time the value of leakage inductance should be measured at different stator current values. The leakage saturation curve is depicted in Figure 8.1.

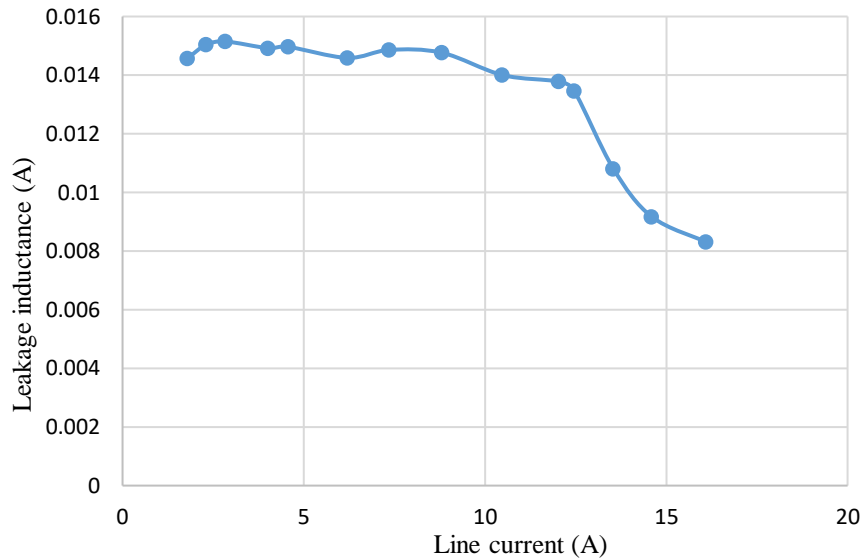


*Figure 8.1 Effect of leakage inductance saturation.*

## 8.3 Modelling leakage saturation

In the analytical model presented in chapter 3 and the results demonstrated in chapters 6 and 7, the leakage saturation is neglected and  $L'_{lsa}$  is assumed to be equal to zero. However, as can be observed from Figure 8.1 the value of leakage inductance is not constant but changes as the stator current changes and therefore  $L'_{sa}$  can be rewritten as follows:

$$\frac{dL_{as}}{dt} = L'_{sa} = L'_{ma} + L'_{lsa}$$

Thus, the dynamic equations of induction machines can be rewritten to include the leakage

saturation as follows:

$$\begin{aligned}
 \begin{bmatrix} v_{as} \\ v_{bs} \\ v_{cs} \\ v_{ar} \\ v_{br} \\ v_{cr} \end{bmatrix} &= \begin{bmatrix} r_{as} & 0 & 0 & 0 & 0 & 0 \\ 0 & r_{bs} & 0 & 0 & 0 & 0 \\ 0 & 0 & r_{cs} & 0 & 0 & 0 \\ 0 & 0 & 0 & r_{ar} & 0 & 0 \\ 0 & 0 & 0 & 0 & r_{br} & 0 \\ 0 & 0 & 0 & 0 & 0 & r_{cr} \end{bmatrix} \begin{bmatrix} i_{as} \\ i_{bs} \\ i_{cs} \\ i_{ar} \\ i_{br} \\ i_{cr} \end{bmatrix} + \begin{bmatrix} L_{sa} & -0.5L_{mb} & -0.5L_{mc} & L_{sr} a_1 & L_{sr} a_2 & L_{sr} a_3 \\ -0.5L_{ma} & L_{sb} & -0.5L_{mc} & L_{sr} a_3 & L_{sr} a_1 & L_{sr} a_2 \\ -0.5L_{ma} & -0.5L_{mb} & L_{sc} & L_{sr} a_2 & L_{sr} a_3 & L_{sr} a_1 \\ L_{sr} a_1 & L_{sr} a_3 & L_{sr} a_2 & L_{ra} & -0.5L_{mb} & -0.5L_{mc} \\ L_{sr} a_2 & L_{sr} a_1 & L_{sr} a_3 & -0.5L_{ma} & L_{rb} & -0.5L_{mc} \\ L_{sr} a_3 & L_{sr} a_2 & L_{sr} a_1 & -0.5L_{ma} & -0.5L_{mb} & L_{rc} \end{bmatrix} \begin{bmatrix} \frac{di_{as}}{dt} \\ \frac{di_{bs}}{dt} \\ \frac{di_{cs}}{dt} \\ \frac{di_{ar}}{dt} \\ \frac{di_{br}}{dt} \\ \frac{di_{cr}}{dt} \end{bmatrix} \\
 - \omega_r & \begin{bmatrix} 0 & 0 & 0 & L_{sr} b_1 & L_{sr} b_2 & L_{sr} b_3 \\ 0 & 0 & 0 & L_{sr} b_3 & L_{sr} b_1 & L_{sr} b_2 \\ 0 & 0 & 0 & L_{sr} b_2 & L_{sr} b_3 & L_{sr} b_1 \\ L_{sr} b_1 & L_{sr} b_3 & L_{sr} b_2 & 0 & 0 & 0 \\ L_{sr} b_2 & L_{sr} b_1 & L_{sr} b_3 & 0 & 0 & 0 \\ L_{sr} b_3 & L_{sr} b_2 & L_{sr} b_1 & 0 & 0 & 0 \end{bmatrix} \begin{bmatrix} i_{as} \\ i_{bs} \\ i_{cs} \\ i_{ar} \\ i_{br} \\ i_{cr} \end{bmatrix} \\
 + \frac{di_m}{dt} & \begin{bmatrix} L'_{sa} + L'_{lsa} & -0.5L'_{mb} & -0.5L'_{mc} & L'_{sr} a_1 & L'_{sr} a_2 & L'_{sr} a_3 \\ -0.5L'_{ma} & L'_{sb} + L'_{lsb} & -0.5L'_{mc} & L'_{sr} a_3 & L'_{sr} a_1 & L'_{sr} a_2 \\ -0.5L'_{ma} & -0.5L'_{mb} & L'_{sc} + L'_{lsc} & L'_{sr} a_2 & L'_{sr} a_3 & L'_{sr} a_1 \\ L'_{sr} a_1 & L'_{sr} a_3 & L'_{sr} a_2 & L'_{ra} + L'_{lra} & -0.5L'_{mb} & -0.5L'_{mc} \\ L'_{sr} a_2 & L'_{sr} a_1 & L'_{sr} a_3 & -0.5L'_{ma} & L'_{rb} + L'_{lrb} & -0.5L'_{mc} \\ L'_{sr} a_3 & L'_{sr} a_2 & L'_{sr} a_1 & -0.5L'_{ma} & -0.5L'_{mb} & L'_{rc} + L'_{lrc} \end{bmatrix} \begin{bmatrix} i_{as} \\ i_{bs} \\ i_{cs} \\ i_{ar} \\ i_{br} \\ i_{cr} \end{bmatrix}
 \end{aligned} \tag{8.1}$$

To represent the variation between the leakage inductance and line current, a numerical curve fitting method to predict the leakage saturation curve is required. To achieve this, a polynomial function from the 12<sup>th</sup> degree is employed such that:

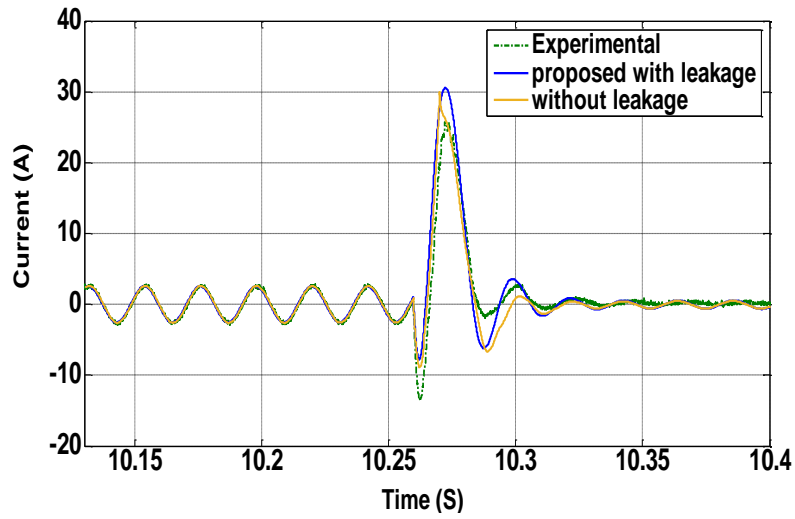
$$\begin{aligned}
 P = & [0.000000 \ 0.000000 \ 0.000000 \ 0.000000 \ 0.000013 \ -0.00014 \ 0.001113 \ -0.005880 \\
 & 0.020929 \ -0.048370 \ 0.067332 \ -0.047838 \ 0.025737]
 \end{aligned}$$

where  $P$  is a row vector of length 12 containing the polynomial coefficients in descending powers.

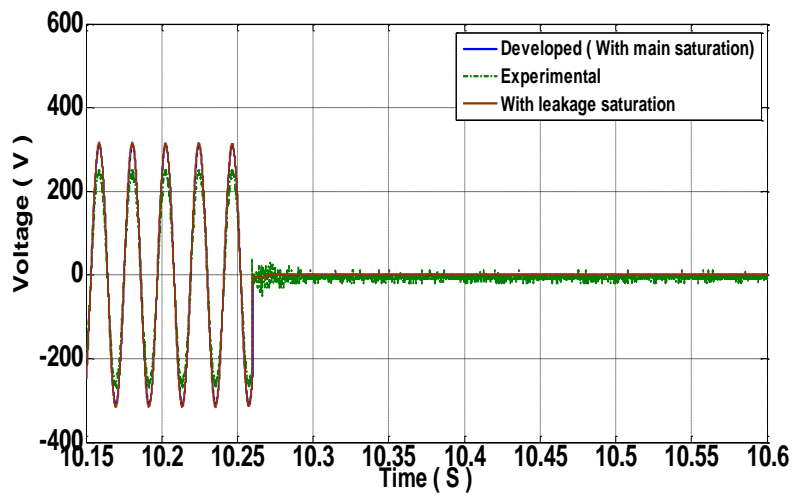
#### 8.4 Model results and experimental validation

In this section, the results obtained by the proposed analytical model presented in chapter 6, which include the main path saturation and neglect the leakage saturation, are compared with those obtained by the model that includes the main saturation as well as the leakage saturation effects presented in section 8.3. Experimental results are used as a reference for this comparison.

The results in Figure 8.2 show the behaviour of the output current and voltage of SEIG after a three-phase fault has occurred between the excitation capacitor and the resistive load. This fault occurred when the generator was feeding a balanced R-L load ( $R_{la} = R_{lb} = R_{lc} = 375 \Omega$ ,  $L_a=L_b=L_c= 1 \text{ H}$ ,  $C_a=C_b=C_c = 37\mu\text{F}$ ) per phase. Those results strengthen the truth that the SEIG is a ‘self-protected’ generator. It is clear that the voltage and current die quickly after the fault. This happens because the excitation capacitor is feeding the fault rather than feeding the generator. From this figure, it can easily be observed that the results generated by the proposed model, which take the leakage saturation and the main saturation effects into consideration, is more accurate in transient conditions ( $RMS_e = 1.57$ ) than results obtained by the model which includes the main path saturation but neglects the leakage saturation ( $RMS_e = 1.80$ ). However, there is no significant difference in the steady state condition. Figure 8.3 can explain this phenomenon, showing that the effect of dynamic inductance appears only for a dynamic response, whereas otherwise it is almost zero (theoretically it is zero but in our case it is a very small value and not equal to zero because the measured speed practically at steady state is not constant perfectly but it changes slightly). It can be seen that the effects of the dynamic matrix (as defined in equation 3.45 on page 47) calculated by the proposed model including leakage saturation is more than that produced when the leakage saturation is neglected as shown in Figure 8.3 and Figure 8.4 respectively.

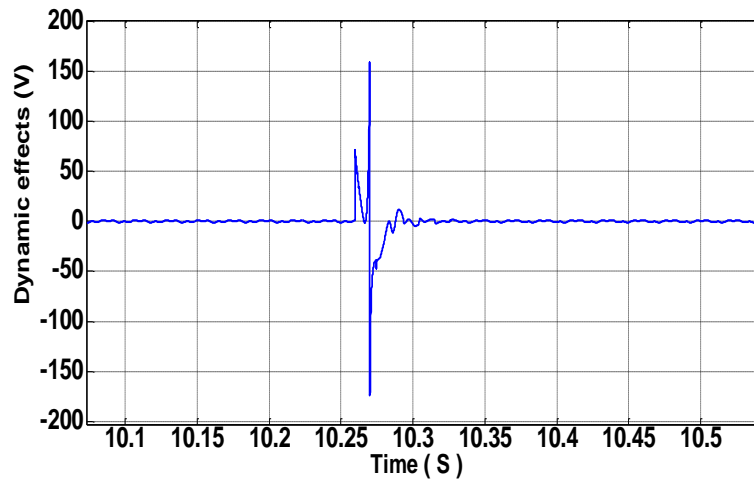


(a)

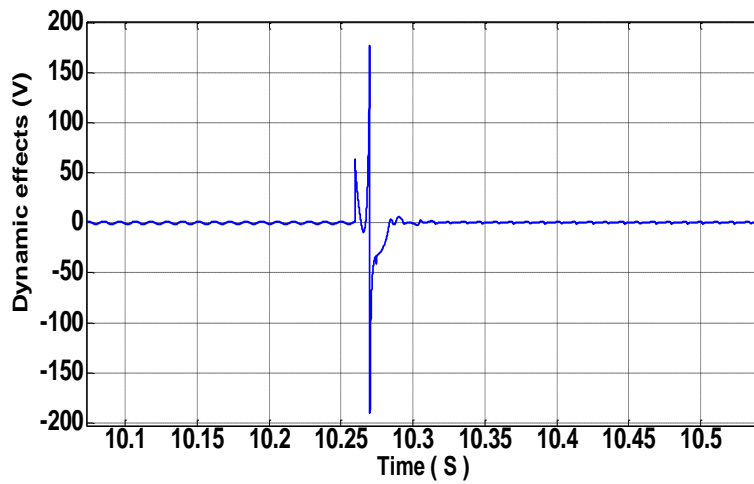


(b)

**Figure 8.2** Behaviour of stator current (a) and output voltage (b) of SEIG during a three-phase fault with and without including leakage saturation.

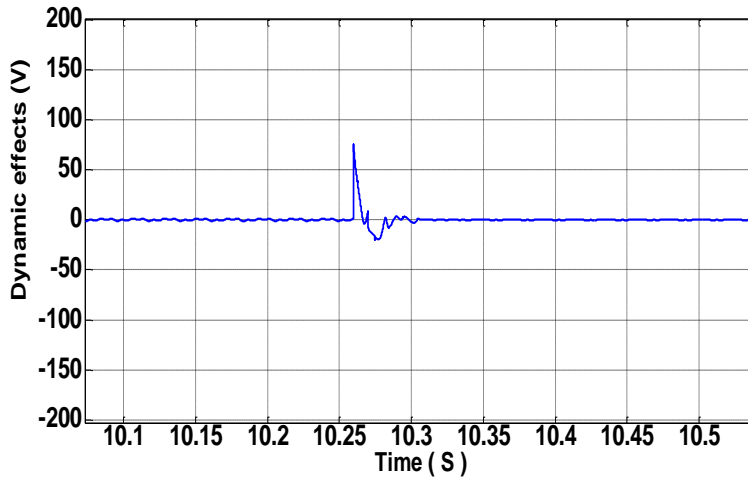


(a)

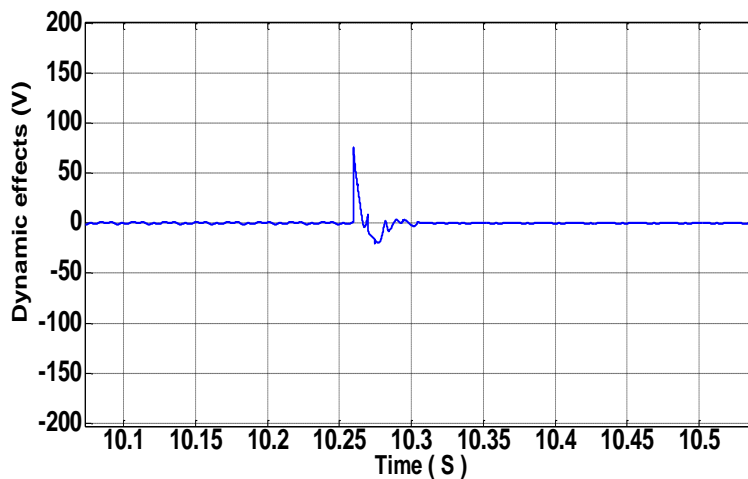


(b)

**Figure 8.3** Behaviour of dynamic inductance of stator (as defined in the equation 3.45) (a) and rotor (b) in phase a during a three-phase fault when leakage saturation is included.



(a)

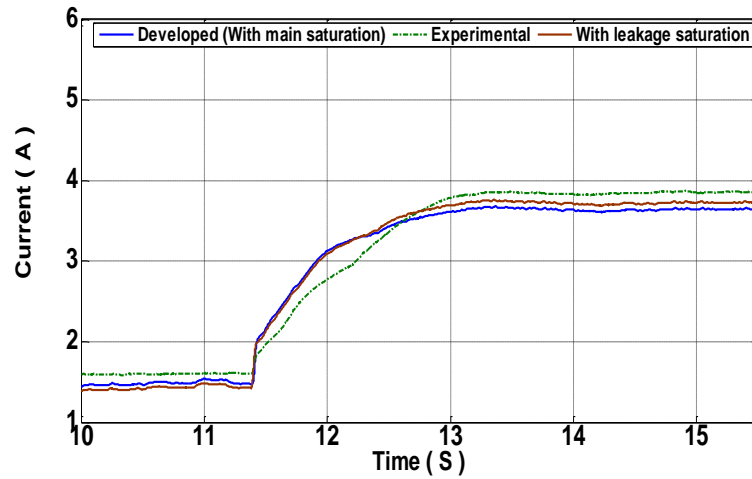


(b)

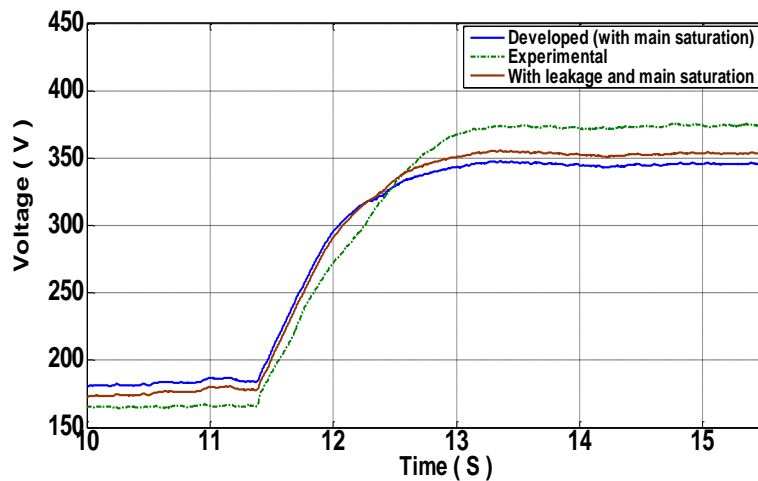
**Figure 8.4** Behaviour of dynamic matrix of stator (as defined in the equation 3.45) (a) and rotor (b) in phase a during a three-phase fault when leakage saturation is not included.

Figure 8.5 shows a comparison between the behaviour of current and voltage when including leakage saturation and main path saturation together in the same model (brown line) and including the main path saturation only (blue line) during the sudden removal of an R-L load ( $L_a=L_b=L_c=1$  H,  $R_a=R_b=R_c=365$ ,  $C_a=C_b=C_c=37$   $\mu$ F) at 11.4 Sec. The effects of the leakage in

this case are small in both steady state and transient conditions such that the  $RMSRMS_e$  without leakage saturation is 0.27, whereas with leakage saturation is 0.21.



(a)

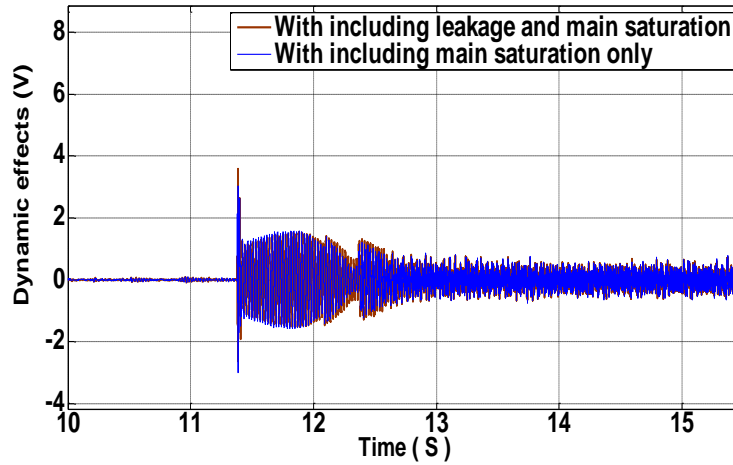


(b)

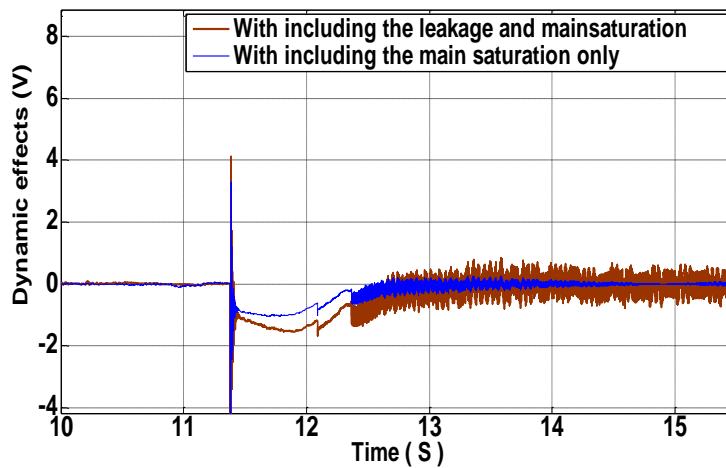
**Figure 8.5** Prediction of the behaviour of current (a) and voltage (b) of the SEIG with and without including leakage saturation after removing a three phase R-L load.

From Figure 8.6, it is clear that there is no effect of dynamic inductance in the steady state;

however, this effect becomes considerable after disturbance has occurred. In addition, it can be seen that the disparity between the dynamic response when the leakage saturation is included and the dynamic response without including leakage saturation is not significant.



(a)



(b)

**Figure 8.6** Behaviour of dynamic matrix of stator phase-a (a) and rotor phase-a (b) during the removal of three-phase load with and without including leakage saturation.

## 8.5 Conclusion

The analytical model developed has been extended to be capable of accounting for the main path leakage saturation besides the main path saturation and mutual saturation between the stator windings as well as that between rotor windings. A polynomial function of degree the 12<sup>th</sup> has been employed to represent the variation in the leakage inductance. The impact of including the leakage saturation on accuracy has been investigated in this chapter.

According to the results presented in this chapter, it can be concluded that the impact on accuracy of the inclusion of the nonlinearity approach to modelling the self-excited induction generator based on the saturation of leakage inductance becomes significant if high current values are reached during the dynamic response. However, during steady-state conditions the impact of including the leakage saturation on the accuracy is not considerable.

# Chapter 9. Conclusion and future work

---

## 9.1 Conclusion

A new, simple and general dynamic model of a three-phase self-excited induction generator with saturable inductances has been presented in this study. This analytical model of the three-phase self-excited induction generator was developed in the natural *abc* frame reference in order to be a universal and applicable model for various unbalanced operating conditions and to allow the tracking of the natural phase currents directly at any time during a transient [52], taking into consideration changes in magnetizing inductance with both rotor position and magnetizing current. The derivative of magnetizing inductance with respect to magnetizing current is included in the model so as to improve the accuracy of the calculation with dynamic responses. In this analytical model the main path saturation and the mutual saturation between stator windings as well as, that between the rotor windings are included.

In the proposed model presented in chapter 3, variation in magnetizing inductance is represented as an exponential function of the magnetizing current that can be derived from only three measured points of the open-circuit magnetizing curve of the machine  $[(I_{m1}, V_{g1}), (I_{m2}, V_{g2}) \text{ and } (I_{m3}, V_{g3})]$ : where  $I_{m3}$  is the maximum magnetising current that could be safely measured. The values of  $I_{m1}$  and  $I_{m2}$  are then determined from  $I_{m2} = \frac{5}{7} I_{m3}$  and  $I_{m1} = \frac{1}{7} I_{m3}$ . This method is safer for the machine under study as well as being simple and its use can avoid the lengthy measurements needed to obtain the measured no-load curve.

The proposed model was implemented in the Matlab/Simulink environment and used to predict the performance of the SEIG's operating characteristics at different operating conditions. The performance of the induction generator was investigated when operating at no-load, and when loaded with a star-connected resistive load and it has been tested at steady state and transient and balanced and unbalanced conditions. In addition, generator performance was investigated when both a resistive and an inductive

load were connected in parallel. Different operating conditions were considered: steady state, balanced and unbalanced load conditions, balanced and unbalanced load perturbation, and balanced and unbalanced fault conditions.

The results produced by the proposed model have been verified experimentally using a 415V, 7.5kW SEIG test machine driven by a DC motor. For successful excitation of the SEIG, a capacitance of 30 $\mu$ F was used in the resistive load tests described in this study whereas, 37 $\mu$ F was used when an R-L load was connected. Results obtained from the proposed model are shown to be in very good concordance with measured waveforms. This agreement is not only in the magnitude value of current and voltage but it is also in the phase angle. Despite that, the SEIG has been exposed to conditions, which may be considered as severe conditions, the proposed model was able to demonstrate a high capability in predicting the performance of induction generator at these severe conditions.

The importance of the derivative of the magnetizing inductance with respect to the magnetizing current has been clearly demonstrated. This has been achieved by comparing the results produced by the analytical proposed model with those using the conventional model. The proposed model accounts for the effect of saturation by including the magnetizing inductance derivative with respect to the magnetizing current, whereas the conventional model neglects the effects of dynamic inductance. In both models the variation in magnetizing inductance is approximated by an exponential function. Both models are employed to predict the dynamic response of the SEIG during different transient conditions, and are validated against experimental results. In all cases, the proposed model produces more accurate results than those from the conventional model, and this is not only true for voltage and current but also flux and torque. Therefore, it can be concluded that the impact of the derivative of the magnetizing inductance with respect to magnetizing current ( $dL_m/di_m$ ) on the accuracy of the simulated results is considerable. particularly during transient conditions whereas during the steady state there is almost no effect and the two sets of results almost coincide.

It can be observed from the results obtained from the comparison of the proposed and conventional models that there is an unexpected small disparity between the results from the proposed model and those produced by the conventional model during some cases in steady state conditions. This disparity may be attributed to a small change in the measured shaft speed which is used as the input speed vector for the simulation model.

The output stator voltage and current of the SEIG during fault events decline quickly, where the voltage collapses to zero immediately while the current takes approximately two cycles to do so. This shows that the SEIG is a self-protecting generator, which supports its use rather than other types of generator. During the first cycle of the three-phase fault current, a surge of current of a magnitude ten times the steady state current occurs. The prefault conditions such as the instant value, the value of excitation capacitance, and the value of the demanded current contribute to determining the magnitude of the current surge. It clear that the developed model has the capability to follow the behaviour of the SEIG accurately during this severe condition.

A DC-drive converter was used to run the generator at a constant speed by controlling the shaft speed of the prime mover (DC motor). It can be observed that the model accounts for any small variations around the average constant speed caused by the DC drive harmonics or mechanical vibrations. This was achieved by measuring and using the actual shaft speed to improve the accuracy of the proposed and the conventional models. In addition to the ability of the proposed model to perform well at constant shaft speed, it can also cope with a sudden change in mechanical speed. Despite a sudden drop and increase in shaft speed, the model succeeded in following this change. Hence, it can be conclude that the developed model can be used for applications with a variable speed within a limited range, which in our results was approximately  $\pm 15\%$  of the shaft speed. This advantage supports the use of the self-excited generator as a viable option for wind turbines applications, whereas, permanent magnet generators are not preferred in such applications since their output voltage increases linearly with prime mover speed.

The proposed model accounts for main path saturation as shown in chapter 3, and has been improved to be able to represent leakage path saturation effects by assuming that leakage inductance is variable, and therefore the derivative of leakage inductance is not equal zero. In this improved model, the derivative of leakage inductance with respect to magnetizing current is included. Additionally, the variation in leakage inductance is represented by a polynomial function of degree 12. The coefficient of this polynomial can be obtained using measured results. The inclusion of leakage saturation was investigated in this study by comparing the model which includes leakage effects with those which ignore it, and both sets of results are validated by experimental results.

According to the results produced by the dynamic model of the SEIG considering leakage saturation, it can be observed that the accuracy of predicting the SEIG performance at different operational conditions is improved noticeably in the dynamic response, whereas taking leakage saturation into account in the steady state condition does not have a significant impact on accuracy.

It has been observed from the experimental work that the ability of the generator to initiate the self-excitation process decreases as the load increases. Hence, for a smooth, reliable and successful start-up process for a SEIG, it is recommended that the load should stay disconnected until the induction generator has built up its voltage successfully and becomes stable. Then the load can be connected while the excitation capacitors are left connected during the process.

The remanent magnetism in the machine under study is represented by a small sinewave voltage source in the simulation model, such that its frequency is a function of rotor speed whereas its magnitude is constant if the speed is constant (almost 7 rms in this study at a speed of about 1500 rpm). It has been observed that this method of representing the residual flux can help in improving the accuracy of the model.

From experimental work, it has been observed that the induction generator may experience a reduction in its remanent magnetization and become de-excited, which results in its voltage failing to build up. This may happen after a fault has occurred on its terminals or if the generator is left to slow down while a small resistive load is connected to its terminal as a result of the reduction of remanent magnetization in the rotor. Thus, it is not possible to initiate the self-excitation process. To overcome the adequacy of the remanent magnetism in the induction generator, several methods can be employed in order to increase the residual flux. From the experimental work, it has been noted that the easiest, most practical, and quickest method is to run the machine when the induction machine is connected to the capacitance. From the experiment, it has been noticed that the higher the capacitance a shortest time is taken to increase the residual flux. When 40  $\mu\text{F}$  is connected, the generator will take approximately one minute to recover its remnant magnetic field.

## 9.2 Future work

For more realistic operation conditions, the investigation of the performance of the SEIG under different operational conditions employing the proposed model accounting for main path saturation can be implemented using a wind/hydro turbine as the prime mover. This has a constant change nature, whereas the DC motor used in the experimental bench in order to emulate the wind turbine by given a constant speed.

For more investigation for the performance of proposed mathematical model developed in ABC/a-b-c frame in predicting the response of the SEIG in different operation conditions. An investigation study can be introduced. This could be implemented by having a path for a zero sequence in the system under study. For a more accurate representation, it is necessary to include the zero component in the mathematical model in the steady state operation. The model can then be improved to have the capabilities of including the zero sequence by using the symmetrical components. In order to find a path in the circuit for the zero sequence, the system is required to be reconnected such that the induction generator is connected to the ground and the induction generator, excitation capacitor, and load should be connected to neutral.

# Appendix A. Derivation of the exponential function

---

The mathematical derivation of the exponential function presented in chapter 4, which is used as a numerical curve-fitting method to predict and approximate the magnetizing curve from the measured three points, can be shown as follows:

By substituting the three measurements points,  $(I_{m1}, V_{g1})$ ,  $(I_{m2}, V_{g2})$  and  $(I_{m3}, V_{g3})$ , in the following equation:

$$V_g = FI_m (K_1 e^{K_2 I_m^2} + K_3) \quad A.1$$

and assuming  $F=1$ , we can get:

$$V_{g1} = (K_1 e^{K_2 I_{m1}^2} + K_3) I_{m1} \quad A.2$$

$$V_{g2} = (K_1 e^{K_2 I_{m2}^2} + K_3) I_{m2} \quad A.3$$

$$V_{g3} = (K_1 e^{K_2 I_{m3}^2} + K_3) I_{m3} \quad A.4$$

Or more specifically,

$$a = \frac{V_{g1}}{I_{m1}} = (K_1 e^{K_2 I_{m1}^2} + K_3) \quad A.5$$

$$b = \frac{V_{g2}}{I_{m2}} = (K_1 e^{K_2 I_{m2}^2} + K_3) \quad A.6$$

$$c = \frac{V_{g3}}{I_{m3}} = (K_1 e^{K_2 I_{m3}^2} + K_3) \quad A.7$$

Manipulation of the last three equations can produce:

$$\frac{c - K_3}{a - K_3} = \left( \frac{b - K_3}{a - K_3} \right)^k \quad \text{A.8}$$

In order to make equation A.8 more beneficial, the value of k should be any real value not equal to 1. And to find the relationship between  $I_{m_1} I_{m_2} I_{m_3}$  which can be memorise and applied in the laboratory:

$$k = \frac{I_{m_3}^2 - I_{m_1}^2}{I_{m_2}^2 - I_{m_1}^2} = 2 \quad \text{A.9}$$

Therefore,

$$I_{m_3}^2 - I_{m_1}^2 = 2(I_{m_2}^2 - I_{m_1}^2) \quad \text{A.10}$$

Or

$$I_{m_3}^2 = (I_{m_1}^2 - I_{m_3}^2)/2 \quad \text{A.11}$$

If this is done in equation 25,  $I_{m_3} = nI_{m_1}$ , and n is an integer, we get:

$$I_{m_2} = I_{m_1} \sqrt{\frac{n^2 + 1}{2}} \quad \text{A.12}$$

In order to have a sequence of minimum integer numbers, it is important to select the smallest convenient value of n; in this case, it could be n=7. So,

$$I_{m_3} = 7I_{m_1} \quad \text{A.13}$$

By substituting n=7 in the equation A.12,

we get:

$$I_{m_2} = 5I_{m_1}$$

Equation A.8 has infinite solutions for integers  $k > 1$ , therefore for trivial solutions the next smallest integer is  $k = 2$ , which is the simplest solution. So,

$$(c - K_3)(a - K_3) = (b - K_3)^2 \quad \text{A.14}$$

Or, simplifying,

$$b^2 - 2bK_3 + K_3(a + c) - ac = 0 \quad \text{A.15}$$

By isolating  $K_3$  we can get:

$$K_3 = \frac{b^2 - ac}{2b - (a + c)} \quad \text{A.16}$$

To find  $K_1$  and  $K_2$  the following derivations can be used.

If equation A.16 is replaced in expression  $a - K_3$  and  $c - K_3$  we get:

$$(a - K_3) = \frac{(a-b)^2}{a+c-2b} \quad \text{A.17}$$

$$(c - K_3) = \frac{(a-b)^2}{a+c-2b} \quad \text{A.18}$$

With further manipulation of the two above equations A.17 and A.18 taking into consideration that:

$$I_{m_1} = \frac{I_{m_3}}{7}$$

we get,

$$K_2 = \frac{49 \ln \left( \frac{b-c}{a-b} \right)}{24 I_{m3}^2} \quad \text{A.19}$$

After some algebraic transformation,

$$K_1 = (c - K_3) \left( \frac{a-b}{b-c} \right)^{49/24} \quad \text{A.20}$$

$$K_3 = \frac{b^2 - ac}{2b - (a+c)} \quad \text{A.21}$$

## Appendix B. The determination of the minimum capacitor value

---

The method used in this study to determine the minimum value of the excitation capacitance required to initiate the build-up process is the formula derived by Eltamaly [69] as follows:

$$C_{min} = \frac{1}{2\pi} \left( \frac{X_L a}{M_3} + \frac{M_4}{M_1^2 + M_2^2} \right)$$

The coefficients  $M_1$ ,  $M_2$ ,  $M_3$  and  $M_4$  are as follows:

$$M_1 = R_s R_r - f(f - v)L_1$$

$$M_2 = R_r f L_3 + R_s(f - v)L_2$$

$$M_3 = R_L^2 + X_L^2 f^2 \text{ and}$$

$$M_4 = R_r^* M_2 - L_2 f(f - v)af \text{ Where}$$

$$L1 = X_s(X_r + X_m) + X_r X_m ,$$

$$L2 = X_r + X_m \text{ and,}$$

$$L3 = X_s + X_m$$

$a$ :  $P_u$  per unit frequency  $f/f_b$

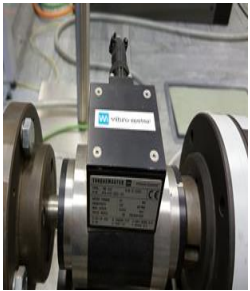
$f$  actual or (generated) frequency (Hz).

$f_b$  based frequency of induction generator (Hz).

## Appendix C. Laboratory tools

<i>Item</i>	<i>Description</i>	<i>Purpose</i>	<i>Photo</i>
Three-phase AC sources	ET system variable voltage, variable frequency three-phase AC power supply, 3×2000VA, 3×0~270V, 3×15A Type: EAC/3P2000/cc/ATI-10/LT Serial No.: 7.13.2389.	Used when calculating the equivalent circuit parameters to carry out the locked rotor and no-load tests and also for the machine magnetic characteristics tests.	
RLC meter	Hameg HM 8118	To measure inductance and capacitance	
Wattmeter	Weston Wattmeter, Model S.67, maximum Current: 5 A, maximum voltage: 300V.	Active and reactive power measurements for the no-load and locked rotor tests carried out to determine the machine equivalent circuit parameters.	
DC Drive	1.5 kW Mentor II Digital DC Drive manufactured by Control Techniques.	Control and rotate the DC motor.	

Item	Description	Purpose	Photo
Three-phase autotransformer	Three-phase autotransformer used as a variable voltage source, maximum winding current: 20 A, maximum winding voltage: 270V.	To provide the induction machine with a three-phase variable voltage, used to find the magnetising of characteristics of the induction machine.	
Voltage probe	Tektronix P5200 high voltage differential probe.	Measurement and recording of the generator output voltages.	
Variable resistive load	Three Curtis variable resistors, 5 A, 300 V, $2 \times 60 \Omega$ .	To provide the generator with a three-phase variable resistive load.	
Induction machine	A 7.5 kW, 415 V, 15A, 50 Hz, 4-pole star connected three-phase squirrel-cage induction machine, manufactured by Brook Hansen.	The machine is Used as induction generator after its terminals connected to capacitors.	

<i>Item</i>	<i>Description</i>	<i>Purpose</i>	<i>Photo</i>
DC motor	A 9 kW, 240 V, 37.5 A, maximum RPM 1800 r.p.m, armature: 240 V, 15 A, fields:240 V, 0.6/0.16 A.	Drives the induction machine.	
Capacitor bank	Three-phase variable excitation capacitor bank	To provide the reactive power needed by induction generator.	
Current probe	Tektronix A622 AC/DC Current probe.	Measure and record generator, load and capacitor currents.	
Oscilloscope	Tektronix MSO 4034 mixed signal oscilloscope, 350 MHz, 2.5Gs/S, voltage 110~240 V, frequency 50~60 Hz, maximum power 250 W  Serial No. MSO04034 C000029	To capture data and export it to an external device for further processing.	
Torque display	Magtrol Model 3411	To read the output signal of the encoder	
Torque and Speed transducer	Torquemaster TM 210  Rated torque: 50 Nm Pulse wheel: 30 pulse/ Rev  Serial No. G-0185	To measure shaft speed	

## Appendix D. Lagrange polynomial

The Lagrange interpolating polynomial is the polynomial  $L(x)$  of degree  $\leq(n-1)$  that passes through the  $n$  points  $(x_1, y_1 = f(x_1)), (x_2, y_2 = f(x_2)), \dots, (x_n, y_n = f(x_n))$ , and is given by:

$$L(x) = \sum_{j=1}^n L_j(x)$$

$$L_i(x) = y_i \prod_{\substack{j=1 \\ j \neq i}}^n \frac{x - x_j}{x_i - x_j}$$

For example to find a polynomial order 3 we need four points which was chosen from magnetising test as follows:

$I_m$	$L_m$
0.270	0.300626
0.403	0.346271
0.934	0.364659
2.640	0.226796

$$L_m = \frac{(x - x_2)(x - x_3)(x - x_4)}{(x_1 - x_2)(x_1 - x_3)(x_1 - x_4)} L_1 + \frac{(x - x_1)(x - x_3)(x - x_4)}{(x_2 - x_1)(x_2 - x_3)(x_2 - x_4)} L_2$$

$$+ \frac{(x - x_1)(x - x_2)(x - x_4)}{(x_3 - x_1)(x_3 - x_2)(x_3 - x_4)} L_3 + \frac{(x - x_1)(x - x_2)(x - x_3)}{(x_4 - x_1)(x_4 - x_2)(x_4 - x_3)} L_4$$

$$\begin{aligned}
&= x^3 - (x_2 + x_3 + x_4)x^2 + (x_3x_2 + x_2x_4 + x_3x_4)x - x_2x_3x_4 \\
&= (0.3006) + \frac{x^3 - (x_1 + x_3 + x_4)x^2 + (x_1x_3 + x_1x_4 + x_3x_4)x - x_1x_3x_4}{(0.403 - 0.27)(0.403 - 0.934)(0.403 - 2.64)} \quad (0.3463) \\
&\quad + \frac{x^3 - (x_1 + x_2 + x_4)x^2 + (x_1x_2 + x_1x_4 + x_2x_4)x - x_1x_2x_4}{(0.934 - 0.27)(0.934 - 0.403)(0.934 - 2.64)} \quad (0.3646) \\
&\quad + \frac{x^3 - (x_1 + x_2 + x_3)x^2 + (x_1x_2 + x_1x_3 + x_2x_3)x - x_1x_2x_3}{(2.64 - 0.27)(2.64 - 0.403)(2.64 - 0.934)} \quad (0.2268)
\end{aligned}$$

$$L(x) = 0.1747x^3 - 0.7463x^2 + 0.7858x + 0.1394 \quad \text{or}$$

$$L(x) = 0.1747i_m^3 - 0.7463i_m^2 + 0.7858i_m + 0.1394$$

# References

---

- [1] F. A. Farret and M. G. Simões, *Integration of alternative sources of energy*: John Wiley & Sons, 2006.
- [2] L. L. Lai, *Power system restructuring and deregulation: trading, performance and information technology*: John Wiley & Sons, 2001.
- [3] N. Jayalakshmi and D. Gaonkar, "Dynamic modeling and analysis of an isolated self excited induction generator driven by a wind turbine," in *Power, Signals, Controls and Computation (EPSCICON), 2012 International Conference on*, 2012, pp. 1-5.
- [4] A. Alfarhan, S. M. Gadoue, B. Zahawi, M. Shalaby, and M. A. Elgendy, "Modelling of magnetizing inductance saturation in self-excited induction generators," in *2016 IEEE 16th International Conference on Environment and Electrical Engineering (EEEIC)*, Florence, 2016, pp. 1-6.
- [5] R. R. Chilipi, B. Singh, and S. S. Murthy, "Performance of a Self-Excited Induction Generator With DSTATCOM-DTC Drive-Based Voltage and Frequency Controller," *Energy Conversion, IEEE Transactions on*, vol. 29, pp. 545-557, 2014.
- [6] S. S. Kumar, N. Kumaresan, M. Subbiah, and M. Rageeru, "Modelling, analysis and control of stand-alone self-excited induction generator-pulse width modulation rectifier systems feeding constant DC voltage applications," *IET Generation, Transmission & Distribution*, vol. 8, pp. 1140-1155, 2014.
- [7] R. R. Chilipi, B. Singh, S. S. Murthy, S. Madishetti, and G. Bhuvaneshwari, "Design and implementation of dynamic electronic load controller for three-phase self-excited induction generator in remote small-hydro power generation," *IET Renewable Power Generation*, vol. 8, pp. 269-280, 2014.
- [8] R. Choudhary and R. Saket, "A critical review on the self-excitation process and steady state analysis of an SEIG driven by wind turbine," *Renewable and Sustainable Energy Reviews*, vol. 47, pp. 344-353, 2015.
- [9] A. Alsalloum, A. Alolah, and R. Hamouda, "Transient performance of isolated induction generator under different loading conditions," in *Systems, Signals & Devices (SSD), 11th International Multi-Conference on*, 2014, pp. 1-6.
- [10] E. E. Agency. (2011, Feb 02). *Renewable energy production must grow fast to reach the 2020 target* [Online]. Available: <http://www.eea.europa.eu/highlights/renewable-energy-production-must-grow>
- [11] R. Bansal, "Three-phase self-excited induction generators: an overview," *Energy*

- Conversion, IEEE Transactions on*, vol. 20, pp. 292-299, 2005.
- [12] F. De Mello and G. Walsh, "Reclosing transients in induction motors with terminal capacitors," *Transactions of the American Institute of Electrical Engineers. Part III: Power Apparatus and Systems*, vol. 3, pp. 1206-1213, 1960.
- [13] J. B. Patton and D. Curtice, "Analysis of utility protection problems associated with small wind turbine interconnections," *Power Apparatus and Systems, IEEE Transactions on*, vol. vol. PAS-101, pp. 3957-3966, 1982.
- [14] G. Raina and O. Malik, "Wind energy conversion using a self-excited induction generator," *Power Apparatus and Systems, IEEE Transactions on*, vol. PAS-102, pp. 3933-3936, 1983.
- [15] L. Wang, Y.-H. Lin, and Y.-T. Chen, "Load-flow analysis of a wind farm containing multiple wind-driven wound-rotor induction generators with dynamic slip control using RX models," *Sustainable Energy, IEEE Transactions on*, vol. 2, pp. 256-264, 2011.
- [16] L. Wang and R.-Y. Deng, "Transient performance of an isolated induction generator under unbalanced excitation capacitors," *Energy Conversion, IEEE Transactions on*, vol. 14, pp. 887-893, 1999.
- [17] S. Murthy, O. Malik, and A. Tandon, "Analysis of self-excited induction generators," *IEE Proceedings C (Generation, Transmission and Distribution)*, vol. 129, pp. 260-265, 1982.
- [18] J. Elder, J. Boys, and J. Woodward, "The process of self excitation in induction generators," *IEE Proceedings B (Electric Power Applications)*, vol. 130, pp. 103-108, 1983.
- [19] L. Quazene and G. Mcpherson, "Analysis Of The Isolated Induction Generator," *IEEE Transactions, Power Apparatus and Systems*, vol. 102, pp. 2793-2798, 1983.
- [20] J. Elder, J. Boys, and J. Woodward, "Self-excited induction machine as a small low-cost generator," *IEE Proceedings C (Generation, Transmission and Distribution)*, vol. 131, pp. 33-41, 1984.
- [21] M. A. Ouhrouche, X. D. Do, Q. M. Le, and R. Chaine, "EMTP based simulation of a self-excited induction generator after its disconnection from the grid," *Energy Conversion, IEEE Transactions on*, vol. 13, pp. 7-14, 1998.
- [22] L. Shridhar, B. Singh, C. Jha, and S. Murthy, "Selection of capacitors for the self regulated short shunt self excited induction generator," *Energy Conversion, IEEE Transactions on*, vol. 10, pp. 10-17, 1995.
- [23] L. Shridhar, B. Singh, and C. Jha, "A step towards improvements in the characteristics of self excited induction generator," *IEEE Transactions on Energy Conversion and Management*, vol. Vol. 1, pp. pp.40-46, 1993.

- [24] D. Watson, J. Arrillaga, and T. Densem, "Controllable dc power supply from wind-driven self-excited induction machines," *Electrical Engineers, Proceedings of the Institution of*, vol. 126, pp. 1245-1248, 1979.
- [25] N. Smith, A. Williams, A. Brown, S. Mathena, and A. Nakarmi, "Stand-alone induction generators for reliable low cost micro-hydro installations, energy and environment," *Proc. World Renewable Energy Congr*, pp. 2904-2908, 1990.
- [26] N. P. Smith, "Induction generators for stand-alone micro-hydro systems," Institute of Electrical and Electronics Engineers, Inc., Piscataway, NJ (United States)1995.
- [27] A. Nejmi, Y. Zidani, and M. Naciri, "Investigation on the self-excited induction generator provided with a hydraulic regulator," ed: FIER, 2002, pp. 494–499.
- [28] N. Ammasaigounden and M. Subbiah, "Microprocessor-based voltage controller for wind-driven induction generators," *Industrial Electronics, IEEE Transactions on*, vol. 37, pp. 531-537, 1990.
- [29] R. Hunter and G. Elliot, *Wind-diesel systems: a guide to the technology and its implementation*: Cambridge University Press, 1994.
- [30] J. Casel and H. Knitterscheidt, "Induction generators for generating and emergency power supplies of the future," *Electrotechnische Zeitschrift*, vol. 102, pp. 139-141, 1981.
- [31] J. Bae, Y. Kim, Y. Son, H. Moon, C. Yoo, T. Jung, *et al.*, "Design and Analysis of a Regenerative Electromagnetic Brake," *Magnetics, IEEE Transactions on*, vol. 50, pp. 1-4, 2014.
- [32] B. Jae-Nam, K. Yong-Eun, S. Young-Wook, M. Hee-Seok, Y. Chang-Hee, and L. Ju, "Self-Excited Induction Generator as an Auxiliary Brake for Heavy Vehicles and Its Analog Controller," *Industrial Electronics, IEEE Transactions on*, vol. 62, pp. 3091-3100, 2015.
- [33] A. Al Jabri and A. Alolah, "Capacitance requirement for isolated self-excited induction generator," *IEE Proceedings B (Electric Power Applications)*, vol. 137, pp. 154-159, 1990.
- [34] T. Chan and L. L. Lai, "Capacitance requirements of a three-phase induction generator self-excited with a single capacitance and supplying a single-phase load," *Energy Conversion, IEEE Transactions on*, vol. 17, pp. 90-94, 2002.
- [35] N. H. Malik and A. A. Mazi, "Capacitance requirements for isolated self excited induction generators," *Energy Conversion, IEEE Transactions on*, pp. 62-69, 1987.
- [36] B. A. Kumar, N. Kamaraj, and C. Subasri, "Voltage Control of a STATCOM at a Fixed Speed Wind Farm Under Unbalanced Grid Faults Using Fuzzy Logic Technique," presented at the Power Electronics and Renewable Energy Systems, 2015.

- [37] R. R. Chilipi, B. Singh, and S. Murthy, "A new voltage and frequency controller for standalone parallel operated self excited induction generators," *International Journal of Emerging Electric Power Systems*, vol. 13, pp. 1-17, 2012.
- [38] B. Singh, S. Murthy, M. Goel, and A. Tandon, "A steady state analysis on voltage and frequency control of self-excited induction generator in micro-hydro system," in *Power Electronics, Drives and Energy Systems, 2006. PEDES'06. International Conference on*, 2006, pp. 1-6.
- [39] L. Wang and S.-C. Kuo, "Steady state performance of a self-excited induction generator under unbalanced load," in *Power Engineering Society Winter Meeting, 2002. IEEE*, 2002, pp. 408-412.
- [40] J. Bhattacharya and J. Woodward, "Excitation balancing of a self-excited induction generator for maximum power output," in *Generation, transmission and distribution, IEE Proceedings C*, 1988, pp. 88-97.
- [41] A. K. Chattopadhyay, "Digital Computer Simulation of an Adjustable-speed induction motor Drive with a cycloconverter-type thyristor-commutator in the Rotor," *Industrial Electronics and Control Instrumentation, IEEE Transactions on*, pp. 86-92, 1976.
- [42] P. C. Krause and C. Thomas, "Simulation of symmetrical induction machinery," *Power Apparatus and Systems, IEEE Transactions on*, vol. 84, pp. 1038-1053, 1965.
- [43] H. E. Jordan, "Digital computer analysis of induction machines in dynamic systems," *Power Apparatus and Systems, IEEE Transactions on*, pp. 722-728, 1967.
- [44] S. Alghuwainem, "Steady-state analysis of a self-excited induction generator self-regulated by a shunt saturable reactor," in *Electric Machines and Drives Conference Record, 1997. IEEE International*, 1997, pp. MB1/10.1-MB1/10.3.
- [45] S. Alghuwainem, "Steady-state analysis of a self-excited induction generator including transformer saturation," *Energy Conversion, IEEE Transactions on*, vol. 14, pp. 667-672, 1999.
- [46] Y. Rahim, "Excitation of isolated three-phase induction generator by a single capacitor," *Electric Power Applications, IEE Proceedings B*, vol. 140, pp. 44-50, 1993.
- [47] S. Murthy, B. P. Singh, C. Nagamani, and K. Satyanarayana, "Studies on the use of conventional induction motors as self-excited induction generators," *Energy Conversion, IEEE Transactions on*, vol. 3, pp. 842-848, 1988.
- [48] S. Murthy and S. Acharya, "MATLAB based steady state analysis of self excited induction generator," in *Power Electronics and Drive Systems, 2003. PEDS 2003. The Fifth International Conference on*, 2003, pp. 749-753.
- [49] O. I. Okoro, "Matlab simulation of induction machine with saturable leakage and magnetizing inductances " *The Pacific Journal of Science and Technology* vol. 5, pp. 5-15, April 2003.

- [50] K. Idjdarene, D. Rekioua, T. Rekioua, and A. Tounzi, "Performance of an isolated induction generator under unbalanced loads," *Energy Conversion, IEEE Transactions on*, vol. 25, pp. 303-311, 2010.
- [51] E. Levi, "Impact of cross-saturation on accuracy of saturated induction machine models," *Energy Conversion, IEEE Transactions on*, vol. 12, pp. 211-216, 1997.
- [52] P. Pillay and V. Levin, "Mathematical models for induction machines," in *Industry Applications Conference, 1995. Thirtieth IAS Annual Meeting, IAS'95., Conference Record of the 1995 IEEE*, 1995, pp. 606-616.
- [53] P. C. Krause, O. Wasynczuk, and S. D. Sudhoff, *Analysis of electric machinery and drive systems*, 2nd ed. New Jersey: IEEE Press Power Engineering Series, 2002.
- [54] O. I. Okoro, "Dynamic and thermal modelling of induction machine with non-linear effects," PhD, Kassel University Press Kassel, 2002.
- [55] A. Alsalloum, R. Hamouda, A. Alolah, and A. Eltamaly, "Transient Performance of an Isolated Induction Generator under Unbalanced Loading Conditions," *Journal of Energy and Power Engineering*, vol. 4, 2010.
- [56] D. Seyoum, C. Grantham, and M. F. Rahman, "The dynamic characteristics of an isolated self-excited induction generator driven by a wind turbine," *Industry Applications, IEEE Transactions on*, vol. 39, pp. 936-944, 2003.
- [57] J. G. Trapp, J. B. Parizzi, F. A. Farret, A. Serdotte, and A. J. Longo, "Stand alone self-excited induction generator with reduced excitation capacitors at fixed speed," presented at the Power Electronics Conference (COBEP), 2011 Brazilian, 2011.
- [58] S. Alghuwainem, "Steady-state analysis of an isolated self-excited induction generator driven by regulated and unregulated turbine," *IEEE Transactions on Energy Conversion and Management*, vol. 14, pp. 718-723, 1999.
- [59] L. Ouazene and G. McPherson, "Analysis of the Isolated Induction Generator," *Power Apparatus and Systems, IEEE Transactions on*, vol. PAS-102, pp. 2793-2798, 1983.
- [60] E. Levi and Y. Liao, "An experimental investigation of self-excitation in capacitor excited induction generators," *Electric Power Systems Research*, vol. 53, pp. 59-65, 2000.
- [61] E. Bassett and F. Potter, "Capacitive excitation for induction generators," *Transactions of the American Institute of Electrical Engineers*, vol. 54, pp. 540-545, 1935.
- [62] B. Doxey, "Theory and application of the capacitor-excited induction generator(Generation of electric power using a squirrel-cage induction motor excited by means of capacitors and employing no external supply)," *The Engineer*, vol. 216, pp. 893-897, 1963.
- [63] M. R. Patel, *Wind and solar power systems: design, analysis, and operation*: CRC press,

- 1999.
- [64] M. Salama and P. Holmes, "Transient and steady-state load performance of a stand-alone self-excited induction generator," *IEE Proceedings-Electric Power Applications*, vol. 143, pp. 50-58, 1996.
- [65] R. Stanislav, S. Pavel, and M. Velešlav, "Research of transients in induction generator for small-scale wind power in Off-the-Grid by using EMTP-ATP," in *Electric Power Engineering (EPE), Proceedings of the 2014 15th International Scientific Conference on*, 2014, pp. 343-347.
- [66] F. Sulla, *Island operation with induction generators: fault analysis and protection*: Department of Measurement Technology and Industrial Electrical Engineering, Lund University, 2009.
- [67] C. Wagner, "Self-excitation of induction motors," *Electrical Engineering*, vol. 58, pp. 47-51, 1939.
- [68] A. Al Jabri and A. Alolah, "Capacitance requirement for isolated self-excited induction generator," in *IEE Proceedings B (Electric Power Applications)*, 1990, pp. 154-159.
- [69] A. M. Eltamaly, "New formula to determine the minimum capacitance required for self-excited induction generator," in *Power Electronics Specialists Conference, 2002. pesc 02. 2002 IEEE 33rd Annual*, 2002, pp. 106-110.
- [70] T. Chan, "Steady-state analysis of self-excited induction generators," *Energy Conversion, IEEE Transactions on*, vol. 9, pp. 288-296, 1994.
- [71] T. Chan, "Capacitance requirements of self-excited induction generators," *Energy Conversion, IEEE Transactions on*, vol. 8, pp. 304-311, 1993.
- [72] L. Wang and C.-H. Lee, "A novel analysis on the performance of an isolated self-excited induction generator," *Energy Conversion, IEEE Transactions on*, vol. 12, pp. 109-117, 1997.
- [73] G. Singh, "Self-excited induction generator research—a survey," *Electric Power Systems Research*, vol. 69, pp. 107-114, 2004.
- [74] J. Björnstedt, F. Sulla, and O. Samuelsson, "Experimental investigation on steady-state and transient performance of a self-excited induction generator," *IET generation, transmission & distribution*, vol. 5, pp. 1233-1239, 2011.
- [75] R. Bonert and S. Rajakaruna, "Self-excited induction generator with excellent voltage and frequency control," *Generation, Transmission and Distribution, IEE Proceedings*, vol. 145, pp. 33-39, 1998.
- [76] E. Suarez and G. Bortolotto, "Voltage-frequency control of a self-excited induction generator," *Energy Conversion, IEEE Transactions on*, vol. 14, pp. 394-401, 1999.

- [77] J. Elder, J. T. Boys, and J. Woodward, "Self-excited induction machine as a small low-cost generator," in *IEE Proceedings C (Generation, Transmission and Distribution)*, 1984, pp. 33-41.
- [78] M. B. Brennen and A. Abbondanti, "Static exciters for induction generators," *Industry Applications, IEEE Transactions on*, pp. 422-428, 1977.
- [79] W.-L. Chen, Y.-H. Lin, H.-S. Gau, and C.-H. Yu, "STATCOM controls for a self-excited induction generator feeding random loads," *Power Delivery, IEEE Transactions on*, vol. 23, pp. 2207-2215, 2008.
- [80] I. Smith and S. Sriharan, "Transients in induction machines with terminal capacitors," in *Proceedings of the Institution of Electrical Engineers*, 1968, pp. 519-527.
- [81] C. Wagner, "Self-excitation of induction motors with series capacitors," *Electrical Engineering*, vol. 60, pp. 1241-1247, 1941.
- [82] M. Nagpal, T. G. Martinich, A. Bimbhra, and M. Ramamurthy, "Hazardous Temporary Overvoltages From Self-Excited Large Induction Motors—A Case Study," *Power Delivery, IEEE Transactions on*, vol. 27, pp. 2098-2104, 2012.
- [83] D. Limebeer and R. Harley, "Subsynchronous resonance of single-cage induction motors," in *IEE Proceedings B (Electric Power Applications)*, 1981, pp. 33-42.
- [84] T. Le and R. Zavadil, "Shunt capacitor failures due to windfarm induction generator self-excitation phenomenon," *Energy Conversion, IEEE Transactions on*, vol. 8, pp. 513-519, 1993.
- [85] A. Kishore and G. S. Kumar, "Dynamic modeling and analysis of three phase self-excited induction generator using generalized state space approach," in *International Symposium on Power Electronics, Electrical Drives, Automation and Motion, 2006. SPEEDAM 2006.*, 2006, pp. 1459-1466.
- [86] L. Wang and C.-H. Lee, "Long-shunt and short-shunt connections on dynamic performance of a SEIG feeding an induction motor load," *Energy Conversion, IEEE Transactions on*, vol. 15, pp. 1-7, 2000.
- [87] O. Ojo, "Performance of self-excited single-phase induction generators with shunt, short-shunt and long-shunt excitation connections," *Energy Conversion, IEEE Transactions on*, vol. 11, pp. 477-482, 1996.
- [88] S. Jain, J. Sharma, and S. Singh, "Transient performance of three-phase self-excited induction generator during balanced and unbalanced faults," *IEE Proceedings-Generation, Transmission and Distribution*, vol. 149, pp. 50-57, 2002.
- [89] G. R. Slemon, "Modelling of induction machines for electric drives," *Industry Applications, IEEE Transactions on*, vol. 25, pp. 1126-1131, 1989.
- [90] J. Reynaud and P. Pillay, "Reclosing transients in induction machines including the

- effects of saturation of the magnetizing branch and a practical case study," *Energy Conversion, IEEE Transactions on*, vol. 9, pp. 383-389, 1994.
- [91] E. Levi, "A unified approach to main flux saturation modelling in dq axis models of induction machines," *Energy Conversion, IEEE Transactions on*, vol. 10, pp. 455-461, 1995.
- [92] P. Leplat, A. Tounzi, S. Clénet, and F. Piriou, "Study of an induction machine using Park's model and finite element method," in *International Conference on Electrical Machines (ICEM 96) Septembre*, 1996, pp. 24-29.
- [93] Y.-K. He and T. Lipo, "Computer simulation of an induction machine with spatially dependent saturation," *Power Apparatus and Systems, IEEE Transactions on*, vol. PAS-103, pp. 707-714, April 1984.
- [94] L. Kalamen, P. Rafajdus, P. Sekerák, and V. Hrabovcová, "A novel method of magnetizing inductance investigation of self-excited induction generators," *Magnetics, IEEE Transactions on*, vol. 48, pp. 1657-1660, 2012.
- [95] Y.-J. Wang and S.-Y. Huang, "Analysis of a self-excited induction generator supplying unbalanced load," presented at the Power System Technology, 2004. PowerCon 2004. 2004 International Conference on, 2004.
- [96] A. Keyhani and H. Tsai, "IGSPICE simulation of induction machines with saturable inductances," *Energy Conversion, IEEE Transactions on*, vol. 4, pp. 118-125, 1989.
- [97] P. Coussens, A. Van den Bossche, and J. Melkebeek, "Parameter estimation for induction motor field oriented control using a non-linear motor model," in *Power Electronics and Variable-Speed Drives, 1994. Fifth International Conference on*, 1994, pp. 198-203.
- [98] A. V. Stanković, E. L. Benedict, V. John, and T. Lipo, "A novel method for measuring induction machine magnetizing inductance," *Industry Applications, IEEE Transactions on*, vol. 39, pp. 1257-1263, 2003.
- [99] M. G. Simoes and F. A. Farret, *Alternative energy systems: design and analysis with induction generators* vol. 13: CRC press, 2011.
- [100] G. Ofualagba and E. Ubeku, "The analysis and modelling of a self-excited induction generator driven by a variable speed wind turbine," *Fundamental and Advanced Topics in Wind Power, InTech*. [http://dx. doi. org/10.5772/18159](http://dx.doi.org/10.5772/18159), 2011.
- [101] K.-E. Hallenius, P. Vas, and J. Brown, "The analysis of a saturated self-excited asynchronous generator," *Energy Conversion, IEEE Transactions on*, vol. 6, pp. 336-345, 1991.
- [102] T. A. Lipo and A. Consoli, "Modeling and simulation of induction motors with saturable leakage reactances," *IEEE Transactions on industry Applications*, vol. 1, pp. 180-189, 1984.

- [103] H. A. Toliyat, E. Levi, and M. Raina, "A review of RFO induction motor parameter estimation techniques," *IEEE Transactions on Energy Conversion*, vol. 18, pp. 271-283, 2003.
- [104] M. Ranta and M. Hinkkanen, "Online identification of parameters defining the saturation characteristics of induction machines," *IEEE Transactions on Industry Applications*, vol. 49, pp. 2136-2145, 2013.
- [105] "IEEE Standard Test Procedure for Polyphase Induction Motors and Generators," *IEEE Std 112-2004 (Revision of IEEE Std 112-1996)*, pp. 0\_1-79, 2004.